University of Kerbala

College of Science

Department of Physics

Improvement of Thermal Imaging Efficiency Using Different Shapes of the Lens Aperture

A Thesis

Submitted to Council of the College of Science, University of Kerbala in Partial Fulfillment of the Requirements for the Master Degree of Science in Physics

By

Fatima Rahim Khalaf

Supervisor

Asst. Prof. Dr.Azhr Abdulzahraa Raheem

2023 A.D   **1445 A.H**

بِسْمِ اللهِ الرَحمَنِ الرَحِيمِ

{ وَلَقَدْ آتَيْنَا دَاوُودَ وَسُلَيْمَانَ عِلْمًا وَقَالَا الْحَمْدُ لِلَّهِ الَّذِي فَضَّلَنَا عَلَى كَثِيرٍ مِنْ عِبَادِهِ الْمُؤْمِنِينَ }

صدق الله العلي العظيم

سورة النمل
الآية (15)

Certificate

We certify that the preparation of this thesis, entitled **"Improvement of Thermal Imaging Efficiency Using Different Shapes of the Lens Aperture"** was made under our supervision by (Fatima Rahim Khalaf) at the Department of physics, College of the Science, University of Karbala in partial fulfillment of the requirements for the degree of Master of Science in Physics.
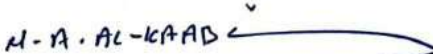
Signature:

Name: Dr.Azhr Abdulzahraa Raheem

Title: Assistant Professor

Address: Department of Physics, College of Sciences, University of Kerbala

Date: 3 / 9 / 2023

In view of the available recommendations, I forward this thesis for debate by the examining committee.

Signature:

Name: Dr.Mohammed Abdulhussain Al-Kaabi

Title: Assistant Professor

Head Department of Physics, College of Science , University of Kerbala

Date: 3 / 9 / 2023

Examination Committee Certification

We certify that we have read this thesis, entitled " *Improvement of Thermal Imaging Efficiency Using Different Shapes of the Lens Aperture* " and as an examining committee, examined the student "*Fatima Rahim Khalaf*" on its contents, and that in our opinion it is adequate for the partial fulfillment of the requirements for the degree of *Master of Science in Physics.*

Signature:

Name: Dr. Fadhil Khaddam Fuliful
Title: Professor
Address: Department of physics, College of Sciences, University of Kerbala
(Chairman)
Date: / / 2023

Signature:
Name: Dr. Adnan Falh Hassan
Title: Professor
Address: Department of physics, College of Sciences, University of Kufa
Date: / / 2023
(Member)

Signature:
Name: Dr. Zaman Hameed Kareem
Title: Assistant Professor
Address: Centre for Research on Environment and Renewable Energy, University of Kerbala
Date: / / 2023
(Member)

Signature: Azhr A.H
Name: Dr. Azhr Abdulzahraa Raheem
Title: Assistant Professor
Address: Department of physics, College of Sciences, University of Kerbala
(Supervisor)
Date: / / 2023

Signature:
Name: Dr. Jasem Hanoon Hashim Al-Awadi
Title: Professor
Dean of the College of Sciences, University of Kerbala
Date: 20 / 9 / 2023

Dedication

To the one who gave me his trust and gave me his strength to the Prophet of love

My respected father

To the most precious of what I have To the perfume of the prophets

My beloved mother

To my soul, my heartbeat and the apple of my eyes

My brother and sisters

To the one who lives in the heart despite her departure to the Lord of the heavens

My beloved grandmother

To the one who supported me in my loneliness

My dear aunt

And to all relatives and friends

Fatima

Acknowledgment

thank God and thank Him as it should be for His Majesty and His greatness. I thank God very much for granting me success and helping me to complete my scientific thesis. I am also pleased to extend my sincere thanks to my father and mother who worked hard and followed my upbringing and education from a young age, and I would like to express my sincere appreciation and gratitude to those who supervised, directed, and helped me, Prof. Dr. Azhr AbdulZahraa Raheem for suggesting the topic of this thesis and for his guidance and continuous encouragement to me throughout this period and in all stages of the research. I also thank everyone who taught me or contributed to my teaching from professors in the Department of Physics - Faculty of Science and everyone who encouraged me and did not forget me in their prayers.

I also extend my sincere thanks and gratitude to all members of the discussion committee of my honorable letter for their acceptance of my letter and thank them for the great effort they made in it.

Fatima

Abstract:

Thermal imaging is an effective form of night vision technology, with the ability to operate in the complete absence of any light. The principle of its work is to capture the infrared part of the electromagnetic spectrum emitted by objects because these objects emit electromagnetic waves when their temperature is higher than absolute zero. Thermal imaging cameras are widely used in military applications for their capabilities to provide night vision, monitoring, and identification of targets. Thermal imaging applications depend on specific wavelengths of infrared radiation (3-5) μm and (8-14) μm.

The quality of the optical system depends on several factors that in turn affect the intensity of the image, such as the geometrical aspects of the optical system design that result in diffraction and aberration, and also depends on factors related to the nature of the target and its surroundings environment (type of target, its speed and weather conditions). will be dealt with in this work, an ideal optical system. That means, studies the effect of factors which related to the target and its surroundings environment, and analyzing the degradation in the image intensity, which gives a blurry image to detect a higher intensity value that required to distinguish the target and not only detect it.

In this study, the thermal imaging conditions was applied to the RSF to find out the intensity distribution of the detected thermal image in the specific place of Karbala governorate. different shapes of camera aperture (circle, square, triangular) were applied and optical filter to improve the thermal camera efficiency. Mathcad software will be used to study and develop the performance of thermal imaging devices using the RSF function as a description of the targets,

as the model it is a promising technology for military applications that try to improve the thermal camera in the environment of the Karbala governorate.

List of Contents

List of Symbols

Symbol	Description	Units
λ	Wavelength	µm
$G(z^{\backslash}, m^{\backslash})$	Point spread function	
(A, B)	Dimensions of object	m
$R(z^{\backslash}, m^{\backslash})$	Rectangular spread function	
(z, m), (z', m')	Reduced coordinates of the point in the object and image planes	
F(x, y)	Pupil function	
$\tau(x, y)$	Function permeability	
k	Wave number	m^{-1}
N	Normalized Factor	
L	Linear Motion Factor	
t_e	Snapshot Time	Sec
$F^{\neq}$	Optical System Focal Number	mm
v_i	Image animation speed	m/sec
f	Focal length	mm

R	Distant of a target from the camera	m
v_0	Speed of the image movement	m/sec
V	Visibility	m
q	Exponent	
C	Concentration of particles	$\mu g/m^3$
τ_S	Transition	
Abs	Absorption of IR	
α	Numerical constant	
β	Apodization parameter	

List of Abbreviations

Symbols	Meaning
IR	Infrared Radiation
IRT	Infrared technology
NWIR	Near-wavelength infrared
SWIR	Short- wavelength IR
MWIR	Medium- wavelength IR
LWIR	Long- wavelength IR
FLWIR	Far long-wavelength IR
EM	Electromagnetic spectrum
ATIR	Atmospheric Transmission of the Infrared Radiations
ESF	Ellipse Spread Function
DSF	Disc Spread Function
PSF	Point Spread Function
LSF	Line Spread Function

BSF	Bar Spread Function
DoF	Depth of focus
RP	Resolving power
PM	Particle Matter

List of figures

4-18	(a) The intensity distribution of the detected thermal image using a system with a filter (at N=1) for moving vehicles with linear motion of (80 Km/h) and at 1 Km of distance.	79
	(b) The intensity distribution of the detected thermal image using a system with a filter (at N=2) for moving vehicles with linear motion of (80 Km/h) and at 1 Km of distance.	79
4-19	(a) The intensity distribution of the detected thermal image using a system with a filter (at N=1) for unmoving vehicles and at 1.5 Km of distance.	80
	(b) The intensity distribution of the detected thermal image using a system with a filter (at N=2) for unmoving vehicles and at 1.5 Km of distance.	80
4-20	(a) The intensity distribution of the detected thermal image using a system with a filter (at N=1) for moving vehicles with linear motion of (80 Km/h) and 1.5 Km of distance.	81
	(b) The intensity distribution of the detected thermal image using a system with a filter (at N=2) for moving vehicles with linear motion of (80 Km/h) and 1.5 Km of distance.	82
4-21	(a) The intensity distribution of the detected thermal image using a system with a filter (at N=1) for unmoving vehicles and at 2 Km of distance.	83
	(b) The intensity distribution of the detected thermal image using a system with a filter (at N=2) for unmoving vehicles and at 2 Km of distance.	83
4-22	(a) The intensity distribution of the detected thermal image using a system with a filter (at N=1) for moving vehicles with linear motion of (80 Km/h) and at 2 Km of distance.	84
	(b) The intensity distribution of the detected thermal image using a system with a filter (at N=2) for moving vehicles with linear motion of (80 Km/h) and at 2 Km of distance.	84

	unmoving vehicles with a concentration of particles PM=30 $\mu g/m^3$ of different distances.	
	(d) The intensity distribution of the detected thermal image using a system operating with the square aperture for unmoving vehicles with a concentration of particles PM=40 $\mu g/m^3$ of different distances.	92
	(e) The intensity distribution of the detected thermal image using a system operating with the square aperture for unmoving vehicles with a concentration of particles PM=50 $\mu g/m^3$ of different distances.	93
4-25	(a) The intensity distribution of the detected thermal image using a system operating with the triangular aperture for unmoving vehicles with a concentration of particles PM=10 $\mu g/m^3$ of different distances.	94
	(b) The intensity distribution of the detected thermal image using a system operating with the triangular aperture for unmoving vehicles with a concentration of particles PM=20 $\mu g/m^3$ of different distances.	94
	(c) The intensity distribution of the detected thermal image using a system operating with the triangular aperture for unmoving vehicles with a concentration of particles PM=30 $\mu g/m^3$ of different distances.	95
	(d) The intensity distribution of the detected thermal image using a system operating with the triangular aperture for unmoving vehicles with a concentration of particles PM=40 $\mu g/m^3$ of different distances.	95
	(e) The intensity distribution of the detected thermal image using a system operating with the triangular aperture for unmoving vehicles with a concentration of particles PM= 50 $\mu g/m^3$ of different distances.	96

List of tables

Chapter One

The introduction

and

Literature Review

1-1 Introduction

In general, most imaging systems do not give perfect images with sharp and regular edges, but they mostly form images with definite clarity with wide edges that have something of a blur. These distortions of images occur due to two main reasons, namely the phenomenon of diffraction of light, and aberrations contained in the optical system. A picture can be defined as a visual representation of what the human eye sees of people, scenes, or anything else, and can be represented through drawing, design, photography, and other means. Many applications may use devices that depend on the formation of images in their work. Such as medical devices that work on imaging using ultraviolet and X-rays to produce a medical image. As well as other devices that use ultrasound in the medical field to produce a medical image for proper medical diagnosis. Additionally, devices are used in the process of geological detection for prospecting. All these fields consider the improvements in image quality is necessary for their quality results. One of these fields is thermal imaging, which relies on infrared rays in the process of producing a thermal image of the body through the so-called thermal imaging image technology developed extensively during the technology [1]. second half of the last century, when different types of devices and sensors were used in the process of producing better images in different fields.

In general, cameras are equipped with detectors to distinguish rays emitted by objects. The thermal camera detects infrared rays based on the fact that all objects whose temperature is above absolute zero can emit radiation in the infrared range of the electromagnetic spectrum. As a result, it works to convert the invisible radiation of objects into visible

images to the human eye, and these images are called thermal diagrams, thermal images, or thermal maps [2]. Thus, all thermal imaging systems consist of radiation detectors, signal processing units, and display units, or what is known as the image acquisition system for the target to be monitored [3].

Accordingly, it has become possible to use the data obtained through thermal imaging, whether directly or indirectly, for many broad and important applications such as military, agricultural, aviation, medical, as well as in the field of veterinary medicine and matters of electrical maintenance [3].

In this study, one can apply the thermal imaging condition to the Rectangular Spread Function (RSF) to find out the intensity distribution of the detected image to stimulate the thermal image that was monitored in the Karbala governorate. The rectangular spread function represents the optimal expression of the real vehicle shape. Different shapes of camera aperture (circle, square, triangular) to improve thermal camera efficiency are applied in this study.

1-2 Infrared Rays

Infrared radiation was discovered by the British astronomer William Herschel, born in Germany in the year 1800, through a simple experiment in which he passed sunlight through a glass prism to produce the spectrum. So, a thermometer was placed at the site of each wavelength of the visible spectrum to measure differences in the temperature. He noticed that an increase in the temperature when the thermometer was moving from the blue color zone to the red color zone of the spectrum. These changing in the measurements even stay after the red color, where

the temperature is higher. The change in the temperature after the red region was explained by "thermal rays" which represent a type of rays that cannot be seen by the human eye. However, when the thermometer was placed far from the red region, it was found that the temperature continued to be increased. This increment in temperature is called infrared. Thus, scientist Herschel defined infrared radiation, which is radiation that exceeds the red end of the visible spectrum, almost from the end of visible light to microwaves. After that, studies took place about to employing and using the infrared radiation it in various fields and applications to serve humanity [4]. In general, one can define infrared rays as a type of radiant energy that cannot be seen by the human eye but can be felt in form of heat.

All organisms on Earth emit a certain level of infrared radiation when their temperature is higher than absolute zero. which can be detected by using thermal cameras. Another source of infrared radiation is the black body, which represents a perfect body that absorbs all the radiation from its environment without any reflection of any radiation, as it is characterized by a high emissivity and accuracy [5].

1-3 Thermal Imaging Technology

Thermal imaging is a very important and indispensable technology in our daily lives because it has many important and useful applications.

The principle of its work is based on capturing infrared rays from objects, leading to detect all objects that emit infrared rays when their temperature is higher than absolute zero degrees. It measures very fine differences in temperature in order to produce a thermogram that helps in detecting targets [6].

The amount of emitted radiation and its radioactive distribution

depends on the objects temperature [7].

According to Stefan Boltzmann Law , which describes an inverse

relationship between thermal radiation and wavelength, the amount of

any thermal radiation depends on the amount of energy that emits from

the body, so the ability of the material surface to produce or emit thermal

radiation is known as emissivity. Thus, all materials have more or less

emissivity depending on their properties [8,9]

Thermal imaging technology is considered one of the best and very

powerful remote sensing techniques, as it collects the data required to

produce a thermal image of the target quickly and with high efficiency. so,

it has been used mainly for military purposes and in field studies related

to the environment of animals [9]. It is superior to visual imaging

technology because thermal radiation can pass through the dark, smoke,

fog, and dust in a better way than it is in visible radiation so that targets

can be detected in all weather conditions and different environments

because it depends on the amount of heat the target emits [9].

The devices that uses this technology are thermal cameras, which

have different types according to the required job or type of

requirements.

The thermal camera produces a grayscale image (the image is black,

which indicates cold objects, and white, which indicates hot objects) [6].

Thermal cameras can be used in many different and useful applications in

daily life. They can be used, for example, in discovering things or people

in complete darkness or even when the environmental conditions are

difficult. In addition, thermal cameras can detect targets in environments

filled with dust or smoke, as well as in environments where lighting is very low [10].

Since the 1940s, the first infrared detector was used with a sensitivity of up to 3 μm for infrared wavelengths. These detectors have advanced significantly to be used in a wide range of applications [11]. Since infrared detectors have been created for a wide range of military and civilian uses, it has proven to determine the spectral range in which the particular detector must operate for many specific purposes in order to achieve optimal performance and reach the most optimal image [12]. Some of the manufacturers offer multi-band detectors, meaning that these devices can work in the middle as well as far infrared ranges, but these detectors are very expensive [13].

1-4 Thermal Imaging Elements

The main elements, that make the thermal imaging system reliable, can be summarized into five elements [13–15]:

1-An optical system through which an image of the required external scenes is created based on the radiation in the favorite thermal wavelength range.

2-One or more of the detector elements can convert this radiation into electrical signals proportional to the captured radiation.

3- Signal amplifiers, which are considered one of the electronic tools through which the input signal can be amplified to obtain a signal similar to the input signal and multiply its value to be processed after that by the electronic processor unit.

4- An electronic processor that translates the electrical signal and converts it into a signal that is sent to the screen in the form of colored areas depending on the temperature.

5- A display unit that converts the recorder's signal into an image visible to the human eye.
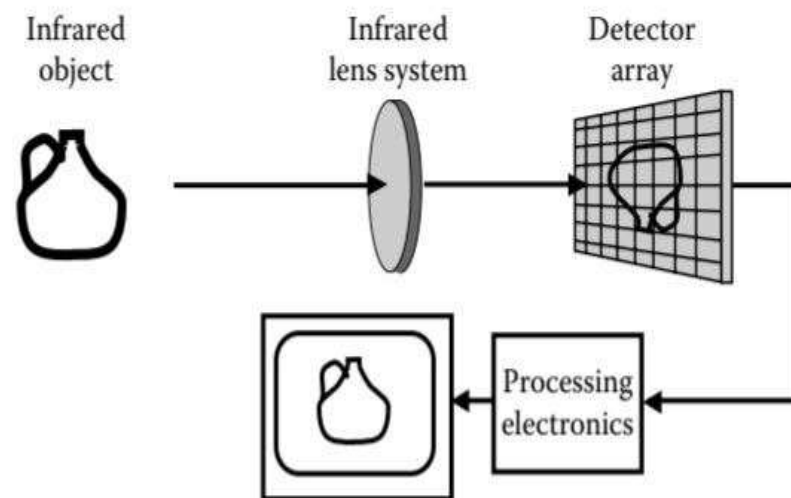
Fig (1-1) Thermal Imaging Elements [13].

1-5 Advantages of The Thermal Imaging

Thermal imaging technology has many characteristics and advantages that make it more used in many applications of our daily life compared to other technologies. These advantages and main features of IRT can be summarized as:

1- IRT is a non-contact technology : the devices used in this technology are not connected to any heat source, so the temperature of extremely hot objects can be estimated and measured with the utmost safety without any direct contact between the target whose temperature is to be measured and the device used in the measurement process.

2-Thermal imaging devices can produce a two-dimensional thermal image in a dark environment, and thus a comparison between different targets and their areas is possible.

3-It can detect moving targets as well as it can detect and monitor fixed targets in different weather conditions such as bad weather (dust or fog) or in the dark.

4-It does not cause in any radiation effects or harmful effects, as in the x-ray imaging technique, so it can be used repeatedly and for long periods without producing any damage to the environment. Therefore, it is considered a technology that does not pollute and is harmless, so it does not cause any biological changes to the target and therefore does not affect or change the nature of the target, which wants to be monitored and tracked, and does not affect the user or the observer [16–18]

1-6 Types of Thermal Cameras

Thermal imaging cameras are produced in different shapes and sizes. There are two types of common thermal imaging cameras, which are classified according to their detectors. The types of thermal cameras are cameras that do not need cooling and others that need cooling. The most common types of thermal imaging devices are non - cooling devices, and this type is widely used because they are suitable in terms of price while cameras that need cooling are very expensive and have a large size, in addition to that they consume more energy, but this type of cameras does not issue Any noise during use (i.e. no sound when used), in addition to that this type of camera is more accurate at work, so

it is increasingly used in thermal imaging applications in particular by the

military forces.

The thermal cameras, which need cooling, were originally using

liquid nitrogen in the processing of the cooling, so they are more

expensive than non-cooled systems, where the elements are contained in

a container that maintains the temperature at $0^{'}$C during use. These

cameras produce images with better accuracy and higher sensitivity. This

is because this type of system can detect differences in temperature of

$0.1^{'}$C at a distance of about 300 meters with a high-quality image

compared to cameras that do not need cooling for their detectors.

Alluringly , it was widely used for monitoring purposes, it was more

popular and used by the military and security forces because it could

determine whether the observed person was carrying a weapon or not

from a certain distance [19–21]

Fig. (1-2) Types of Thermal Cameras [22].

1-7 The Night Vision and Thermal Imaging Technologies

In general, thermal imaging technology is a shape of night vision technology. Night vision is divided into two different technologies depending on the need and the technology applications. The first technique is used to improve the image, where this technology works in a low-light environment. This technique works by collecting a small amount of light in the region so that these quantities of light are imperceptible and difficult for the human eye to notice. Then, in these devices, some amplifiers amplify the visible light available in the dark environment to form a focused image. The principle of this type of night vision technology is based on the reflectivity of light. So, the reflected light from natural sources (such as moonlight, stars, and artificial sources such as the light of street lamps) is amplified even if the reflected light has a very low intensity and as shown in the following table (1-1) . However, this technique is ineffective in the case of complete darkness .

The second technique is the thermal imaging technique, which can work in regions where light cannot be fully sensed by the eye. In this region, light emits by objects in the form of heat. Thus, the principle of this technique is based on emissivity. In particular, in this technique, the devices can capture the light emitted by objects in the form of heat instead of reflected light. So that the hotter objects are more emissive than other cooler objects. Moreover, the hotter the objects, the higher the percentage of infrared radiation to be converted into a visible image, and this technology can work in complete darkness and even in environments where the lighting is completely absent, unlike image enhancement technology [19,23].

Table (1-1) luminous intensity [24].

Object	illumination (Lux)

Street lights	40-10
The moon	0.1
Stars	0.001
The sun	100000
The brightness of the night sky	0.2-0.5

1-8 Applications of Thermal Imaging Technology

The thermal imaging technology was initially used in particular by the military as a detection method and surveillance for military purposes. Nowadays, it has become more spread in many fields and thus has a wider range of applications [25].

Based on the fact that all objects are capable of emitting an amount of infrared radiation when their temperature is above absolute zero in the form of heat emitted at different levels, it has been considered a feature that has been used in infrared thermography for a variety of purposes [26].

In addition to other advantages that make thermal imaging technology more used than other technologies. For example, this feature can be used for electrical maintenance purposes to discover and identify any defect that may occur in electrical circuits, for its ability to estimate the temperature of different parts to avoid costly breakdowns and to avoid disasters major that may result from it [27].

This feature is also an indicator of health in medical applications, and in particular, this technology has contributed to the advancement of the medical field through its use for many medical purposes, by estimating the temperature. It is successfully used in the process of diagnosing breast cancer, diagnosing diabetic neuropathy, and identifying disorders in

peripheral blood vessels and the heart. It has also been used in dentistry, measuring fever, monitoring the temperature of people with infectious diseases, as well as monitoring the functions of newborn organs [28,29]. It is mainly used by the army, navy, defense, and air forces, as well as in civil fields for many purposes. This technology was used by the army in border control and the implementation of air operations in the controlling and monitoring of targets.

It is also used in the navy by the coast guard at night to avoid ship collisions and for guidance purposes, due to the ability of thermal imaging devices to work at night or in low-light environments in bad weather conditions. In the case of a low level of illumination, it had a great contribution to the development of military aviation in identifying the location of the enemy forces. In addition, it can also be contributed to the development of civil aviation, which was used for the monitoring of aircraft [30,31].

The firefighter may face many difficulties during the rescue operation. Experiencing high temperatures and very thick smoke. In this case, ordinary imaging devices become unsuitable to operate in such environments. Therefore, thermal imaging devices were used when fire accidents occurred, because these devices may work better in such dense environments than in normal imaging devices. Therefore, thermal imaging devices were used in firefighting applications because these devices provide firefighters with important information about the accident, such as the source of the fire and an estimate of the extent of the fire in the place, on the basis of which appropriate decisions will be taken in the rescue operation [32,33].

Depending on this feature (as the temperature is a very important

parameter in all fields), thermal imaging technology can also be used in

the field of agriculture for various agricultural purposes, as the devices

used in this technology are more accurate and more effective in working

in this field than other technologies. Based on the data provided by the

thermal cameras, appropriate decisions are taken in the cultivation

process [34,35].

The low cost of thermal imaging technology in the past decade was

a reason to make imaging devices more widely available and accessible to

everyone and thus to employ it in various fields depending on needs. Since

the process of monitoring animals and their activities in the natural

environment is very difficult for researchers and workers, thus, this

technique was used to survey and observe animals at night, as well as to

solve many problems related to monitoring wildlife [9,36].

1-9 Transmission of The Thermal Radiation Through Atmosphere

In general, the atmosphere consists of various natural gases, some

of these gases cannot absorb infrared rays, whereas many of them can

absorb these rays. Many air molecules will absorb these infrared rays

when it transmits through the air like carbon dioxide CO_2 and H_2O. The

wavelength of the thermal rays determines the amount of infrared rays

absorbed by the air, the quantity of infrared rays absorbed by the air

decreases as the wavelength decreases [37,38] .

The infrared region of the electromagnetic spectrum is divided into

several regions [37,38]:

Near-wave infrared (NWIR) at the range of 0.75–1.4 μm

Short wavelength IR (SWIR) at the range of 1.4–3 μm

Medium wavelength IR (MWIR) at the range of 3–8 μm

Long wavelength IR (LWIR) at the range of 8–15 μm

Far-long wavelength IR (FLWIR) at the range of 15-10000 μm

The MWIR region is considered the most suitable area to do in the

thermal imaging process, while the wavelength range of 8-5 micrometers

is practically not usable in the thermal imaging process because of the

higher absorption of this range by the atmosphere.

If the spectral bands 3-5 μm of the MWIR region and the spectral

bands 12-8 μm of the LWIR region are considered bands in which a

thermal image of the target can be produced [37,38].

After testing the imaging systems operating in these infrared bands

in ground conditions, it was found that the detectors operating in the

MWIR band have good performance compared to their performance in

the LWIR band in most cases. But it was later found that the performance

of detectors in the MWIR band deteriorates more quickly compared to

the performance of detectors in the LWIR band in the case where the

observed targets are cooler [39,40].

This absorption is achieved at low rates in the MWIR and LWIR

bands, allowing more radiation to reach the camera sensor.

The figure below shows the transmittance of the atmosphere for

many different wavelengths. It shows that in the visible part of the

spectrum, ranging from (0.4 - 0.7) μm, only about 60% of the emitted

radiation is transmitted, while in the range between (5 - 7.5) μm.

Approximately, there is no transmission of radiation, and all this radiation

is absorbed by the atmosphere as shown in figure (1-3) [27].
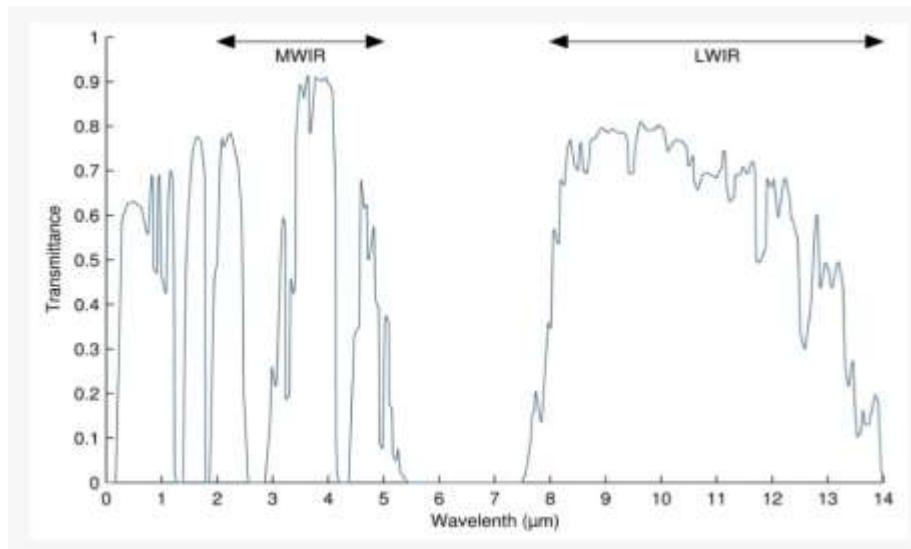
(1-3) Atmospheric transmittance [41] Fig

1-10 Literature Review

W. K. Wong, *et al* [42], in 2010 proposed a new algorithm, used to identify targets (humans) by analyzing the data obtained from the thermal image, to create fast and effective intelligent detection systems to monitor intruders. This technology is used for the purpose of distinguishing and identifying any human element, its shape, location, and dimensions that are examined for better identification. The experimental results of this research revealed that the proposed intruder detection algorithm was effective, very fast, and accurate, with an accuracy of 98.62% in the optimal setting .

K. V. Kumar, *et al* [43] presented in 2013 another study aimed at improving the efficiency of an optical system suffering from spherical aberration through the use of Hanning Amplitude Filters, which is considered one of the most important filters used in optical systems. The efficiency of this filter is verified in the presence of different parameters

through the point spread function, as This filter contributed to improving the accuracy of the resulting image in a way that allows objects to be distinguished efficiently.

U. Gupta, *et al* [44], a studying, in 2013, discussion provides a quick overview of various methods for tracking numerous targets while using infrared imaging. Every branch of security, including border security, seashore security, traffic monitoring, and robotics-based rescue operations, needs an intruder detection and tracking system. The performance of the tracking is hampered by a number of factors, including noise, directional view, pose, and illumination. When numerous targets are being tracked in thermal imagery, the performance of the temporal median filter (TMF) with kalman filter (KF) is improved. When compared to other approaches, TMF with KF has a higher positive predictive value and is more sensitive to target recognition and tracking.

R. Ishimwe, *et al* [45], offered in 2014 a assessment of infrared thermal imaging technology applications with a focus on their using for agricultural purposes. Monitoring nurseries and greenhouses, scheduling irrigation, discovering plant diseases, and predicting fruit crops are possible applications of thermal sensing in the field of agriculture. Where this technique is considered a non-contact and not harmful technique in for determining the thermal characteristics of any particular organism, was marked for study.

M.Venkanna1, *et al* [46] presented in 2015 a study aimed at improving the efficiency of the optical system by using Amplitude filters for the purpose of producing a clear image and thus increasing the object recognition distance. The efficiency of this filter was verified by using the point spread function, while the results of this study proved the

effectiveness of this filter in improving The efficiency of an optical system

that operates using circular and annular apertures

M. Štumper and J. Kraus [47], presented an article in 2015, which

was a study aimed to investigate the advantage of using thermal imaging

technology in the field of aviation. Thermal imaging technology is used to

maintain the security of the airport perimeter, and the establishment of

the ground control system.

N. Saunier, *et al* [48], presented in 2016 a study aimed at detecting

and tracking pedestrians. This study discussed the success of using

thermal imaging technology devices in traffic control operations on

internal or external roads, compared with visual imaging devices, due to

the possibility of thermal imaging devices working in all bad weather

conditions of the environment, whether represented by dust, fog, smoke

or darkness, where the resulting image is with visual imaging devices, less

accuracy, and clarity than in thermal imaging devices, so traffic can be

monitored and pedestrians can be tracked well.

M. Bardou, *et al* [49], presented in 2017 a work in which he

discussed the possibility of using thermal imaging devices in measuring

fever for travelers and examining persons suspected of having infectious

diseases at airports by estimating the temperature emitted from bodies

to avoid human disasters.

A work was presented, in 2018 by S. J. Mambou, *et al* [50], aimed

at employing thermal imaging technology in the field of medicine to

detect breast cancer. Radiography techniques have been widely used in

the diagnosis of breast cancer. In addition, one of the important methods

used is infrared imaging. A diseased breast always shows an increase in

thermal activity in potentially cancerous tissues and the surrounding

areas.

 B. T. Miethig [51], presented, in 2019, a study of knowing using

infrared imaging in improving the system in self-driving vehicles.

Self-driving vehicles contain thermal imaging techniques that can

identify and track objects that are surrounding the vehicle, leading to

collecting information to help in appropriate driving decisions. The

information that infrared cameras may provide can help in improving

driving by detecting all objects in the vehicle's environment.

a group of researchers, E.H. Kiashari, *et al* [52], in 2020, presented

a work aimed at reducing road accidents. As the drowsiness of drivers, it

was necessary to work on finding ways to reduce and limit these

accidents. In this research, a new and innovative method was proposed

for detecting the drowsiness of the driver. This is performed depending

on the difference in the driver's breathing rate detected by thermal

imaging technology for the driver's face.

M. Mileckaet, *et al* [53], presented in 2021 a work aimed to provide

a summary of the findings from fire trials. The project's goal was to create

novel fire detection techniques employing IR thermal imaging technology

and specialized image processing. We carried out four studies using

various setups and objects in each experiment. The results of the trials

have demonstrated the enormous value of infrared cameras for spotting

the beginnings of a fire. Hot areas can be found using even inexpensive,

low-resolution bolometric detector modules.

A. A. Kharnoub, *et al* [54], offered, in 2021, a theoretical model

aimed to study the image intensity distribution of a point object detected

by an optical system containing a single and multi-hexagonal aperture.

The point spread function used in this study showed the preferring of the multi-hexagonal aperture and the single hexagonal aperture, where the multi-hexagonal aperture gave a high resolution compared to the single hexagonal aperture .

In 2022, another research was performed by A. A. Kharnoub, *et al* [55], which aims to study the efficiency of an optical system that works using a single hexagonal aperture in the case where the optical system contains aberrations. The results of this work showed a very clear increase in the value of central intensity in an optical system that works using a hexagonal optical aperture compared to an optical system that works using a circular optical aperture. This is an indicator for improvement in the used optical system, which is one of the most important factors affecting the accuracy of resulting images .

A. F. Abdul Rahim, *et al* [56], performed in 2022 a study to investigate the effect of dust particles on the intensity distribution of the detected thermal image by an optical system works using a circular optical aperture. Air pollution with surrounding particles, such as dust particles, is one of the most important factors negatively affecting the intensity of the image. It was found in this research that the amount of thermal radiation emitted from the target to the thermal camera detectors is affected by the concentration and sizes of the dust particles which is containing in the atmospheric of the environment surrounding the target .

In 2022 A. F. Abdul Rahim, *et al* [57], also presented a work in which a new mathematical model was created that simulates bar-shaped objects by a MathCAD program known as the bar spread function. In this work, the transmittance of infrared rays in the atmosphere at

wavelengths (5,10) micrometers is studied in foggy environments. The obtained results proved that the thermal camera that operates at a wavelength of 10 micrometers is better than the camera that operates at

a wavelength of 5 micrometers under foggy conditions .

Moreover, A. F. Abdul Rahim, *et al* [58], presented, in 2023, another work aimed to detect moving objects at different ranges. The intensity distribution of the detected thermal image of an optical system operating using a circular aperture was calculated by solving the Bar Spread Function (BSF) in the case of moving and stationary objects. The theoretical results obtained in this research were compared with the experimental images taken by the thermal camera in the Ain Al-Tamor

area of the holy city of Karbala .

This study was close to our study, but by comparing the intensity distribution in the thermal image produced for moving objects by an optical system operating with a circular aperture using both the BSF and RSF equation, it was found that RSF had a better effect on the accuracy of

the resulting image of moving objects.

1-11 Aim of Work

This work aims to improve the efficiency of thermal imaging by using the optical filter and different shapes of lens apertures to make more improvements in the distribution of the intensity at the image level of the detecting objects at Karbala Governorate at the Ain Al-Tamr. This study was performed under certain conditions (different ranges and different speeds of the detecting target).

Chapter Two

Theoretical Part

Introduction 2-1

The photography technique was one of the best inventions of science in the documentation process at that time. This technique allowed the documentation of many results.

In general, the picture was used mainly for documentation, clarification, and interpretation of the observed phenomena. Because of the rapid progress in this technology, the concept of the image has been developed to include more advanced and useful techniques, whereas personal computers and workstations are powerful and good enough to handle image data processing [59].

Since the first use of imaging techniques, researchers and scientists have tried to improve the quality of the resulting images. All properties, qualities, and features are always represented at the edges of the image. The designing imaging devices have the goal of representing the most accurate and important details in the image.

On another side, the clarity of the image is mostly determined by the effect of both the aberration factor and the diffraction that occur in optical imaging systems. These factors are the most affected the accuracy of images. In addition to the factor of distortions that can occur during the process of recording the signal, the used sensor, its exposure time to the signal, and the speed of the sensor response, all these factors have a clear effect on the processing of the image and its contrast. Therefore, any distortion that occurs and affects the image will affect the amount of information in the image [1].

Also, the bad quality of the imaging equipment used or the environmental conditions at the time of image acquisition is one of the

factors affecting the accuracy of the image, leading to creating an image

with a bad clarity or completely distorted [60].

2-2 Image Distortion Factors

Aberration and diffractions of light in the optical systems

represent the main factors, that affect the image quality, leading to

distortion and blurring of the image features [1].

There is no perfect image that can be produced in any optical

system. Producing the perfect image is related to many things like optical

elements manufacturing, and optical system designing. Optical designers

have the main goal to improve image accuracy so that the results of the

optical systems would be more suitable for a specific purpose that is made

for [47]. Modern algorithms, software innovations, and developments are

methods that may be used to solve problems and can help in improving

images.

2-2-1 The diffraction

One of the most important and common physical phenomena in

optical systems is diffraction, which occurs when the light ray travels

through a specific aperture, causing a deviation in the path of this light

ray [61].

The diffraction is also an inherent property of the nature of light in

the sense that when an optical system is essentially free of aberrations,

its performance is limited only by diffraction. Thus, it is referred to as a

diffraction-limited optical system [62].

High-quality lenses can be created leading to eliminating the
aberration effects, whereas, the diffraction effect cannot be ignored
because it is related to light properties [63].
The details and information, that obtain from an optical system,
show the effect of diffraction more clearly when the optical aperture is
small (Unlike aberration, whose effect will be less). Meanwhile, this does
not mean that the large optical apertures will be free from this effect, so,
the diffraction effect will also be present [64].
When the light rays pass through a circular optical aperture, the
image of a point source will appear in the form of a bright central disk
containing (84%) of the total energy. Surrounding that bright disk is many
less bright rings in which the rest of the total energy is distributed (16%).
This central disk is called the Airy disk, relating to the scientist Airy,
who considered calculating the intensity of the image of a point object,
which was formed as a result of diffraction, as shown in figure (2-1) [65].
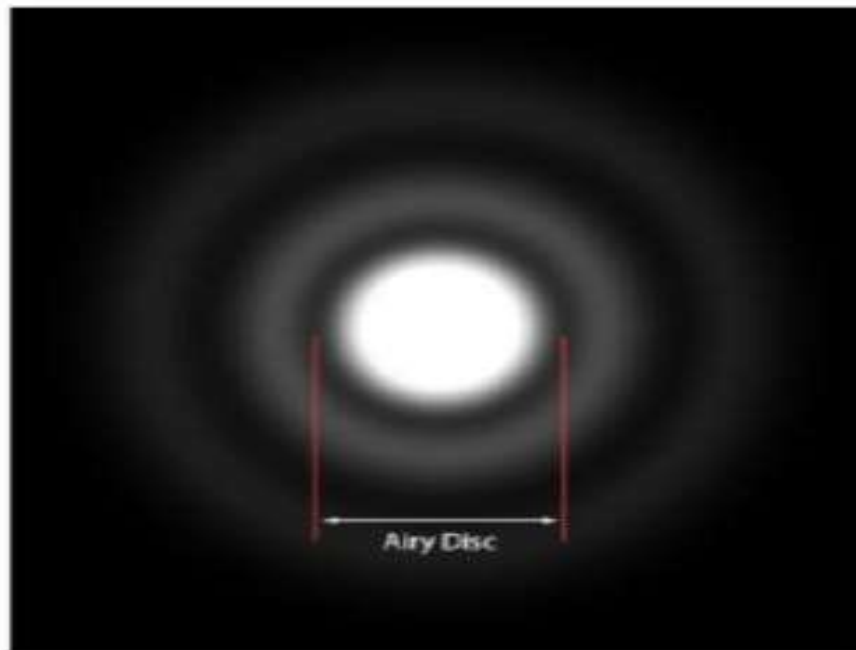
2-1) Airy disk [65])Fig.

The angular diameter of Airy disk (B_{ang}) which is assumed to be the diameter of the first dark ring is [66]:

$$B_{ang} = 2.44\lambda/D \qquad (2\text{-}1)$$

The Airy disk diameter B_{diff} is:

$$B_{diff} = B_{ang}\, f = 2.44\lambda f/D = 2.44\lambda(f/NO) \qquad (2\text{-}2)$$

2-2-2 The aberration

Optical aberration is one of the most common sources of image degradation that affects nearly all lens-based imaging systems. Optical aberration is widely found in optical imaging systems. The advanced lenses are carefully designed to minimize optical aberration. In general, a better lens with lower optical aberration is usually larger and has a much higher cost to manufacture, and thus may not be viable in consumer-grade cameras [67].

Light reflection, refraction, and diffraction are the reasons for creating images in imaging systems. Imaging systems are designed to form images of self-luminous or light-reflecting objects. The created images are not ideal due to the inherent nature of optical systems as optical aberrations diminish their accuracy Deviations from optimal conduct are referred to as aberrations. Traditionally, extended image analysis has begun with the examination of images of point sources within the optical system's field of view. A non-physical entity called a point source is used to determine the point from which light rays come. The geometrical wave front, which is defined as a surface with an equal optical path measured along the rays and from the point source.

Every point of an object that travels through the optical system while maintaining its spherical shape is an indication that the optical

system is perfect. However, sometimes the converging wave front may

not be spherical but distorted due to the inherent geometry of the optical

surfaces in the system. [68,69].

In general, aberration can be defined as the failure of the rays

emitted from any point in the body to gather at a single point, or the

inability of the wavefront to maintain its spherical during the transition

between optical systems [68,69].

There are two main types of aberration: chromatic aberration and

achromatic aberration, and the latter is classified into five types [70]:

1- Spherical aberration.

2- Coma Aberration.

3- Astigmatism aberration.

4- Field curvature aberration.

5- Distortion aberration.

2-3 Optical system design

The process of producing or manufacturing an optical system goes

through many very important steps that cannot be dispensed with in the

manufacturing process of any optical system. The optical design is the first

step in the production process. The second step is manufacturing the

optical components. Evaluating the manufactured optical components

are the last step before using the optical compounds for what it was

designed for it.

Because the optical system manufacturing process is highly

dependent on the information that the designer determines and through

which the designer can derive the parameters of the optical system. The

optical design is thus the most important step in the manufacturing

process among the other steps, as it is the basis in the production of

optical systems.

Many specifications, included in the optical design, are the thickness and diameters of the different components, the radius of curvature of the surfaces, the air spaces, the distances between the optical elements and objects, the type of glass that will be used, and the refractive index of the material from which the lens is made, as well as the shape of the lens apertures. These parameters can be defined as (degrees of freedom), where the designer can change it to maintain the required

order.

In general, formed images cannot be completely perfect due to the designed system may suffer from aberration and diffraction. The main reason for aberration and diffraction in the formed image is the wave nature of light. In addition, there are many other factors that in turn affect the process of evaluating the quality and accuracy of the image that makes up the optical system. One of these important factors is the measured spread function, whether it is for a point, a bar, or a line, which in turn represents the descriptions of the intensity distribution in the image plane for a specific object (bar, line, point and etc…). The spread function is dependent on the aberrations occurring in the optical system or the lens and also on the diffraction resulting from the lens aperture. The point spread function is one of the very important parameters used in the process of determining the efficiency of the optical system, where

many functions are derived from this function [62,71,72].

Also, thermal cameras do not differ much in design and manufacturing steps from optical cameras, with some differences, such as a difference in the working principle, the spectral range in which they

operate, and some of the parts that make up each camera, such as the lens and the sensor used. The principle of operation of optical cameras is based on the reflection of light on objects coming from lighting sources present in the scene, so that this reflected light is converted into electrical signals to then be displayed on the display screen, as these cameras only work in the range of visible rays [73].

Whereas thermal imaging cameras, their working principle is based on capturing infrared rays emitted from objects in the form of thermal radiation and converting them into electrical signals to be later displayed in the form of diagrams or thermal images with grayscale, regardless of the lighting, as these cameras only work in the infrared range [74]. These are the most important differences between thermal cameras and optical cameras. They also each have their own uses and may have overlap in some applications for the purpose of improving work efficiency [75].

2-4 Optical Systems Examination

After Finishing the design and manufacturing of the optical element processes, the inspection process of these optical elements is the next. This step represents the last step before the optical system is used. The main purpose of the examination process is:

1- To determine if the optical elements are suitable for a particular application and meet the purpose.

2- Ensure that the optical elements fit to design characteristics as much as possible.

3- Investigate the limitations of image resolution.

The examination process can help in determining the suitability of
the optical elements for the purpose that was designed for and improving
the formed image quality. Two methods are used to examine the optical
system or the lens: quantitative or qualitative [62,71].

2-4-1 Qualitative Examination

The qualitative test allows to determine if the lens contains
aberration or not. The star test is one of the qualitative test methods. A
collimator is used in the star test to create a plane wave that falls directly
on the lens being evaluated. As shown in figure (2-2), the created image
by the tested lens is studied under a microscope.
If the lens under test is perfect, the viewer will perceive a brilliant
circular ring surrounded by many rings of gradually decreasing brightness,
which is known as the Airy pattern. The central disk contains about (84%)
of the intensity, while the rest is distributed over the rings surrounding
the disk, represented by (16%) of the intensity. The human eye is
employed in this process, and while it is a good detector for asymmetry
and shape changes, it cannot display the exact difference in
intensity [66,76].
Where the range of the human eye's ability to distinguish the
lowest possible light intensity reaches approximately 0.1 Lux (and this
amount is represented by the intensity of the moon's illumination) [77].
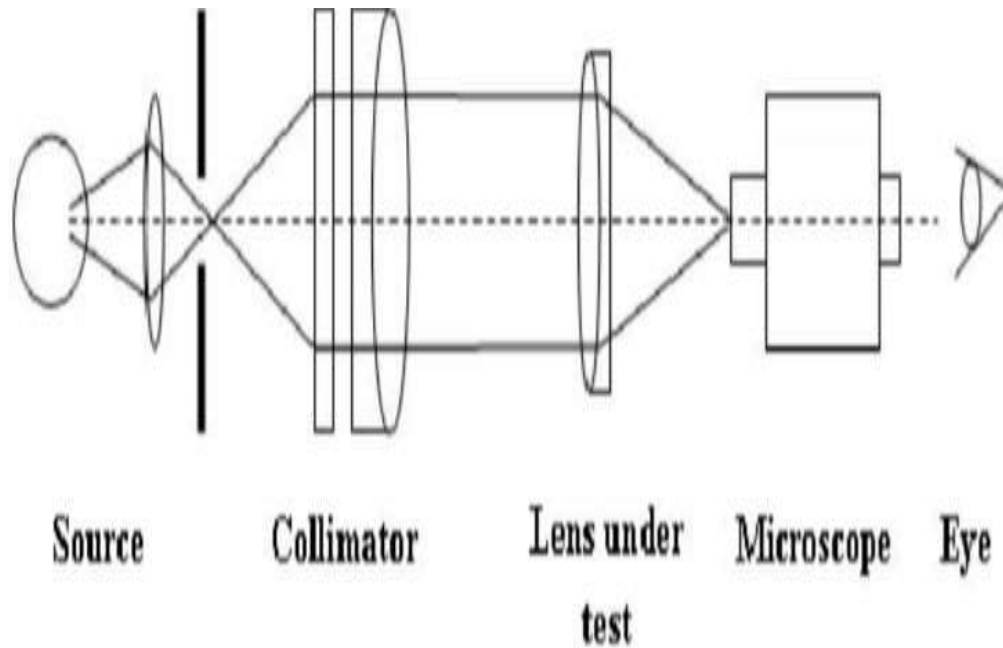
Fig. (2-2) star test [76]

2-4-2 Quantitative Examination

The Quantitative test is divided into two types:

2-4-2-1 Visual Examination Methods:

The visual test is based on the interference between the wavefronts coming from the under-checking lens when using an ideal single-wavelength wave from a point source.

The Twyman-Green interferometer is simply a Michelson interferometer with a few differences, as illustrated in figure (2-3).
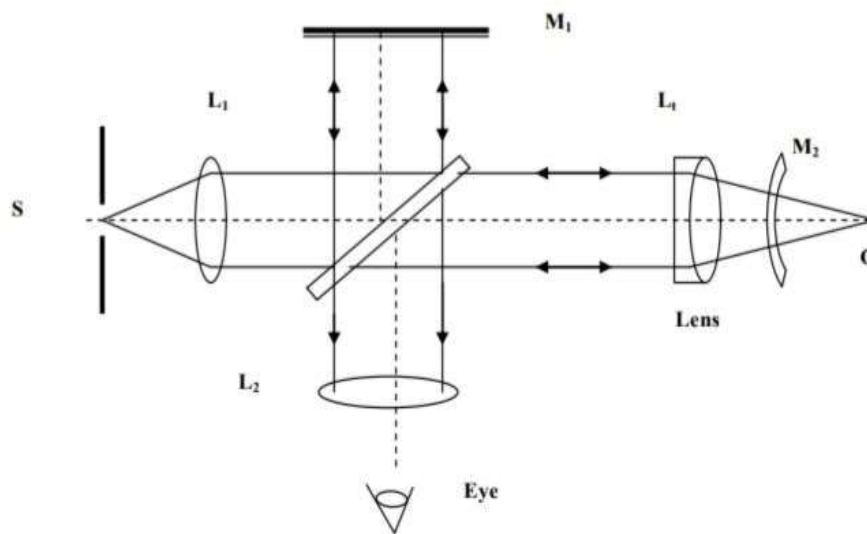
Twyman-Green interferometer [76].   ((2-3 Fig.

The principle of operation of this scale is based on the interference

of the two waves, one of which is reflected from the mirror, M1, which is

usually flat, and the other is reflected from the mirror, M2, and this is

done after the rays pass twice through the under examining lens. If the

lens used is perfect, the front of the wave reflected from M2 will be flat,

and thus the resulting fringe will be homogeneous and straight in shape.

As a result, the shape of the fringes determined if the lens contains

aberration or not [66,76].

2-4-2-2 The Photometer Examination

This type of evaluation is based on the definition of spread

functions. Many spread functions are calculated like the Point spread

function, Line spread function (simulated for linear objects that are

composed of an infinite number of bright points), Ellipse spread function,

Disk spread function, and Bar spread function are calculated to a specific

case of the optical system and shape of the detected objects [58,78–82].

This kind of evaluation provides a good description of the intensity
distribution in the image plane that results from an object by the optical
system under investigation.

The spread function is determined by the aperture lens diffraction
as well as the type of aberrations present in the lens or optical
components.

Such functions characterize the image quality of the optical system
under investigation [62,71]

2-5 Depth of Focus

Thus, the depth of focus can be defined as the ability of the lens to
maintain the sharpness of the image and its clarity and what is adjacent
to it [83].

 It is considered one of the most important conditions in how to
judge whether the formed image is good or not. In general, the depth of
focus (DoF) of the intensity distribution of the formed image which is
produced by an optical system gives good information and details for the
acceptance of the results of such an optical system.

The simplest example to make the concept of depth of focus clear
and understandable is an image, which is formed to an object located in a
place, where the image of the object is clear while the background of the
object weak and the rest of the details are blurred. This is because the
image was taken with a sharp depth of focus. While, for the same object
if the image shows all the details of the scene and all the image is clearly
defined for the object and its surroundings, which means the background
of the object, this is because the captured image was with a wide depth
of focus.

Also, the less the distance between the object and the lens aperture, weak, the object becomes closer to the imaging device, weak more the background of the object becomes less clear and more blurred, that is, it becomes out of focus, unlike the clear object.

Also, when the aperture is small, the greater the depth of focus, so the image is clear with all its details (object and background) and vice versa [84,85]

2-6 Resolving Power

Resolving power (RP) can be described as the possibility of any optical system or the ability of the eye to distinguish or separate the two images of two bright and adjacent points or the separation between two images of two lines[65].

The first which describes the ability of analysis and set a standard for it is Rayleigh [64].

One of the most important physical laws that have a great and important impact on daily life is related to describing the extent of the eye's ability to separate and distinguish between any two sources far from the eye, close to each other, and not consistent.

Thus, the analysis ability can be relied upon in determining the quality and efficiency of any optical system.

So Rayleigh's criterion was as the following: in the case in which the central light point of the image of one of the two stars is located on the first dark ring of the other star. This means that both images will be within the limits of distinction, separation or analysis, as in the following figure (2-4) [64,86–88]:
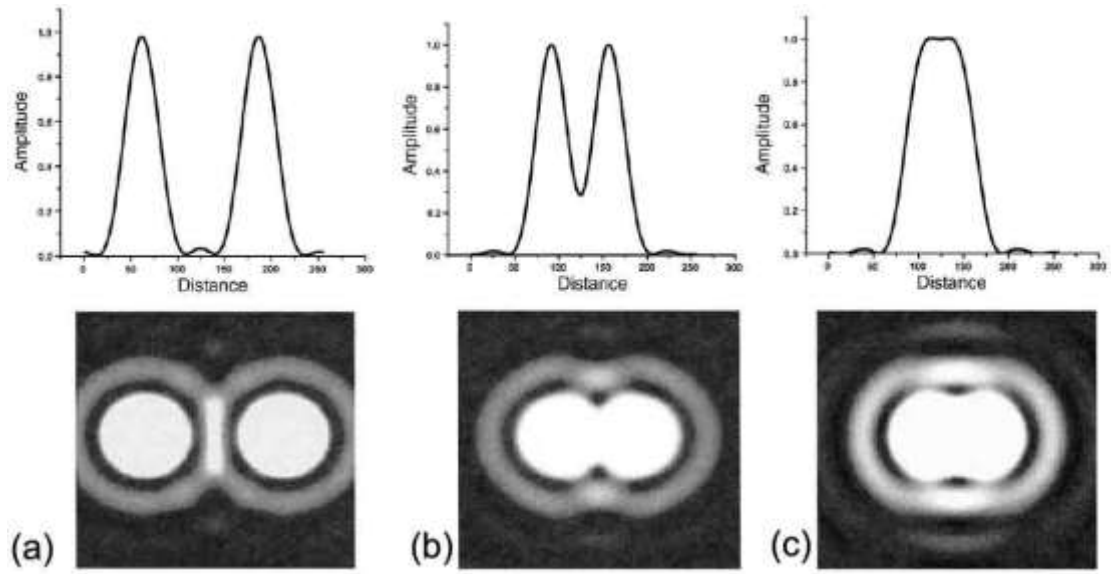
Fig. (2-4) Resolving Power (a) fully resolved. (b) just resolved. (c) unresolved [89].

Chapter Three

Rectangular Spread Function

3-1 Introduction

Measuring image resolution has been a difficult process, so when evaluating the performance of any optical imaging system used, it is necessary to consider the system's response to the nature of the object and the conditions of the environment in which the object is to be imaged and the location at which it is located [90].

Image resolution and clarity are a measure of image quality, so images with high resolution and high contrast in particular will be easier to distinguish the detected object visually with high accuracy and its surroundings in the observation environment. While the image has a low resolution, the process of identifying and distinguishing the object is limited.

As for the used methods in the image enhancement process, all methods have been aimed to increase the clarity of the details in the image by increasing the intensity and the resolution of the image. As mentioned earlier, there are many methods used in the process of improving image quality, and among these methods, the most important and most widely used are the spread functions. Where the spread functions are one of the most important tools used to determine the quality of the detected image and the efficiency of the optical system. In general, it can be said that the process of evaluating the performance and efficiency of any optical system is done through the use of certain functions, and The spread functions are interesting in evaluating the intensity distribution of images at image plane for a specific shape of the object [91–93].

3-2 Point Spread Function

The spread point function (PSF) is the optimal measure used in testing and evaluating optical systems, so the adopted measure to know the efficiency of optical systems becomes a very important role in the process of developing the methods used in data processing to the best possible. [93,94]. It is known that the resulting image of any point source is not, in fact, a point image, but it is in the form of a spot of light distributed over a specific area of the image plane. This is called the point spread function (PSF) [43,95]. The point spread function depends on the diffraction resulting from the used aperture and aberrations contain in the optical system [68].

The point spread function, which has other names, such as impulse response, Green function, and the Fraunhofer diffraction pattern, is a characteristic of the system under test [62]. When the system does not contain any aberration, the image of a bright point appears as a finite disk of intensity distribution surrounded by a series of weak diffraction rings; only the first is usually bright enough to be visible. This phenomenon was early expanded by Airy [96].

To estimate and calculate the intensity distribution in the image plane for a point source, suppose that an optical system contains a lens forming an image for a point source. It is known that all optical systems have an aperture placed somewhere in the optical system, where the image of this aperture is at the object space called (Entrance pupil) and in the image space called (Exit pupil) [97].

As it is known that the image cannot be perfectly formed unless the lens used is perfect and capable of accurately reproducing the object. The reason for the failure of the used lens to achieve such perfection is due to both the diffraction phenomenon that occurs by the aperture and the aberrations. The Point Spread Function (PSF) of a lens is the image of a point source object created by an optical system, or it is the distribution of intensity in the image plane of a point object using different apertures. The complex amplitude in the image plane of a point source located

at the origin (0, 0) in the object plane is given by [98]:

$$(3\text{-}1) F(u', v') = \iint_{-\infty}^{+\infty} f(x, y) . e^{i2\pi(u'x + v'y)} dx dy$$

f(x, y) is the pupil function, which is finite within the used aperture and

equal to:

$$f(x, y) = \tau(x, y) e^{ikw(x,y)} \ for \ inside \ aperture \ f(x, y)$$
$$= 0 \qquad for \ outside \ aperture$$

Where: K is the wave number and equal to $(2\pi/\lambda)$, and λ is the wavelength of the applied source. w(x,y) is the aberration function .τ represents the transparency of the pupil and is equal to one for the uniform aperture.

As a result, the integral's limits -∞ to +∞ are limited by the finite extent of the used aperture.

The image profile's intensity is derived by multiplying F(u', v') with the complex conjugate F*(u', v') as follows:

$$G (u', v') = F (u', v') . F^*(u', v') \qquad\qquad (3\text{-}2)$$

The image intensity of a point source located at the point (0, 0) in the

image plane is given by:

$$(3\text{-}3)\, G\,(u',v')\ =\ |F(u',v')|^2$$

Or:

$$(3\text{-}4)\, G(u^{\backslash},v^{\backslash}) = \left| \int_y \quad \int_x \quad f(x,y)\cdot e^{i2\pi(u^{\backslash}x+v^{\backslash}y)}dxdy \right|^2$$

Assuming that $z^{\backslash} = 2\pi u^{\backslash},\, m^{\backslash} = 2\pi v^{\backslash}$, thus, eq. (3-4) can be written as:

$$(3\text{-}5)\, G(z^{\backslash},m^{\backslash}) = \left| \int_y \quad \int_x \quad f(x,y)\cdot e^{i(z^{\backslash}x+m^{\backslash}y)}dxdy \right|^2$$

Or:

$$G(z^{\backslash},m^{\backslash}) = \int_y \quad \int_{y_1} \quad \int_x \quad \int_{x_1} \quad f(x,y)\cdot e^{i(z^{\backslash}x+m^{\backslash}y)}f^*(x_1,y_1)\cdot$$
$$e^{-i(z^{\backslash}x_1+m^{\backslash}y_1)}dx_1dxdy_1dy$$

(3-6)

Equation 3-6 represents the point spread function.

3-3 Rectangular Spread Function (RSF)

In this study, a new spread function was considered for rectangular objects which are similar in shape to different cars, known as the rectangular spread function (**RSF**).

Rectangular objects were chosen because such objects are common in military applications for surveillance and border security. This function is used to study the image intensity distribution in the image plane of an optical system operating using an optical aperture of different shapes.

Rectangular objects are two-dimensional objects consisting of two dimensions of length and width represented by the dimensions of cars (A, B) that contain infinite point sources of non-homogeneous illumination.

Since the rectangular object has a two-dimensional axis (A, B) and contains unlimited incoherent point sources, thus, by making the double-dimensional integral of the point spread function and multiplying with the intensity function of the rectangular object, the intensity distribution equation for the rectangular image (rectangular spread function) is produced as follows:

$$(3\text{-}7) R\big(z^{\backslash}, m^{\backslash}\big) = \int_{-\infty}^{\infty} \int_{-\infty}^{\infty} R(z,m).\,G\big(z^{\backslash} - z, m^{\backslash} - m\big) dz\,dm$$

Where (z,m) and (z$^{\backslash}$,m$^{\backslash}$) are the dimensionless coordinates in the object and image, respectively. R(z,m) is the distribution spectrum of the rectangular object, G(z$^{\backslash}$-z,m$^{\backslash}$-m) represents the point spread function resulting from a single source at the rectangular object.

From eq. (3-6) we can write:

$$G(z^{\backslash} - z, m^{\backslash} - m) = \int_y \quad \int_{y_1} \quad \int_x \quad \int_{x_1} \quad f(x,y).\,f^*(x_1, y_1) \cdot$$
$$(3\text{-}8) e^{i(z^{\backslash} - z)(x - x_1)} . \qquad\qquad e^{i(m^{\backslash} - m)(y - y_1)} dx_1\,dx\,dy_1\,dy$$

By substituting eq. 3-8 in eq.3-7 we get:

$$R\big(z^{\backslash}, m^{\backslash}\big) =$$
$$\int_{-\infty}^{\infty} \quad \int_{-\infty}^{\infty} \quad \int_y \quad \int_{y_1} \quad \int_x \quad \int_{x_1} \quad R(z,m).\,f(x,y).\,f^*(x_1, y_1) \cdot$$
$$(3\text{-}9) \; e^{i(z^{\backslash} - z)(x - x_1)} . e^{i(m^{\backslash} - m)(y - y_1)} dx_1\,dx\,dy_1\,dy\,dz\,dm$$

The distribution spectrum of the rectangular object is determined by the following conditions:

$$R(z,m) = 1 \, for \; \{z \; or \; m \qquad \leq A \; z \; or \; m$$
$$\leq B \,\} R(z,m)$$
$$= 0 \, for \; \{z \; or \; m \qquad > A \; z \; or \; m \qquad > B \,\}$$

Where A and B are the main axes of the rectangular object, so

equation (3-9) becomes:

$$R\left(z^{\backslash}, m^{\backslash}\right)$$

$$= \int_{y} \int_{y_1} \int_{x} \int_{x_1} f(x,y) . f^*(x_1, y_1) . e^{iz^{\backslash}(x-x_1)} . e^{im^{\backslash}(y-y_1)} dx_1 dx dy_1 dy$$

$$(3\text{-}10) \int_{-A}^{+A} e^{-iz(x-x_1)} dz \int_{-B}^{+B} e^{-im(y-y_1)} dm$$

Using Mathematical relation, the last two integrals in equation 3-10

are equal to [81]:

$$\int_{-A}^{+A} e^{-iz(x-x_1)} dz = \frac{sinsin\,[(x-x_1)A]}{(x-x_1)} \qquad (3\text{-}11)$$

$$\int_{-B}^{+B} e^{-im(y-y_1)} dm = \frac{sinsin\,[(y-y_1)B]}{(y-y_1)} \qquad (\,3\text{-}12)$$

From equations 3-10, 3-11, and 3-12, the rectangular spread function can

be expressed as:

$$R\left(z^{\backslash}, m^{\backslash}\right) =$$

$$\int_{y} \int_{y_1} \int_{x} \int_{x_1} f(x,y) . f^*(x_1, y_1) . e^{iz^{\backslash}(x-x_1)} . e^{im^{\backslash}(y-y_1)} \frac{sin\,sin\,[(x-x_1)A]}{(x-x_1)} . \frac{sin\,sin\,[(y-y_1)}{(y-y_1)}$$

$$(3\text{-}13)$$

Since the intensity distribution on the image level is symmetrical,

therefore, only one coordinate is taken (z$^{\backslash}$), so the coordinate (m$^{\backslash}$) assume

to be equal to zero, and after substituting the values of the functions (f, f^*)

in the equation 3-13, it results:

$$R\left(z^{\backslash}\right) =$$

$$\int_{y} \int_{y_1} \int_{x} \int_{x_1} e^{iz^{\backslash}(x-x_1)+ikw(x,y)-ikw(x_1,y_1)} \frac{sin\,sin\,[(x-x_1)A]}{(x-x_1)} . \frac{sin\,sin\,[(y-y_1)B]}{(y-y_1)} dx_1 dx$$

Where:

$$e^{iz^{\backslash}(x-x_1)+ikw(x,y)-ikw(x_1,y_1)}$$

$$=cos\,cos\,\{z^{\backslash}(x-x_1)+kw(x,y)-kw(x_1,y_1)\}+i$$
$$sin\,sin\,\{z^{\backslash}(x-x_1)+kw(x,y)-kw(x_1,y_1)\}$$

Since the intensity is real, therefore the imaginary part of the above equation must be equal to zero, thus [81]:

$$R(z^{\backslash})$$
$$=N\int_y\;\int_{y_1}\;\int_x\;\int_{x_1}$$
$$cos\,cos\,\{k[w(x,y)-w(x_1,y_1)]$$
$$+z'(x-x_1)\}.\frac{sin\,sin\,[(x-x_1)A]}{(x-x_1)}\cdot\frac{sin\,sin\,[(y-y_1)B]}{(y-y_1)}dx_1dxdy_1dy$$

(3-14)

If $w(x,y)$=0 and $w(x_1,y_1)=0$ for an ideal system, the last equation becomes:

$$R(z^{\backslash})=N\int_y\;\int_{y_1}\;\int_x\;\int_{x_1}\;cos\,cos\,\{z'(x-$$
$$x_1)\}.\frac{sinsin\,[(x-x_1)A]}{(x-x_1)}\cdot\frac{sinsin\,[(y-y_1)B]}{(y-y_1)}dx_1dxdy_1dy$$

(3-15)

The last equation (3-15) represents the final formula of the rectangular spread function (RSF). A and B: represent the length and width of the rectangle object.

(N): is the normalized factor whose value can calculated when z=0, and R(z$^{\backslash}$)=1, so:

$$1$$
$$=N\int_y\;\int_{y_1}\;\int_x\;\int_{x_1}\;\frac{sin\,sin\,[(x-x_1)A]}{(x-x_1)}\cdot\frac{sin\,sin\,[(y-y_1)B]}{(y-y_1)}dx_1dxdy_1dy$$

$$(3\text{-}16)$$

Or:

$$N = 1 / \left(\int_y \int_{y_1} \int_x \int_{x_1} \frac{\sin \sin\left[(x - x_1)A\right]}{(x - x_1)} \cdot \frac{\sin \sin\left[(y - y_1)B\right]}{(y - y_1)} dx_1 dx dy_1 dy \right)$$

$$(3\text{-}17)$$

The normalized factor will be calculated for each case of the aperture shape of the optical system in this work.

3-4 Estimation of the Length and Width (A, B) of the Rectangular Shape

To estimate the dimension (A, B), referring to the length and width of the rectangular objects, measurements of different sizes of the vehicle are performed in this work, where dimension (A) represents the average vehicle lengths and (B) represents the average vehicle width. Since the shape of vehicles can be estimated as a rectangular shape, many lengths and widths of different sizes of vehicles were taken. The measured vehicles are divided into three groups depending on the size, which are small-sized vehicles, medium-sized vehicles, and large-sized vehicles. As shown in table (3-1), the vehicles on which the study was theoretically conducted are small-sized vehicles.

Table (3-1) The average vehicle dimensions**.**

Type Vehicles	Average Length (m)	Average Width (m)
Small vehicles	3	1.6
Medium vehicles	4.3	1.8
Large vehicles	13.7	2.6

In the present study, the values of (3 and 1.6) were taken into account representing the dimensions (A, B), respectively. One can mention that just numbers of length and width of rectangular objects were included.

3-5 Different Aperture Shapes of the Optical System:

In this part of the work, the effect of the shape of used aperture in the optical system will be studied on the density distribution of the detected thermal image (image clarity). The shape of the used aperture in the optical system is one of the most important factors that greatly affect the intensity distribution in the plane of the captured image for all optical systems [99].

Different shapes of apertures are applied in this work. Circular, square, and triangular aperture shapes are chosen for the thermal system. For comparison, the same area, which is (π), was assumed for all shapes of the used apertures to study the effect of just changing the shape of the used aperture on the intensity distribution of the image.

The limits of the integration in the equation (3-15) represent the shape border of used aperture in the optical system to produce the thermal image. When the effect of the shape of the used optical aperture is involved, the equation of RSF of each optical aperture can be presented as the following:

1- **Circular Aperture**:

A circular aperture is considered one of the most widely used optical apertures compared to other optical apertures such as rectangular,

square, elliptical, or triangular apertures. Because of the characteristics of the image formed by the optical system that works using a circular aperture, it is commonly used in most optical devices. Many advantages of such aperture compared to other optical aperture shapes can be mentioned as the goodness at the case when used optical system suffers from diffraction. On the other hand, the circular optical aperture is free of sharp edges or corners, unlike other optical apertures such as square, triangle, and rectangular, which usually affect the intensity distribution of

detected image [100].

The limits of the integral of the rectangular spread function equation are determined through the circular aperture, which has a normalized area equal to (π) and a radius equal to (1). The limits of integrals can be included by calculating the distance to any point on the

circle, as shown in figure (3-1) [101]:

$$r^2 = x^2 + y^2$$

$$x^2 = r^2 - y^2$$

$$x = \mp\sqrt{r^2 - y^2}$$

$$r^2\pi = \pi$$

$$r^2 = 1$$

$$when\ r = \mp 1$$

$$x = \mp\sqrt{1 - y^2}$$
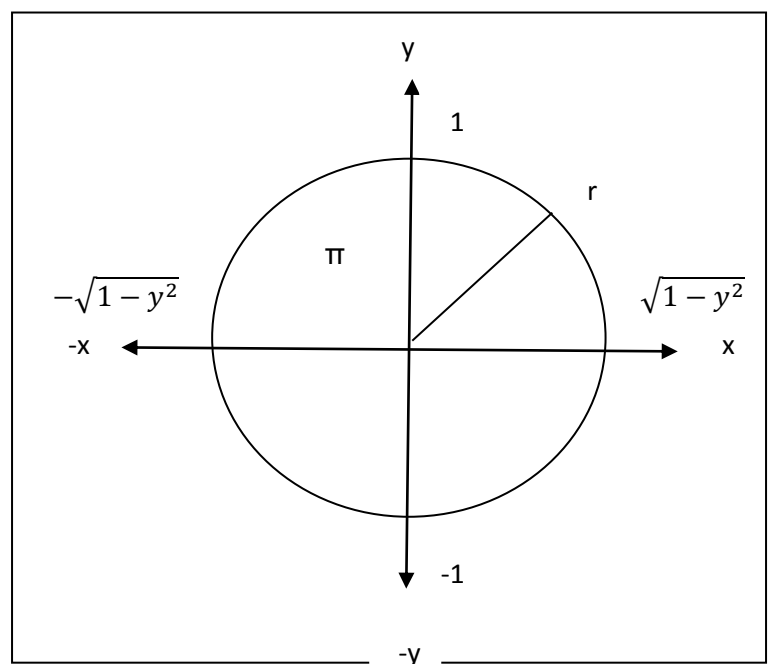
Fig. (3-1) Circular optical aperture

Thus, equation (3-15) can be written as the following:

$$R(z\backslash)$$

$$= N \int_{-1}^{1} \int_{-1}^{1} \int_{-\sqrt{1-y^2}}^{\sqrt{1-y^2}} \int_{-\sqrt{1-y_1^2}}^{\sqrt{1-y_1^2}}$$

$$cos \; cos \; z'(x$$

$$- x_1) \frac{sin \; sin \; [(x-x_1)A]}{(x-x_1)} \frac{sin \; sin \; [(y-y_1)B]}{(y-y_1)} dx_1 dx dy_1 dy$$

$$(3\text{-}18)$$

2- **Square Aperture**:

Another optical aperture that was used in this work is the square aperture. The limits of the integral of the rectangular spread function equation are determined via the square aperture that has a normalized area equal to (π) and a side length of ($\sqrt{\pi}$), The limits of the integral can be calculated through the following [101]:

$$Area = \pi = L^2$$

$$L = \mp\sqrt{\pi}$$

$$\frac{\sqrt{\pi}}{2}$$

$-x$ ←————————————————→ x

$$-\frac{\sqrt{\pi}}{2}$$

$-y$
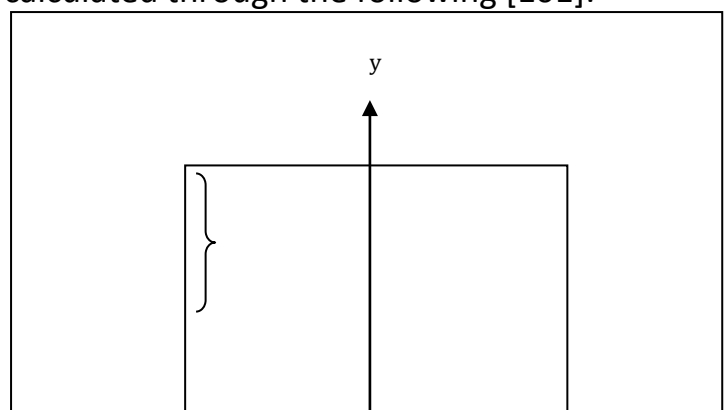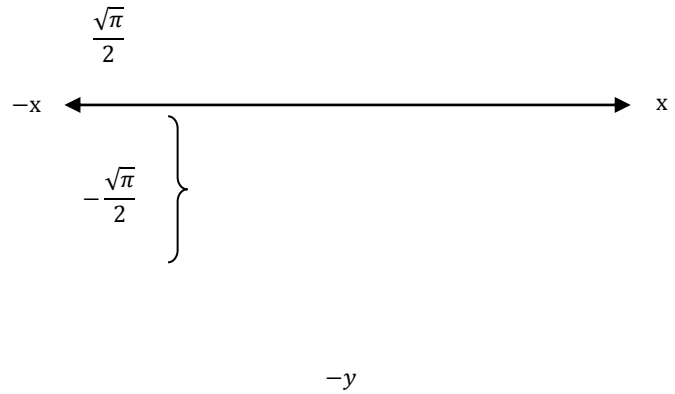
Fig. (3-2) Square optical aperture

Equation (3-15) can be written as the following:

$R(z\backslash)$

$$= N \int_{-\frac{\sqrt{\pi}}{2}}^{\frac{\sqrt{\pi}}{2}} \int_{-\frac{\sqrt{\pi}}{2}}^{\frac{\sqrt{\pi}}{2}} \int_{-\frac{\sqrt{\pi}}{2}}^{\frac{\sqrt{\pi}}{2}} \int_{-\frac{\sqrt{\pi}}{2}}^{\frac{\sqrt{\pi}}{2}}$$

$cos\, cos\, z'(x$

$$- x_1) \frac{sin\, sin\, [(x - x_1)A]}{(x - x_1)} \frac{sin\, sin\, [(y - y_1)B]}{(y - y_1)} dx_1 dx dy_1 dy$$

(3-19)

3- Triangular Aperture:

he third used aperture in this work is the triangular aperture. The limits of the integral in the equation of the rectangular spread function are determined by the equilateral triangular aperture that has a normalized area equal to (π) and the length of the horizontal side is (2x). So, the distance from the middle of the base to the top is (2y). Based on this, the area of the triangle is A = 2xy=π. Since the triangular optical

43

aperture taken in this work is equilateral, the angles of the triangle will be equal to (60°), so that [101]:

$$\tan\theta = \frac{2y}{x} = \tan(60) = \sqrt{3}$$

So: $y = \frac{\sqrt{3}}{2}x$

Area=2xy=π

So: $x = \frac{\pi}{2y}$
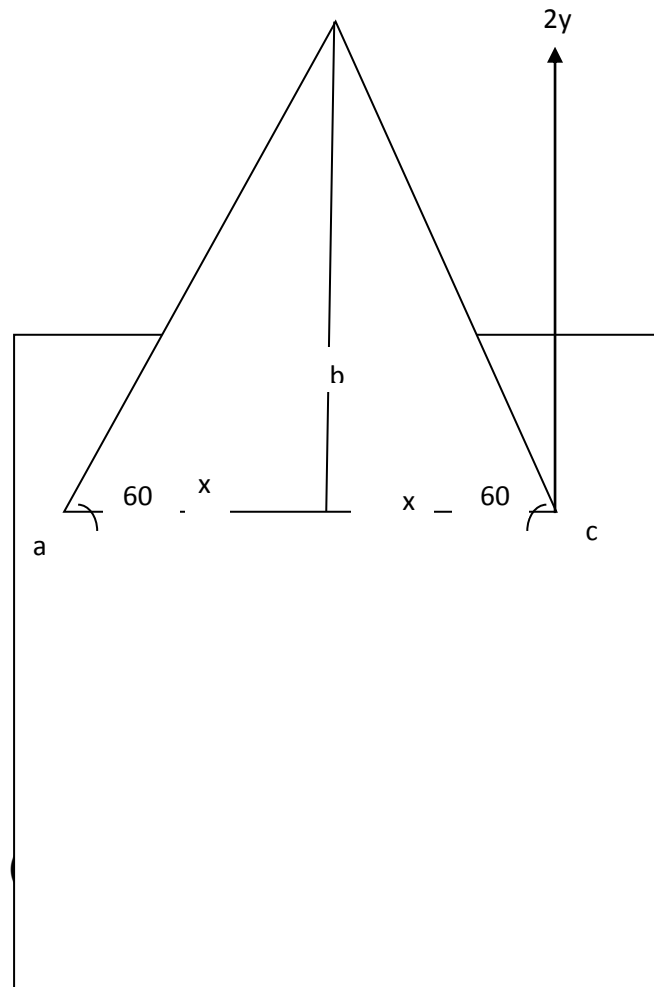
$$y = \mp 1.166$$

From the equation of the line (

$$y = \mp 1.166$$

$$x = \frac{y - 1.166}{\sqrt{3}}$$

Therefore, equation (3-15) can be written as:

$$R(z\backslash)$$

$$= N \int_{-1.166}^{1.166} \int_{-1.166}^{1.166} \int_{-\frac{y-1.166}{\sqrt{3}}}^{\frac{y-1.166}{\sqrt{3}}} \int_{-\frac{y_1-1.166}{\sqrt{3}}}^{\frac{y_1-1.166}{\sqrt{3}}}$$

$$cos\ cos\ z'(x$$

$$- x_1) \frac{sin\ sin\ [(x - x_1)A]}{(x - x_1)} \frac{sin\ sin\ [(y - y_1)B]}{(y - y_1)} dx_1 dx dy_1 dy$$

44

$$(3\text{-}20)$$

The Effect of the Distance Factor on the Rectangular   3-6

Spread Function:

The distance factor or the distance between the observer and the observing object, which is represented by the thermal camera and target, represents an important factor that is investigated in this work. Effects of such a parameter on the density distribution in the detected thermal image required to identify the object.

When the influence of this factor is involved in the equation (3-15),

the RSF equation can be defined as:

RSF equation for Circular Aperture: -A

$$R(z\backslash)$$

$$= N \int_{-1}^{1} \int_{-1}^{1} \int_{-\sqrt{1-y^2}}^{\sqrt{1-y^2}} \int_{-\sqrt{1-y_1^2}}^{\sqrt{1-y_1^2}}$$

$$\cos \cos z'(x$$

$$- x_1) \frac{\sin \sin [(x-x_1)A]}{(x-x_1)} \frac{\sin \sin [(y-y_1)B]}{(y-y_1)} \frac{\sin \sin (\pi R(x-y))}{\pi R(x-y)} dx_1 dx dy_1 dy$$

$$(3\text{-}21)$$

RSF equation for Square Aperture: -B

$$R(z\backslash)$$

$$= N \int_{-\frac{\sqrt{\pi}}{2}}^{\frac{\sqrt{\pi}}{2}} \int_{-\frac{\sqrt{\pi}}{2}}^{\frac{\sqrt{\pi}}{2}} \int_{-\frac{\sqrt{\pi}}{2}}^{\frac{\sqrt{\pi}}{2}} \int_{-\frac{\sqrt{\pi}}{2}}^{\frac{\sqrt{\pi}}{2}}$$

$$\cos \cos z'(x$$

$$- x_1) \frac{\sin \sin [(x-x_1)A]}{(x-x_1)} \frac{\sin \sin [(y-y_1)B]}{(y-y_1)} \frac{\sin \sin (\pi R(x-y))}{\pi R(x-y)} dx_1 dx dy_1 dy$$

(3-22)

RSF equation for Triangular Aperture: -C

$$R(z\backslash) =$$

$$N \int_{-1.166}^{1.166} \int_{-1.166}^{1.166} \int_{-\frac{y-1.166}{\sqrt{3}}}^{\frac{y-1.166}{\sqrt{3}}} \int_{-\frac{y_1-1.166}{\sqrt{3}}}^{\frac{y_1-1.166}{\sqrt{3}}}$$

$$cos\, cos\, z'(x - x_1) \frac{sin\, sin\, [(x-x_1)A]}{(x-x_1)} \frac{sin\, sin\, [(y-y_1)B]}{(y-y_1)} \frac{sin\, sin\, (\pi R(x-y))}{\pi R(x-y)} dx_1 dx dy_1 dy$$

(3-23)

R: is the distance between the camera and the target (Vehicle).

3-7 The Effect of the Linear Motion Factor on the Rectangular Spread Function:

The efficiency of a thermal camera depends mainly on the accuracy of the captured thermal image or the ability to detect and identify the target. The situation of moving objects at different speeds is considered one of the most important factors that affect the intensity distribution in the thermal image. The linear movement of targets and the distance between the thermal camera and the target affect the accuracy of the detected thermal images significantly.

In this work, a theoretical calculation of the effect of the linear motion of the objects represented by the vehicles on the intensity distribution in the thermal image detected by the thermal camera. The effect of the linear motion was studied by including a part of the linear motion in the RSF equation, where the intensity distribution of the detected thermal

image is determined, and thus, the quality of the thermal image is determined. The linear motion factor part can be presented as [58,102]:

$$(3\text{-}24)L = \frac{t_e v_i}{\lambda F^{\neq}}$$

Where L: is the linear motion factor.

Is the snapshot time for the used thermal camera equal to ($t_e = t_e$:

$$\frac{1}{25} \; sec).$$

λ: The used infrared wavelength, which is for the used thermal camera is

$$\lambda = 10\mu m.$$

is the optical system focal number, which for the used thermal $F^{\neq}$:

camera is equal to 18.

: is the lens focal length of the thermal camera and it is equal to 36 mm.f

v_i : is the image motion and can be found from the following relationship:

$$\text{or } v_i = \frac{f \, v_0}{R} \quad \frac{v_0}{v_i} = \frac{R}{f}$$

Where:

: is the speed of the object's motion and was determined for a moving v_0

target at a different speed in this research.

R: is the distance of the target from the camera.

Including the effect of linear motion factor (L) into the RSF equation, three different equations will appear depending on the type of the used aperture as follows:

RSF equation for Circular Aperture: -A

$R(z\backslash)$

$$= N \int_{-1}^{1} \int_{-1}^{1} \int_{-\sqrt{1-y^2}}^{\sqrt{1-y^2}} \int_{-\sqrt{1-y_1^2}}^{\sqrt{1-y_1^2}}$$

$\cos \cos z'(x$

$$- x_1) \frac{\sin \sin [(x-x_1)A]}{(x-x_1)} \frac{\sin \sin [(y-y_1)B]}{(y-y_1)} \frac{\sin \sin (\pi L(x-y))}{\pi L(x-y)} dx_1 dx dy_1 dy$$

$$(3\text{-}25)$$

RSF equation for Square Aperture: -B

$R(z\backslash)$

$$= N \int_{-\frac{\sqrt{\pi}}{2}}^{\frac{\sqrt{\pi}}{2}} \int_{-\frac{\sqrt{\pi}}{2}}^{\frac{\sqrt{\pi}}{2}} \int_{-\frac{\sqrt{\pi}}{2}}^{\frac{\sqrt{\pi}}{2}} \int_{-\frac{\sqrt{\pi}}{2}}^{\frac{\sqrt{\pi}}{2}}$$

$\cos \cos z'(x$

$$- x_1) \frac{\sin \sin [(x-x_1)A]}{(x-x_1)} \frac{\sin \sin [(y-y_1)B]}{(y-y_1)} \frac{\sin \sin (\pi L(x-y))}{\pi L(x-y)} dx_1 dx dy_1 dy$$

$$(3\text{-}26)$$

RSF equation for Triangular Aperture: -C

$$R(z\backslash) =$$

$$N \int_{-1.166}^{1.166} \int_{-1.166}^{1.166} \int_{-\frac{y-1.166}{\sqrt{3}}}^{\frac{y-1.166}{\sqrt{3}}} \int_{-\frac{y_1-1.166}{\sqrt{3}}}^{\frac{y_1-1.166}{\sqrt{3}}}$$

$\cos \cos z'(x$

$$- x_1) \frac{\sin \sin [(x-x_1)A]}{(x-x_1)} \frac{\sin \sin [(y-y_1)B]}{(y-y_1)} \frac{\sin \sin (\pi L(x-y))}{\pi L(x-y)} dx_1 dx dy_1 dy$$

$$(3\text{-}27)$$

Effect of Optical Filter on the Rectangular Spread   3-8

Function) RSF):

The optical filter is considered one of the most important methods used to improve the efficiency of optical devices. Such an effect leads to an increase in the resolution of the image produced by optical systems and thus, an increase in the distance of recognizing targets. Various types of optical filters have been used to improve the efficiency of optical systems. These optical filters such as Hanning filters [103,104], amplitude filters [105], Hamming Amplitude Filter [106], the parabolic optical filter [107,108], Complex Pupil Filters [109], and the Gaussian filter [110]. All of these filters work to improve the accuracy of the detected image to distinguish the target more accurately and not just discover it.

In this work, the optical filter (Parabolic Filter) was used, which concentrates the thermal photons, that come from the targets, in the form of a Parabolic shape. The expression equation of the parabolic filter is [108]:

(3-28) $f(r) = (\alpha + \beta r)^N$

Where: represents the filter power order and is equal to N=1, 2, …...

: is a numerical constant. α

: represents the apodization parameter and indicates the degree of non- β uniformity of pupil transmission.

r : filter coordinates.

So, equation (3-15) will be in the following form when the effect of the optical filter factor is included for the circle apertures:

RSF equation for Circular Aperture:

$$R(z\backslash) =$$

$$N \int_{-1}^{1} \int_{-1}^{1} \int_{-\sqrt{1-y^2}}^{\sqrt{1-y^2}} \int_{-\sqrt{1-y_1^2}}^{\sqrt{1-y_1^2}} \cos\cos z'(x -$$

$$x_1) \frac{\sin\sin [(x-x_1)A]}{(x-x_1)} \frac{\sin\sin [(y-y_1)B]}{(y-y_1)} [(\alpha + \beta(x^2 +$$

$$y^2)^N] \, dx_1 dx dy_1 dy$$

$$(3\text{-}29)$$

3-9 The Effect of Attenuation Factor on the Rectangular Spread Function

Attenuation of the incoming thermal radiation to the camera detector is another factor that is investigated in this section. This attenuation is caused by the dust particles that are contained in the environment of the detection. The attenuation represents one of the most important factors affecting negatively the intensity distribution of the detected thermal image. It leads some time to completely distorted the detected thermal image [111].

In this part, we will study the effect of circular, square, and triangular optical apertures on the thermal image captured in an environment containing different percentages of these particles to improve the thermal image.

The equation of the rectangular spread function with the effect of the attenuation factor is introduced by going through a series of physical equations. The empirical expression used to calculate atmospheric attenuation is given by the following equation [112,113]:

$$(3\text{-}30) \quad \tau_s = exp\left[\left(\frac{-3.91}{V}\right)\left(\frac{\lambda}{0.55}\right)^{-q} \times R\right]$$

Where:

τ_s: is the transition

λ: is the wavelength of IR.

R: is the distance range.

V: is the visibility.

q: is a number, that depends on the size distribution of scattering particles or the visibility. The value of q can determine as: when the visibility range is 0.5(km) <V<1(km), the value of q=V -0.5, and if V is V<0.5 (km), the value of q is zero.

The Visibility values can be calculated using the following equation [112,113]:

$$V = 7080 \times C^{-0.8} \qquad (3\text{-}31)$$

Where **C** is the concentration of particles. The concentration (**C**) of the particulate matter, PM, equal to (10, 20, 30, 40, 50) µg/m³, which is recorded by the meteorological station in Ain al-Tamer area, Kerbala city.

After extracting values of (**V**) for each concentration, they are substituted into the equation (3-30) to calculate the values of (**τₛ**) for each case. The absorbance is calculated for each value (**τₛ**) as the following [113,114]

$$(3\text{-}32) \qquad\qquad A = 2 - log_{10}(\tau s\%)$$

Where: A is the absorption of IR at the wavelength of 10 µm. Thus, the equation of RSF (3-15), after including the effect of the absorbance factor, becomes as the following for different optical apertures:

A-Optical system working using a circular

aperture:

$$R(z\backslash) =$$

$$N \int_{-1}^{1} \int_{-1}^{1} \int_{-\sqrt{1-y^2}}^{\sqrt{1-y^2}} \int_{-\sqrt{1-y_1^2}}^{\sqrt{1-y_1^2}}$$

$$\cos \cos z'(x$$

$$- x_1) \frac{\sin \sin [(x - x_1)A]}{(x - x_1)} \frac{\sin \sin [(y - y_1)B]}{(y - y_1)} \frac{\sin \sin (\pi Abs(x - y))}{\pi Abs(x - y)} dx_1 dx dy_1 dy$$

$$(3\text{-}33)$$

B-Optical system working using square aperture:

$$R(z\backslash) =$$

$$N \int_{-\frac{\sqrt{\pi}}{2}}^{\frac{\sqrt{\pi}}{2}} \int_{-\frac{\sqrt{\pi}}{2}}^{\frac{\sqrt{\pi}}{2}} \int_{-\frac{\sqrt{\pi}}{2}}^{\frac{\sqrt{\pi}}{2}} \int_{-\frac{\sqrt{\pi}}{2}}^{\frac{\sqrt{\pi}}{2}}$$

$$\cos \cos z'(x$$

$$- x_1) \frac{\sin \sin [(x - x_1)A]}{(x - x_1)} \frac{\sin \sin [(y - y_1)B]}{(y - y_1)} \frac{\sin \sin (\pi Abs(x - y))}{\pi Abs(x - y)} dx_1 dx dy_1 dy$$

$$(3\text{-}34)$$

C-Optical system working using triangular aperture:

$$R(z\backslash) =$$

$$N \int_{-1.166}^{1.166} \int_{-1.166}^{1.166} \int_{-\frac{y-1.166}{\sqrt{3}}}^{\frac{y-1.166}{\sqrt{3}}} \int_{-\frac{y_1-1.166}{\sqrt{3}}}^{\frac{y_1-1.166}{\sqrt{3}}}$$

$$\cos \cos z'(x$$

$$- x_1) \frac{\square\square\square \sin [(x - x_1)A]}{(x - x_1)} \frac{\sin \sin [(y - y_1)B]}{(y - y_1)} \frac{\sin \sin (\pi Abs(x - y))}{\pi Abs(x - y)} dx_1 dx dy_1 dy$$

$$(3\text{-}35)$$

Characteristics of the used Thermal Camera   3-10

(PT-602CZ HD):

The type of thermal camera that was studied theoretically in this

work is the PT-602CZ HD camera. This type of camera is considered one

of the most advanced security systems that are equipped with advanced

dual sensors. It has the advantage to combine a visible-light imaging

sensor and a thermal sensor. It is also able to track a moving system high

speed with wide ranges. This type of thermal camera has many special

characteristics that make it widely used in many applications and for

different purposes. Especially for surveillance purposes in completely dark

or bright environments or bad weather conditions. There are many other

properties of such cameras making them very attractive for use in

different applications. These characteristics can summarize the most

important of them:

1-PT-602CZ HD Thermal Security Camera works in the detection

range from 3000m to 3300m.

2 - The PT-602CZ HD camera has a high sensitivity, so it works in

broad daylight and at night when it is completely dark.

3 - PT-602CZ HD produces high-resolution thermal images through

which the target can be detected in all weather conditions in the

environment in which the target is located, compared to other types of

cameras.

4 - The PT-602CZ HD camera is equipped with a high-precision

infrared detector operating in the (3-5) μm and (8-14) μm wavelength

range. This detector helps users to detect all objects in the image, so the

product image is of high efficiency.

5 - This type of thermal imaging camera is equipped with an

advanced optical zoom, where the optical zoom is considered one of the

best zoom methods because it gives clear and real results with the best

possible accuracy. So, zoom helps through the use of a series of lenses elements by moving these lenses to zoom in or out. This technique provides an excellent field of view allowing the ability to get more accurate images.

6 - The PT-602CZ HD camera can be used with the other cameras as a collection system or it can be used as a stand-alone monitoring unit.

7- The PT-602CZ HD thermal camera comes equipped with an advanced and accurate pan/tilt mechanism, allowing the user to freely rotate the camera 360 degrees. This feature helps to scan the area widely.

8- The PT-602CZ HD camera can be connected to the radar system.

In this unit system operation, if the radar detects an object, the PT-602CZ HD will automatically turn in the right direction and give a good recognition so that it will be a unique system with radar.

In the present model of the PT-602CZ HD camera, many parameters are included in the RSF to stimulate the intensity distribution of the detected object. These parameters are:

- The focal length of the lens is 36 mm.
- The focal number is 18.
- snapshot time of each captured snapshot is 0.04 sec.
- The used infrared wavelength, which is for the used thermal camera is $\lambda = 10\mu m$.

Note: All the features of the camera that we mentioned here were taken from the catalog of the camera provided by the manufacturer, make: FLIR Systems.

Fig. (3-4) The PT-602CZ HD camera

Zone of Study: 3-11

The study area that was chosen in this work is the Ain Al-Tamr area located west of Karbala Governorate, where this area was chosen based on the multiple military operations that terrorists and infiltrators are exposed to. The importance of thermal imaging technology appears here in detection to counter attacks surprise by the terrorist. So, the information provided by the thermal imaging cameras is employed to monitor the enemy's military targets, which is very important in this area of the city of Kerbala.

In this area, there are several thermal cameras installed in different places. A study is being done to improve the efficiency of thermal imaging devices by using different aperture shapes and by using a filter on the thermal image for different cases.

This area also suffers from many environmental cases (dust), which negatively affect the performance of these cameras during the monitoring process. The effect of different concentrations of particles on the clarity of the detected image was studied when it is (10, 20, 30, 40, 50) µg/m^3 which was recorded by the Iraqi Meteorological Organization located in Ain Al-Tamr   area   of   the   holy   city   of   Karbala   in 2021 [56].

Chapter Four

Results and Discussion

4-1 Introduction

This chapter includes the results obtained by solving the rectangular spread function equation for diffraction limit system. The effects of different parameters were taken into the calculations, such as the distance factor in which vehicles are located and whether vehicles don't move or move linearly. Moreover, the linear motion factor of the rectangular objects represented by the vehicle is investigated, and the effect of the filter on the optical system that is working with the thermal range of wavelength is considered. Finally, the effect of the attenuation factor is represented by the dust particles with different concentrations. All the previous parameters or effects are included in the rectangle spread function (RSF) equation to calculate the intensity distribution of the detected thermal images for each case. All work-related calculations were made using infrared wavelength (10 μm) and in the Ain Al-Tamr area of Kerbala city for the thermal camera (PT-602CZ HD). All results in this work are performed via programming the equation that simulates the shape of vehicles known as the Rectangular Spread Function (RSF) by using Mathcad software.

4-2 Effect of Vehicle Linear Motion on the Intensity Distribution of the Detected Thermal Image.

In this part of the results, the effect of linear motion on the intensity distribution of the detected thermal image is investigated. Different velocities of the vehicle will take into account to realize the effect of such parameters on the quality of the detected thermal image. The speed of a vehicle is chosen as (40, 80, 120) Km/h for various distances.

4-2-1 Effect of the Linear Motion on the Detected Thermal Image for System Operates with Circular Aperture

The velocity values for the detected object are assumed to be equal to (40, 80, 120) Km/h for different distances (250, 500, 750, 1000, 1500, 2000, 3000, 4000) m. The effect of linear motion on the intensity distribution of rectangular objects is performed using the RSF equation through compute the equation (3-25) for a circular aperture. Figures (4-1), (4-2), and (4-3) show the intensity distribution of the thermal image of an ideal optical system operating with a circular aperture for an object with a linear motion of (40, 80, 120) Km/h, respectively. Distances between the thermal camera and the object were chosen as (250, 500, 750, 1000, 1500, 2000, 3000, 4000) m. It is clear in figure (4-1) the RSF curves comprise a main peak starting at (0.952, 0.929, 0.857, 0.762, 0.567, 0.431, 0.29, 0.218) for the case of (250, 500, 750, 1000, 1500, 2000, 3000, 4000) m of distances, respectively. This peak represents the intensity distribution of the rectangular thermal image at the image plane. One can observe that a vehicle at a distance of (250 m) has the best quality compared to the other distances. As, in this case, the detected thermal image has a high value of intensity, leading to get a high-clarity thermal image that can be recognized and distinguished evidently. Figures (4-2) and (4-3) have the same behavior as figure (4-1) for the intensity distributions at two different linear motions, which are 80 Km/h and 120 Km/h. From these two figures and for all cases of different distances, the main peak of intensity decreases as the distance increases. Nevertheless, the observation of intensity distribution in all cases of different linear motion verifies that with the increase of the linear

motion, the intensity values become less, and thus, the image is getting blurrier. In the case of 80 and 120 Km/h of linear motion, the best image clarity is at the range of (500 m). This indicates that the effect of a high linear motion of the detected thermal image overcomes the effect of distances, meaning that the image of a high-speed vehicle makes a significant effect on the image resolution.

In addition, at the distance of 3000 m for all different linear motions, the intensity is very low and the main peak becomes extinct, leading to cases where the object cannot be recognized. Nevertheless, the thermal images will be completely non-existent at distances of (3000 m and 4000 m).
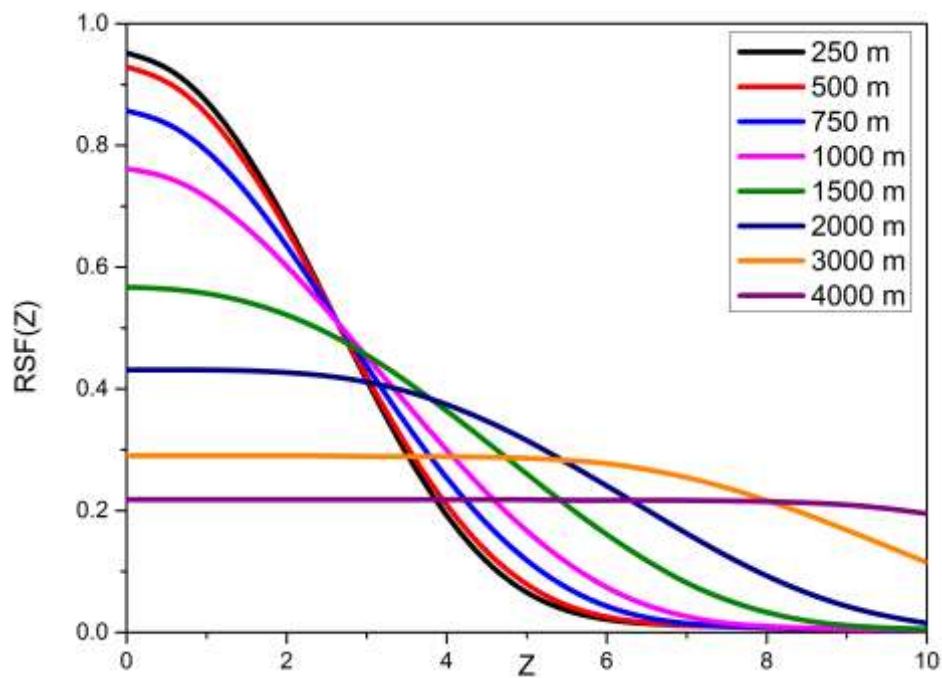

Fig. (4-1) The intensity distribution of the detected thermal image of a vehicle moving at 40 Km/h for a system operating with a circular aperture.
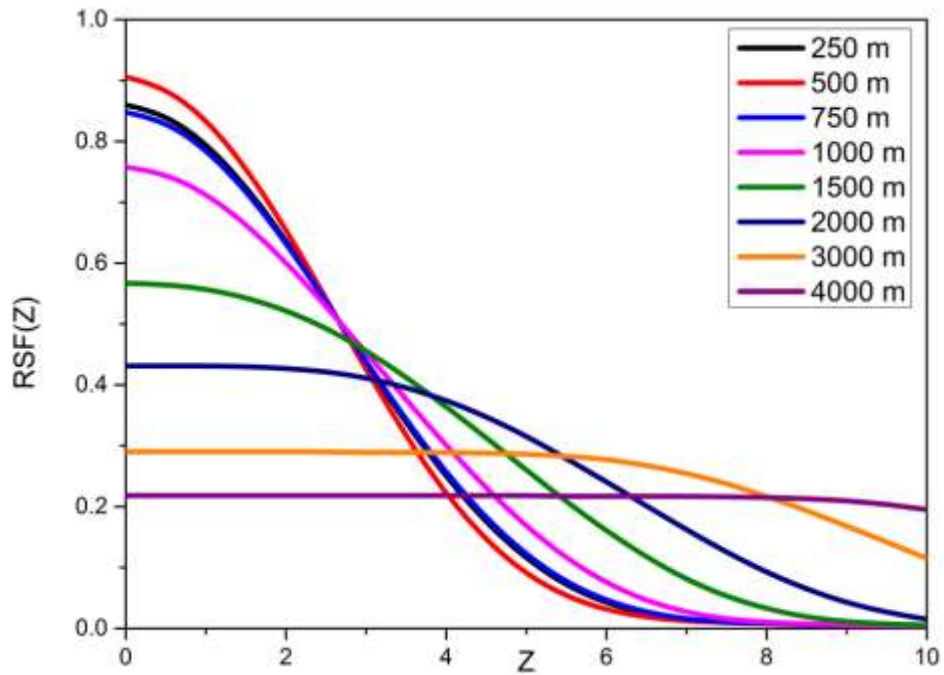
Fig. (4-2) The intensity distribution of the detected thermal image of a vehicle moving at 80 Km/h for a system operating with a circular aperture.
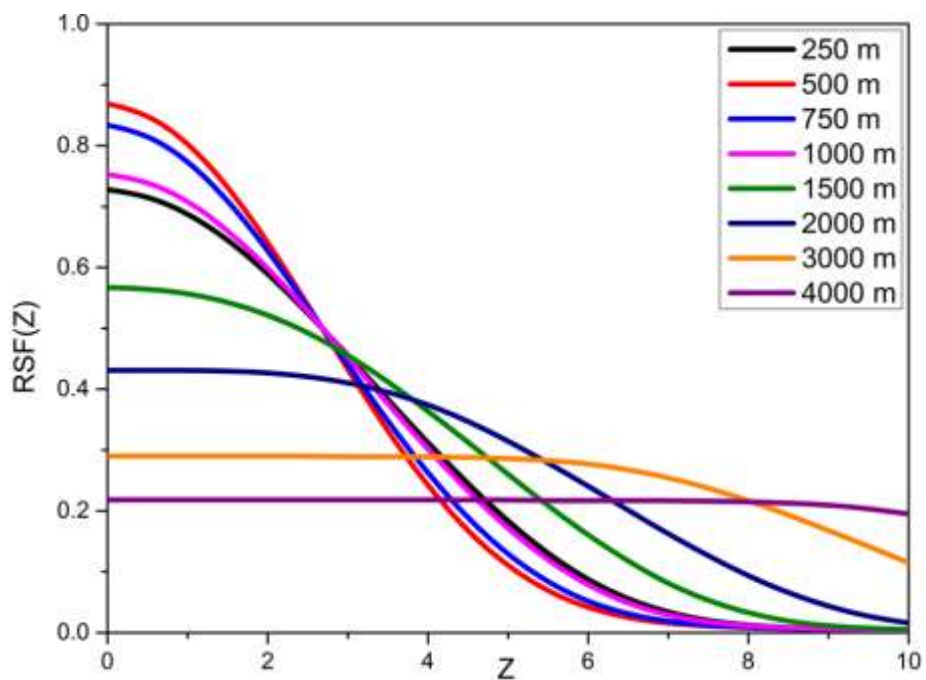

Fig. (4-3) The intensity distribution of the detected thermal image of a vehicle moving at 120 Km/h for a system operating with a circular aperture.

Table (4-1), represent the comparison between the intensity distribution of the detected thermal images at different linear motions of the system operates with a circular aperture at specific distances (250, 500, 750, 1000) m between the thermal camera and object. Comparing the linear motion (40,80, 120) Km/h for a vehicle at (250 m) and (500 m) of distance, one can be noticed that the intensity of the thermal image decreases whenever the linear motion of the moving vehicle increases. Therefore, the best detected thermal image is at a speed of (40 Km/h). Also, there is a clear difference in the maximum point of intensity among the three different speeds of the object. These differences in intensity become less at (750 and 1000) m of distances. This means that the effect of distance overcomes the effect of vehicle speed, in addition, the effect of the transversal motion becomes less for a large distance.

Table (4-1) Maximum intensity at different distance and linear motions using a circular aperture **.**

Distance (m)	RSF(z=0) At v_0=40Km/h	RSF(z=0) At v_0=80Km/h	RSF(z=0) At v_0=120Km/h
250	0.952	0.86	0.728
500	0.929	0.906	0.869
750	0.857	0.848	0.834
1000	0.762	0.758	0.753

4-2-2 Effect of the Linear Motion on the Detected Thermal Image for System Operates with Square Aperture

A square aperture is one of the advantageous apertures that utilize in optical systems. In this part, the intensity distribution of the detected thermal image is calculated for the system operating with a square

aperture. The effect of linear motion on the intensity distribution of rectangular objects is achieved using the RSF equation through compute the equation (3-26) for square aperture.

Figures (4-4), (4-5), and (4-6) show the intensity distribution of the detected thermal images at the linear motion of (40, 80, 120) Km/h, respectively. The RSF calculations are performed at different distances between the thermal camera and the object (250, 500, 750, 1000, 1500, 2000, 3000, 4000) m. Form figures, the intensity distribution of the RSF is affected by the distances and linear motion, where the maximum value of the intensity is decreasing by the increasing of distances as in the illustrated figures. It is also clear that the detected thermal image has a very weak intensity at a distance of 2 Km compared to the best case in the same figure. Thus, in such case, the detected thermal image will be blurred, deformed, and difficult to distinguish between its components. Moreover, at distances of 2 Km or more, the detected thermal image cannot be completely recognized.
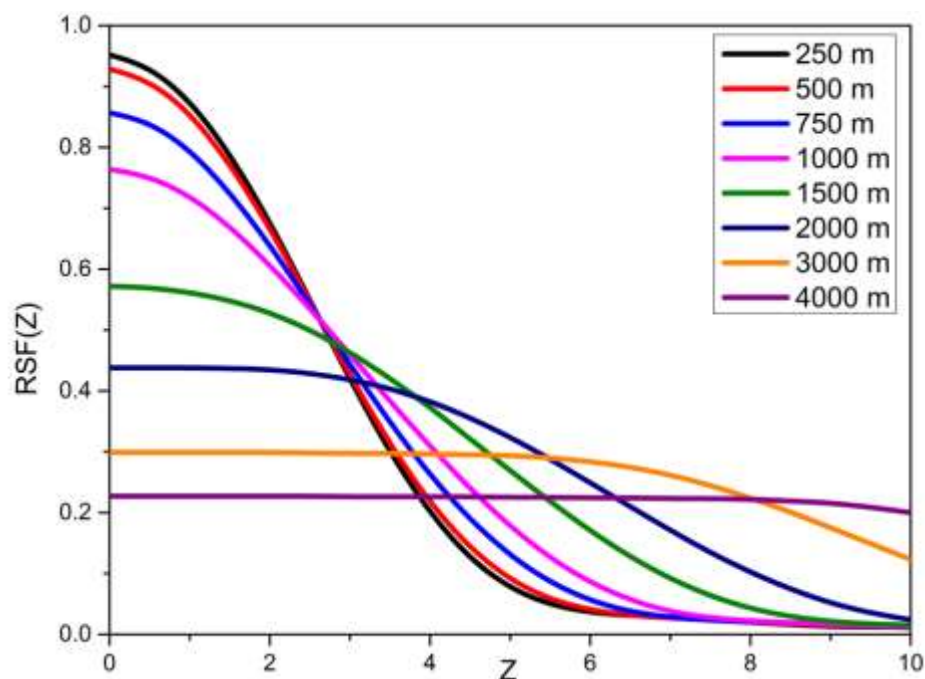
Fig. (4-4) The intensity distribution of the detected thermal image of a vehicle moving at 40 Km/h for a system operating with a square aperture.
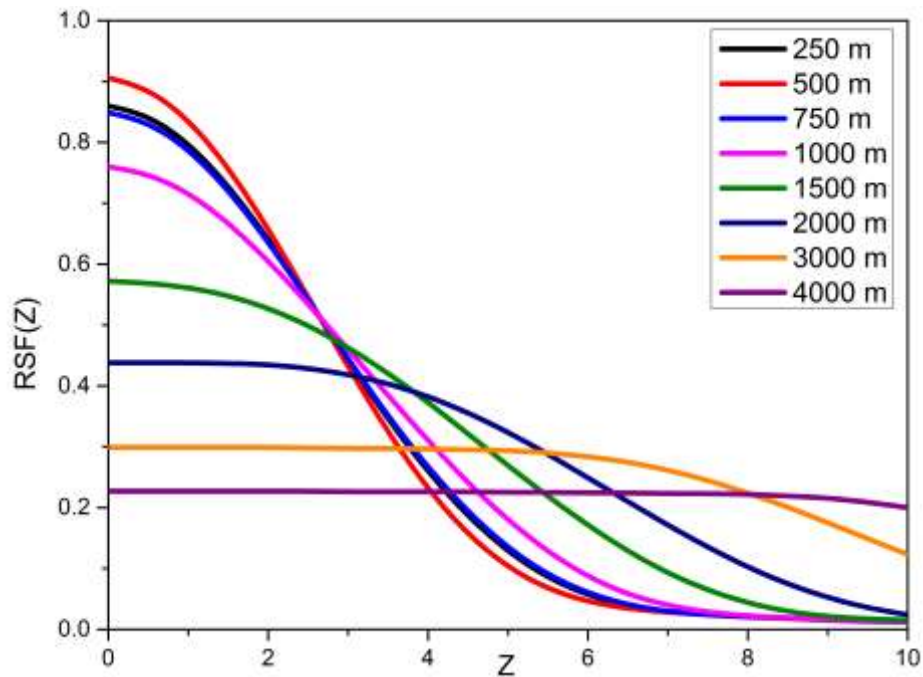

Fig. (4-5) The intensity distribution of the detected thermal image of a vehicle moving at 80 Km/h for a system operating with a square aperture.
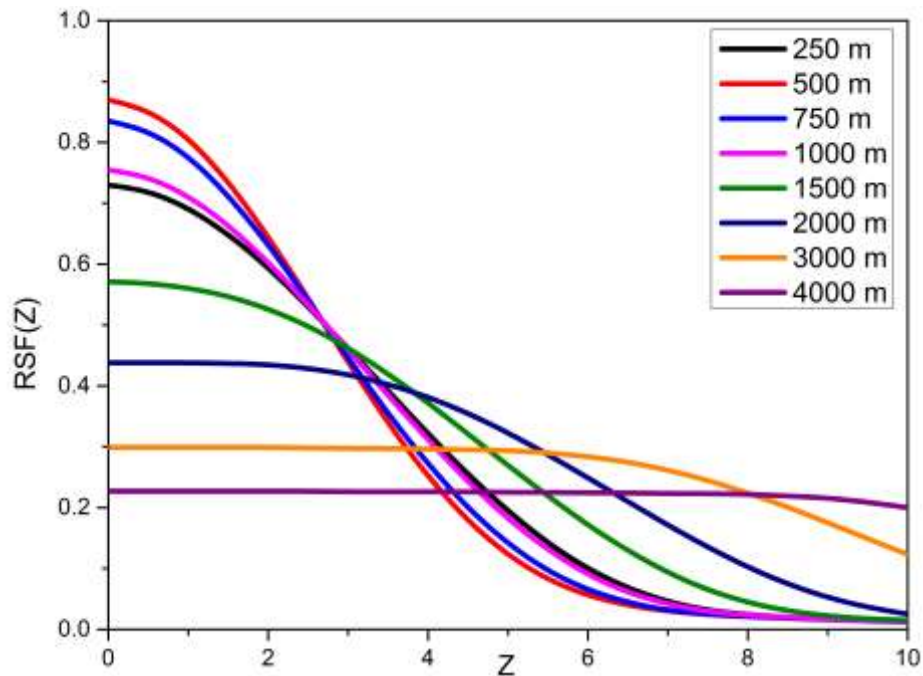

Fig. (4-6) The intensity distribution of the detected thermal image of a vehicle moving at 120 Km/h for a system operating with a square aperture.

As well as the effect of linear motion on the thermal image clarity

is apparent in the three cases. Moreover, at the linear motion of 40 Km/h,

the best value of the central peak is at the distance of 250 m, as shown in

figure (4-4). Nevertheless, in the other cases of 80 Km/h and 120 Km/h,

the best case is at a distance of 500 m. In addition, the cases where the

distance is 250 m become to be worse, as shown in figures (4-5), (4-6).

A comparison is necessary between the intensity of the detected

thermal image for different linear motions (40, 80, 120) Km/h. This

comparison is performed for an optical system operating with a square

aperture at the following distances (250, 500, 750, and 1000 m) to identify

the best detected thermal image of each case.

Table (4-2), illustrated the comparison between the intensity

distribution of the detected thermal images at different linear motions of

the system operates with a square aperture at specific distances (250,

500, 750, 1000) m between the thermal camera and object. The linear

motion affects the central peak values of the RSF intensity for each

distance. From table (4-2), the value of the main peak of intensity in the

image plane decreases when the linear motion is increased. This effect

appears obviously at the range of 0.25 Km. From the figures, the change

in the main peak is insignificant when the distances are large. Therefore,

the effects of linear motion occur at short distances more than the long

distances. Finally, one can judge that the lower value of linear motion has

the best image clarity. Likewise, the effects of the linear motion are very

small at long distances.

Table (4-2) Maximum intensity at different distance and linear motions using a square aperture .

Distance (m)	RSF(z=0) At v_0=40Km/h	RSF(z=0) At v_0=80Km/h	RSF(z=0) At v_0=120Km/h
250	0.952	0.86	0.73
500	0.929	0.906	0.87
750	0.857	0.849	0.835
1000	0.764	0.76	0.755

4-2-3 Effect of the Linear Motion on the Detected Thermal Image for System Operates with Triangular Aperture

The linear motion effect is calculated for different values of distances between the thermal camera and the object for the system operates with a triangular aperture. The triangular apertures considered a promising optical system aperture. The calculations are performed with different linear motions of the object under investigation. These linear motions are (40, 80, 120) Km/h. The effect of linear motion on the intensity distribution of rectangular objects is performed using the RSF equation through compute the equation (3-27) for triangular aperture. Figures (4-7), (4-8), and (4-9) display the intensity distribution of the thermal image at the image plane of a rectangular object for different ranges and a specific linear motion of the object under investigation. From figure (4-7), a distance of 250 m at the linear motion of 40 Km/h is the best case compared to other cases. Otherwise, when distances increase the intensity decreases. In addition , the shape and character of the intensity distribution main peak changes at long distances (< 2000 m), leading to the deformation of the detected thermal image. In addition, the peak intensity

value of the RSF has a higher value, when the object is at a distance of 500 m, in the case when the linear motion is 80 and 120 Km/h, compared to the case where the linear motions of the object are 40 Km/h. The behavior of the intensity curves at the triangular aperture is the same as the system operates at the square aperture, where these two apertures give a good resolution of the thermal images at middle distances compared to the short one at the low speed of the detected object. In general, the result from the previous three cases is the thermal camera can detect and predict objects at

a range of less than 2 Km.
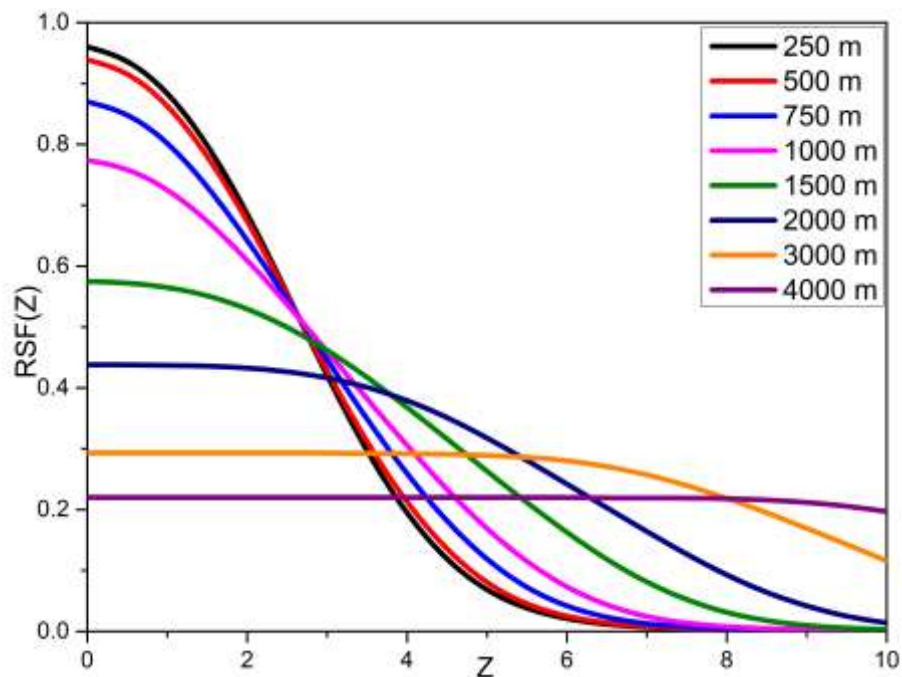
Fig. (4-7) The intensity distribution of the detected thermal image of a vehicle moving at 40 Km/h for a system operating with a triangular aperture..
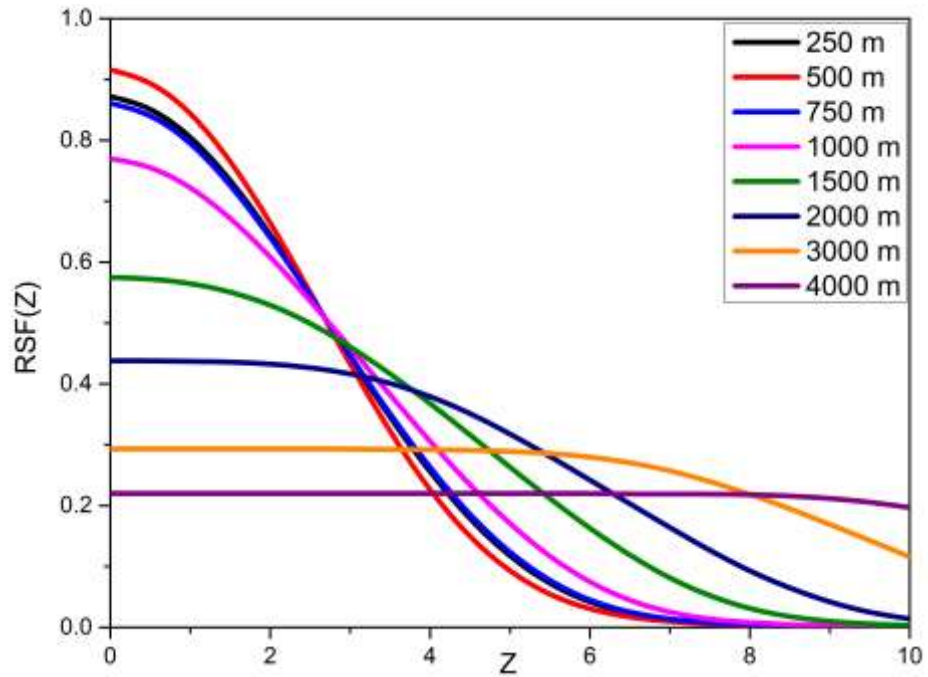
Fig. (4-8) The intensity distribution of the detected thermal image of a vehicle moving at 80 Km/h for a system operating with a triangular aperture.
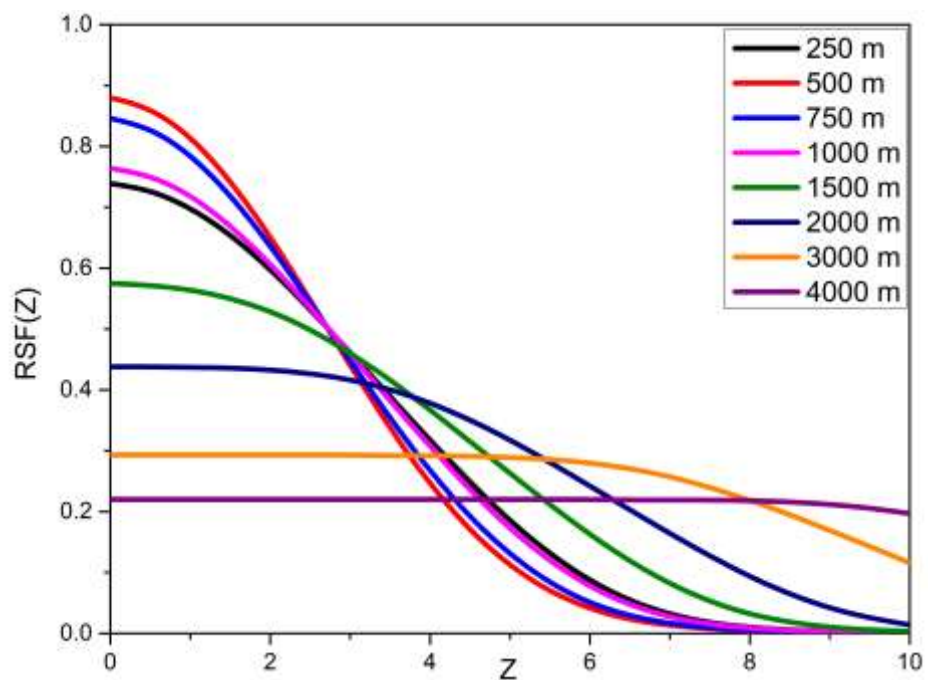

Fig. (4-9) The intensity distribution of the detected thermal image of a vehicle moving at 120 Km/h for a system operating with a triangular aperture

Results are applied to obtain a comparison of detected images of a vehicle moving at a speed of (40, 80, and 120 Km/h) at each of the following dimensions (250 m, 500 m, 750 m, and 1000 m) using an optical system that works with a triangular aperture. Table (4-3), show the accuracy of the detected thermal image by showing a comparison between the detected thermal image at a specific distance of (250, 500, 750, and 1000) m for the linear motion of (40, 80, 120) Km/h for each case. The linear motion of 40 Km/h is the best value of the intensity distribution compared to all cases.

Generally, the short distances are better than the long distances for the low object speed. This is indicated from the previous figures and it is clear for different apertures.

Table (4-3) Maximum intensity at different distance and linear motions using a triangular aperture .

Distance (m)	RSF(z=0) At v_0=40Km/h	RSF(z=0) At v_0=80Km/h	RSF(z=0) At v_0=120Km/h
250	0.96	0.872	0.739
500	0.939	0.916	0.88
750	0.87	0.861	0.846
1000	0.774	0.77	0.764

4-3 The Effect of the Distance Between the Object and the Thermal Camera on the Intensity Distribution of the Detected Thermal Image

One of the factors that affect the image quality is the distance between the detected object and the thermal camera. This factor is investigated in this section for a vehicle without any linear motion

(unmoving vehicles). Such a factor affects the intensity distribution of the detected thermal image of vehicles represented by a rectangular object. Results of the distance effect on the intensity distribution of RSF are achieved by solving equations (3-21), (3-22), and (3-23) for circular, square, and triangular apertures, respectively.

Figures (4-10), (4-11), and (4-12) show the intensity distribution of the thermal image with different apertures, which are circular, square, and triangular, respectively. The thermal image of a car target is detected at ranges of (250, 500, 750, 1000, 1500, 2000, 3000, 4000) m. From the figures we find that the thermal image detected for a vehicle, that has no linear motion (unmoving or stopped vehicle), decreases in intensity value and begins to reduce as the distance increases for any optical system that works with any of the three apertures (circular, square, and triangular). Likewise, the image detected by the thermal camera for a stopped vehicle at a distance of 250 m has the best thermal image quality, where the thermal image, in this case, has a higher value of intensity, this means that the clarity of such an image is the best compared to the other cases of distances. This result is similar for all applied apertures (circular, square, and triangular). Besides, at a distance of more than 2 Km, the thermal image is difficult to be distinguished, and the difficulty in distinguishing increases as the distance increases. For all used apertures, the same behavior appears for the detected thermal image.
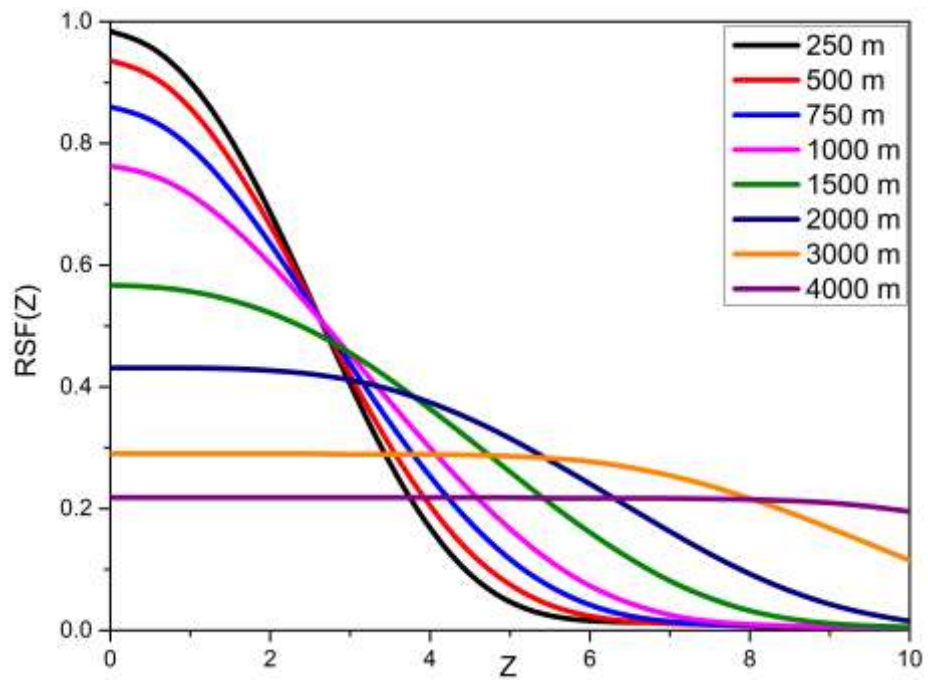
Fig. (4-10) The intensity distribution of the detected thermal image of an unmoving vehicle at different distances for a system operating with a circular aperture.
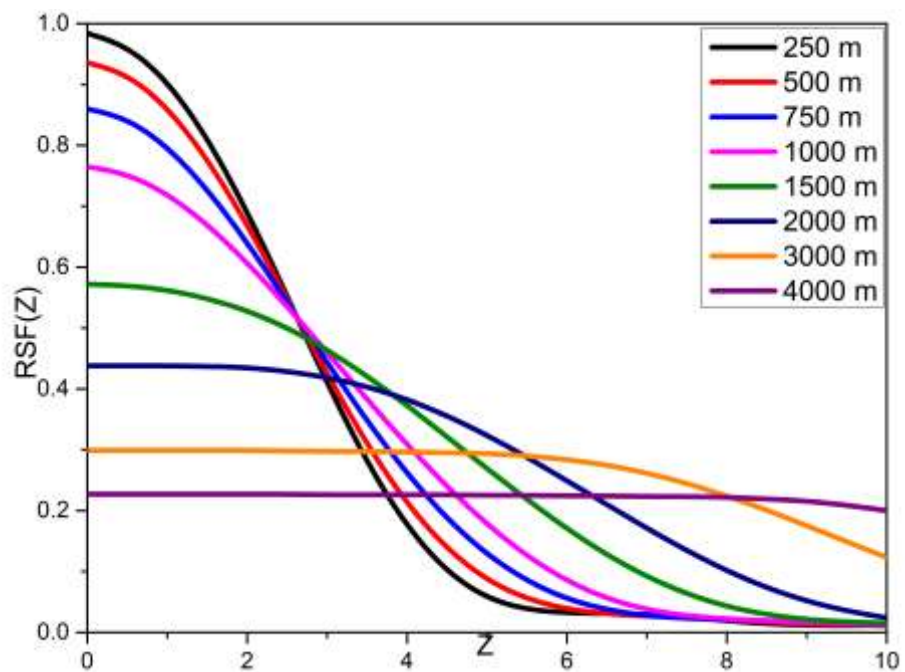

Fig. (4-11) The intensity distribution of the detected thermal image of an unmoving vehicle at different distances for a system operating with a square aperture.
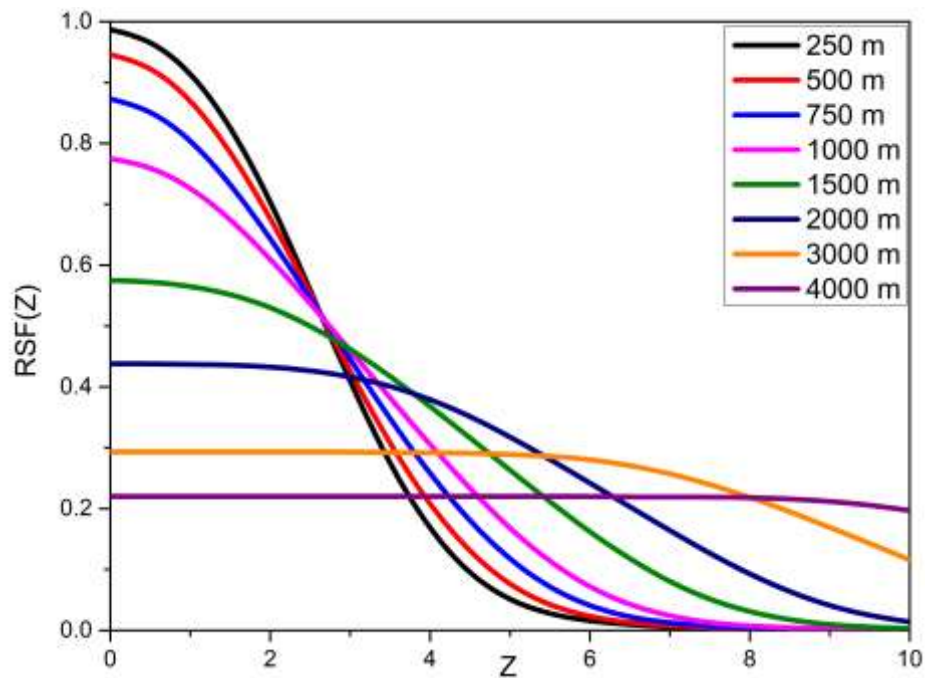
Fig. (4-12) The intensity distribution of the detected thermal image of an unmoving vehicle at different distances for a system operating with a triangular aperture.

4-4 A comparison Between the Effect of Different Apertures on the Intensity Distribution of the Detected Thermal Image

Comparing the three apertures, which were considered (circular, square, and triangular) to produce a thermal image of the vehicle at different distances of (250, 500, 750, 1000, 2000, 3000, 4000) m, is necessary to find out the best image quality. In such cases, all parameters are similar to show the effect of just the shape of the used aperture on the intensity values. Since the behavior of the intensity distribution is approximately similar, therefore, the maximum values of RSF (at z=0) are taken into account to compare the effect of the aperture on the image quality. Thus, for all the following figures in this section, the maximum values of RSF are only used for the unmoving /moved objects.

4-4-1 unmoving Objects

Figure (4-13) shows the intensity distribution of the detected thermal image for a system that operates with different apertures (circular, square, triangular). In this case, the intensity distribution of the detected thermal image depends only on the aperture shape. The values of object distances are (250, 500, 750, 1000, 2000, 3000, and 4000) m for unmoving vehicles.

From the intensity values in figure (4-13), it is found that the intensity values of the detected thermal image decrease with increasing the distance for all different apertures. Consequently, the best possible detected thermal image of the unmoving vehicle is obtained at a distance of 250 m, where the intensity value is maximum. Besides, the differences between intensity curves, which represent the system operating with circular and square, and triangular, are small. Anyway, one can say that there is evidence indicating that the triangular aperture represents the best aperture for the system activates for distances less than 2 Km. Moreover, all square and circular apertures are considered the best-used apertures for systems operating to detect objects at long distances (more than 2 Km), nevertheless, the intensity at such distances is very low, leading to non-distinguish detected images. These indications arise from high values of intensity at different ranges and for different apertures.
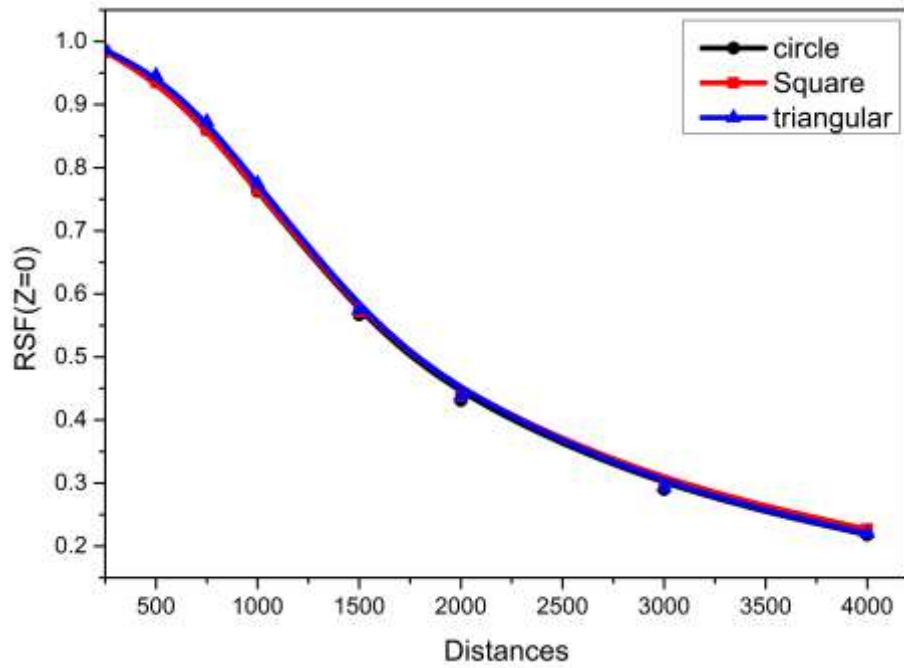
Fig. (4-13) The intensity distribution of the detected thermal image for the unmoving vehicle at different distances and for different apertures.

Table (4-4) Maximum intensity at different distances for the unmoving vehicle for different apertures.

Distance (m)	RSF(z=0) At circular aperture	RSF(z=0) At square aperture	RSF(z=0) At triangular aperture
250	0.984	0.984	0.987
500	0.936	0.936	0.946
750	0.86	0.86	0.873
1000	0.763	0.765	0.775
1500	0.567	0.572	0.575
2000	0.431	0.438	0.438
3000	0.29	0.299	0.293
4000	0.218	0.227	0.22

4-4-2 Moving Objects

The effect of the aperture shape on the intensity distribution of the object (vehicle) has linear motion and at different distances is investigated in this section.

Figure (4-14) shows the intensity distribution of the detected thermal image of an object with linear motion of 40 Km/h for the system operating with different apertures (circular, square, triangular). Distance values of objects are considered as (250, 500, 750, 1000, 2000, 3000, and 4000) m for different apertures.

Due to the best values of the intensity, it is clear that the best detected thermal image obtained from the system works using the triangular aperture, as well as the best distance of detection is 250 m for all apertures.
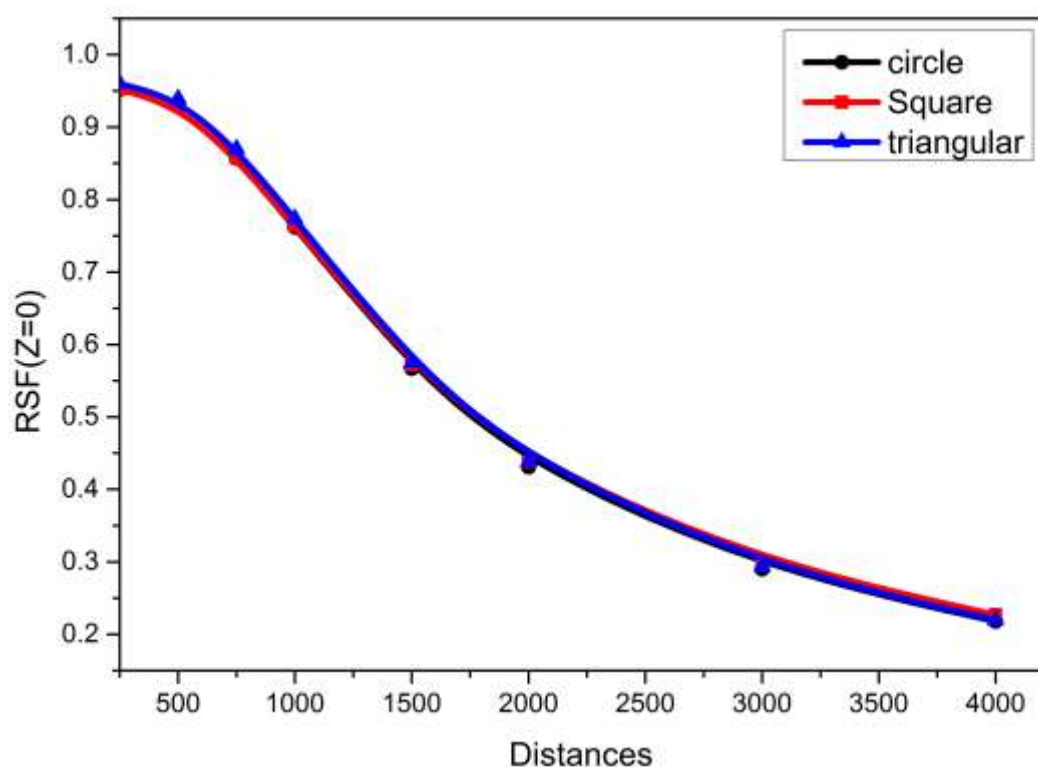

Fig. (4-14) The intensity distribution of the detected thermal image for a vehicle moving at 40 Km/h at different distances and for different apertures.

Table (4-5) Maximum intensity at different distances for the moving vehicle v_0=40Km/h for different apertures.

Distance (m)	RSF(z=0) At circular aperture	RSF(z=0) At square aperture	RSF(z=0) At triangular aperture
250	0.952	0.952	0.96
500	0.929	0.929	0.939
750	0.857	0.857	0.87
1000	0.762	0.764	0.774
1500	0.567	0.572	0.575
2000	0.431	0.438	0.438
3000	0.29	0.299	0.293
4000	0.218	0.227	0.22

The detection of the thermal image of a vehicle moving at a speed of 80 and 120 Km/h is presented in figures (4-15), and (4-16), respectively. It is obvious that the triangular aperture still gives the best intensity values over distances in case of less than 2 Km. This range of detection (less than 2 Km) is the effective distance for recognition of an image with good quality. Thus, one can say that the triangular aperture is the best aperture for moving objects. Additionally, the best distance for detecting the thermal image, in the case where the linear motions are 80 and 120 Km/h, is at the distance of 500 m, which is different that the unmoving object. This indicates that the higher the linear motion the higher the effective distance of detection. This is clear from figures (4-28), where the effective distance of detections started when 500 m.

Finally, in all cases of moving/unmoving objects, the image produced through an optical system that works using a square and circular aperture, are similar in the intensity value and RSF behavior.
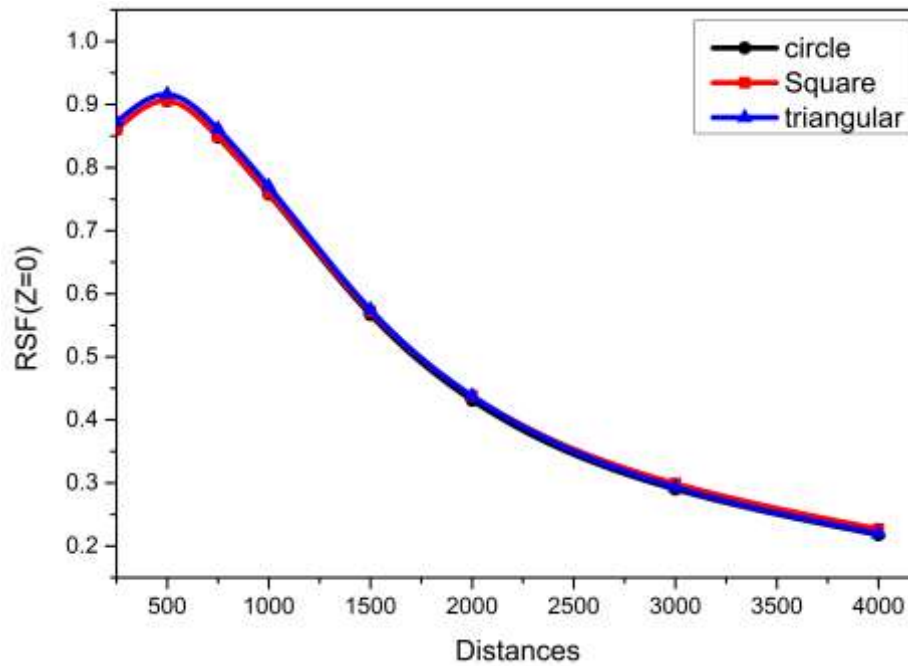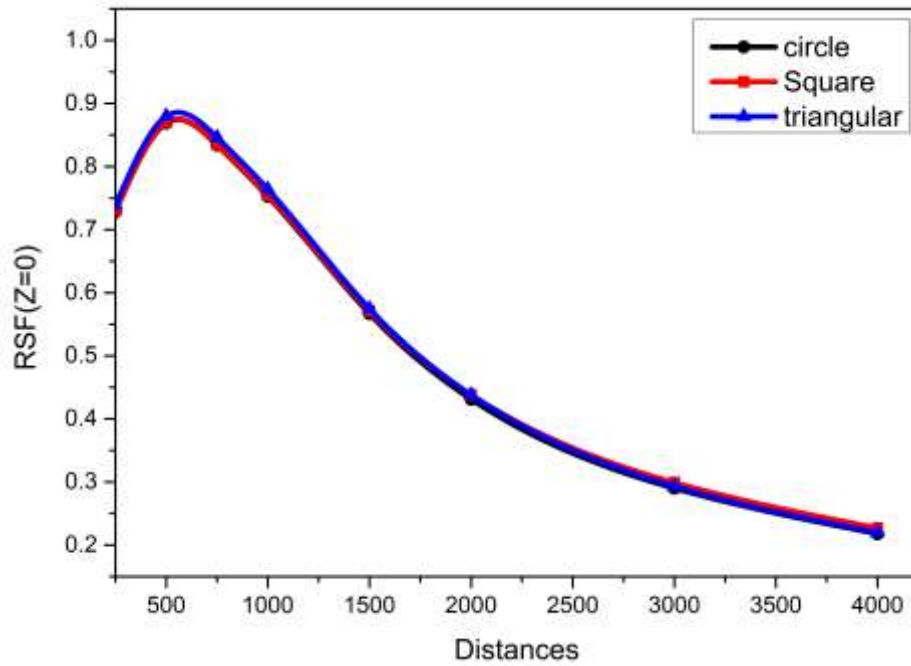
Fig. (4-15) The intensity distribution of the detected thermal image for a vehicle
moving at 80 Km/h at different distances and for different apertures.

Table (4-6) Maximum intensity at different distances for the moving
vehicle v_0=80Km/h for different apertures.

Distance (m)	RSF(z=0) At circular aperture	RSF(z=0) At square aperture	RSF(z=0) At triangular aperture
250	0.86	0.86	0.872
500	0.906	0.906	0.916
750	0.848	0.849	0.861
1000	0.758	0.76	0.77
1500	0.567	0.572	0.575
2000	0.431	0.438	0.438
3000	0.29	0.299	0.293
4000	0.218	0.227	0.22

Fig. (4-16) The intensity distribution of the detected thermal image for a vehicle moving at 120 Km/h at different distances and for different apertures.

Table (4-7) Maximum intensity at different distances for the moving vehicle v_0=120Km/h for different apertures.

Distance (m)	RSF(z=0) At circular aperture	RSF(z=0) At square aperture	RSF(z=0) At triangular aperture
250	0.728	0.73	0.739
500	0.869	0.87	0.739
750	0.834	0.835	0.846
1000	0.753	0.755	0.764
1500	0.567	0.571	0.575
2000	0.431	0.438	0.438
3000	0.29	0.299	0.293
4000	0.218	0.227	0.22

4-5 The Effect of Using A filter on the Intensity Distribution of the Detected Thermal Image

In this section, a filter is used to increase the quality of the detected thermal image via increasing the intensity value and thus, increasing the clarity of the detected thermal image for an optical system works with a circular aperture to detect a rectangular object represented by vehicles to obtain a better image through which objects can be straightforwardly distinguished. This filter works to change and focus the incoming thermal ray to the thermal camera.

Practically, this work can be performed by inserting a filter in front of the entrance aperture of the thermal camera that works with a circular aperture to investigate the effect of the filter on the intensity distribution of the detected thermal image. Theoretically, all results are achieved, in this section, by calculating equation (3-29) with Mathcad software. Since utilizing such filters with many parameters gives many different cases in this work, thus using specific parameters is the best choice to focus on improving the image quality. In addition, for the same reason using one aperture (circle aperture which is the aperture that is used in the thermal camera under investigation) is favored in this case. Therefore, the parameters that are applied for the filter in this study are:

$$\text{Circular aperture. -1}$$

$$\beta = 0, 0.25, 0.5, 0.75, 1 \text{ -2}$$

$$\alpha = 0.6 \text{ -3}$$

$$\text{N=1,2 -4}$$

The thermal image is enhanced for images that are detected but not recognized, and where the intensity value is very low. This is carried out at a long range and a high linear motion of the object under detection.

Hence, just long distances are applied in this section to improve the thermal image. Distances of (1, 1.5, 2) Km are explored in this section to improve the image intensity. The linear motion, that is considered in this part of the research, is 80 Km/h. From the previous sections, it is clear that the effect of the linear motion becomes less at long distances so in this section just one linear motion is considered to investigate. This linear motion (velocity) is 80 Km/h for all cases of moving vehicles under thermal detection.

Figures (4-17) (a, b) display the intensity distribution of the detected thermal image for rectangular unmoving objects at a distance of 1 Km. This filter is inserted in this case with different values of β and for N=1 and 2, respectively.

The effect of the inserted filter appears obviously on the intensity distribution of the detected thermal image. Where the intensity increases when the value of β increases. β=1 represents the best case compared to the other cases. Increasing the N value leads to an improvement in the intensity value in the detected image, leading to an improvement of the image quality, as shown in figure (4-17) (b).
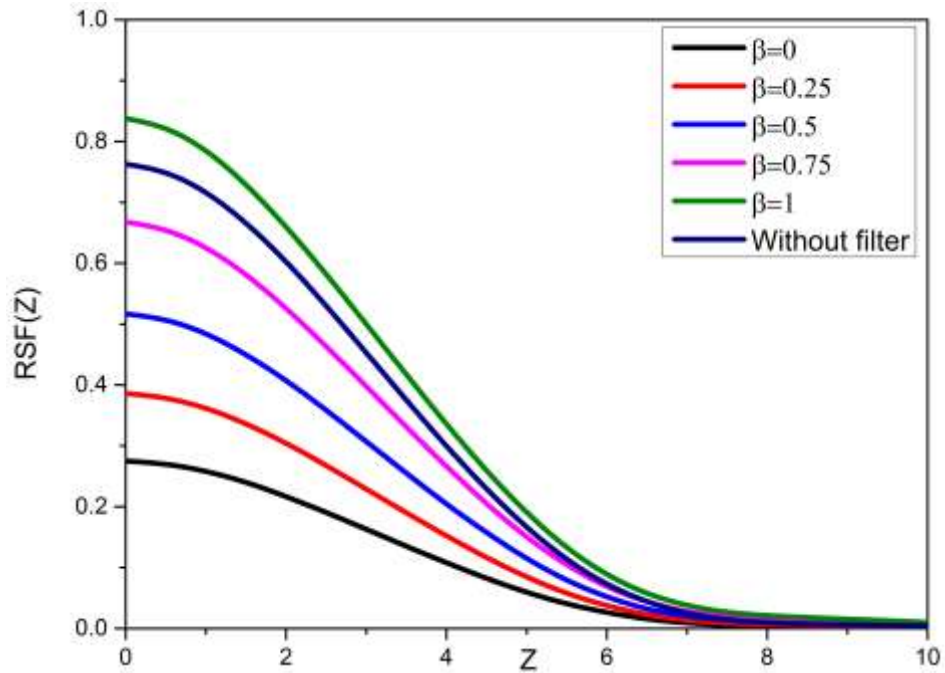
Fig. (4-17): (a) The intensity distribution of the detected thermal image using a system with a filter (at N=1) for unmoving vehicle and at 1 Km of distance
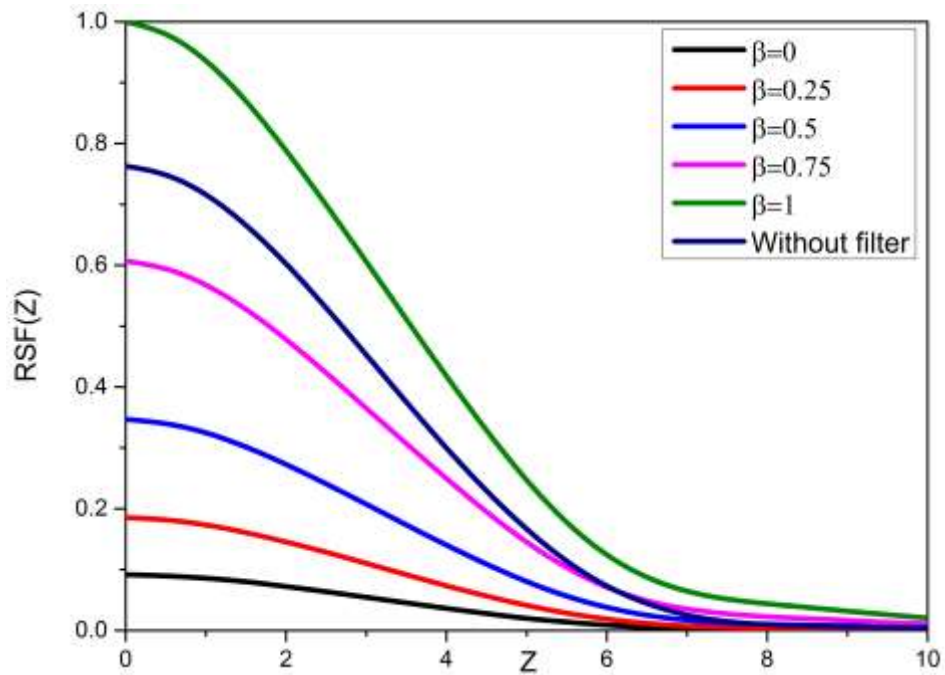

Fig. (4-17): (b) The intensity distribution of the detected thermal image using a system with a filter (at N=2) for unmoving vehicle and at 1 Km of distance

Figures (4-18) (a, b) display the intensity distribution of the detected thermal image for rectangular objects with linear motion of

(80Km/h) at a distance of 1 Km. This filter is inserted in this case with different values of β and for N=1 and 2, respectively. The figures indicate that the filter can be used to improve the detected thermal image for a moving vehicle at a distance of 1Km and speed of 80 Km/h when the value of β=1 and for both N=1 and 2. In both cases, the detected image is improved and the quality is better compared to the case where the system operates without filter.

At a distance of 1.5 Km, the intensity distribution of the detected thermal image of an unmoving vehicle is shown in figures (4-19): (a, b). Similarly, the filter is very useful, when it is used to improve the maximum intensity of RSF, especially at N=2. By using the filter, the intensity value arrives at the high corrected point and the detected thermal image becomes very clear.
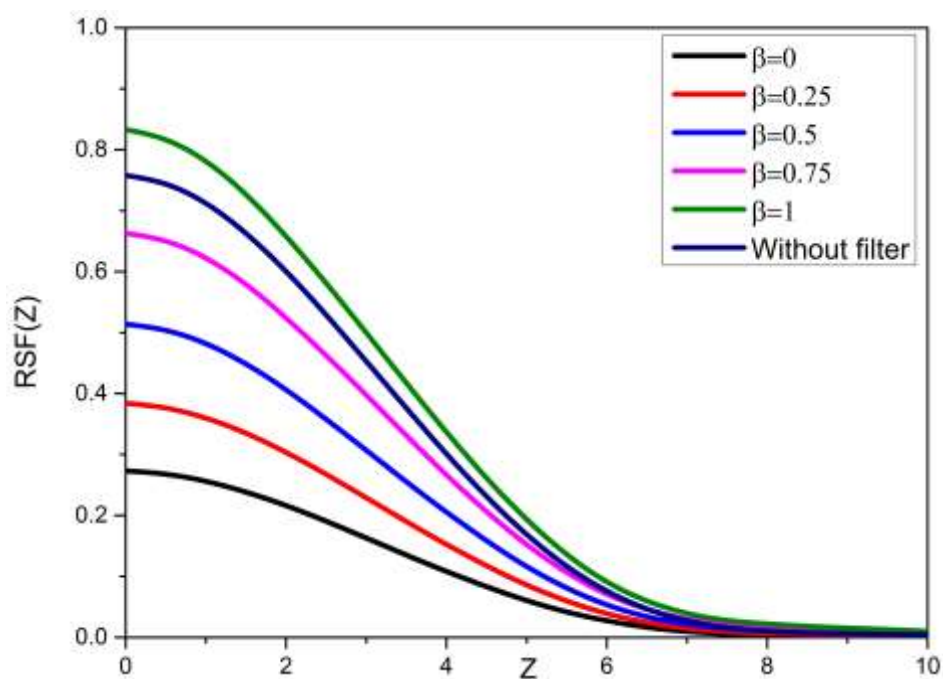

Fig. (4-18): (a) The intensity distribution of the detected thermal image using a system with a filter (at N=1) for moving vehicles with linear motion of (80 Km/h) and at 1 Km of distance.
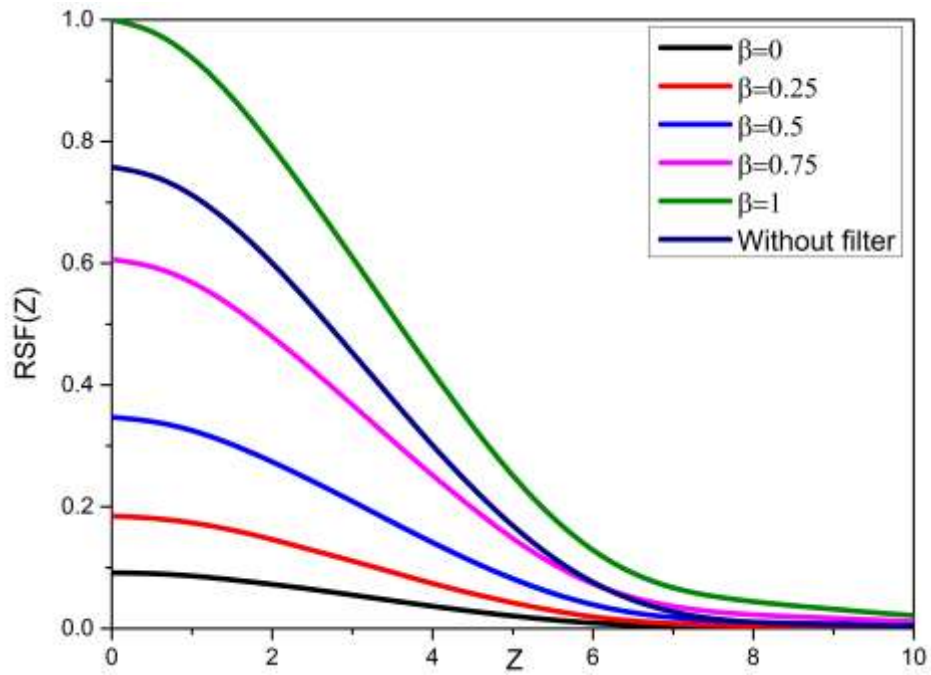
Fig. (4-18): (b) The intensity distribution of the detected thermal image using a system with a filter (at N=2) for moving vehicles with linear motion of (80 Km/h) and at 1 Km of distance.
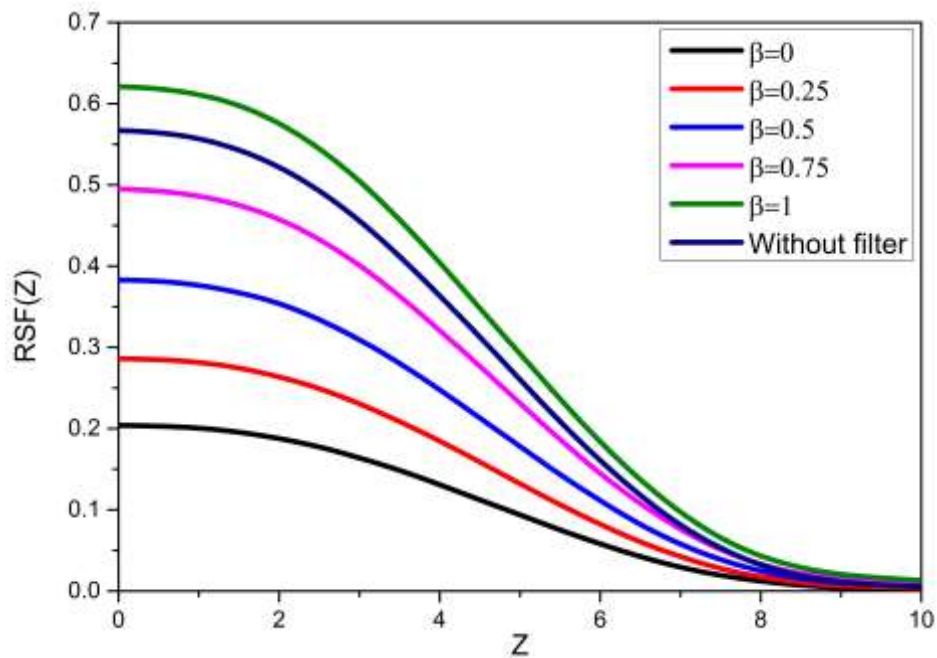

Fig. (4-19): (a) The intensity distribution of the detected thermal image using a system with a filter (at N=1) for unmoving vehicles and at 1.5 Km of distance.
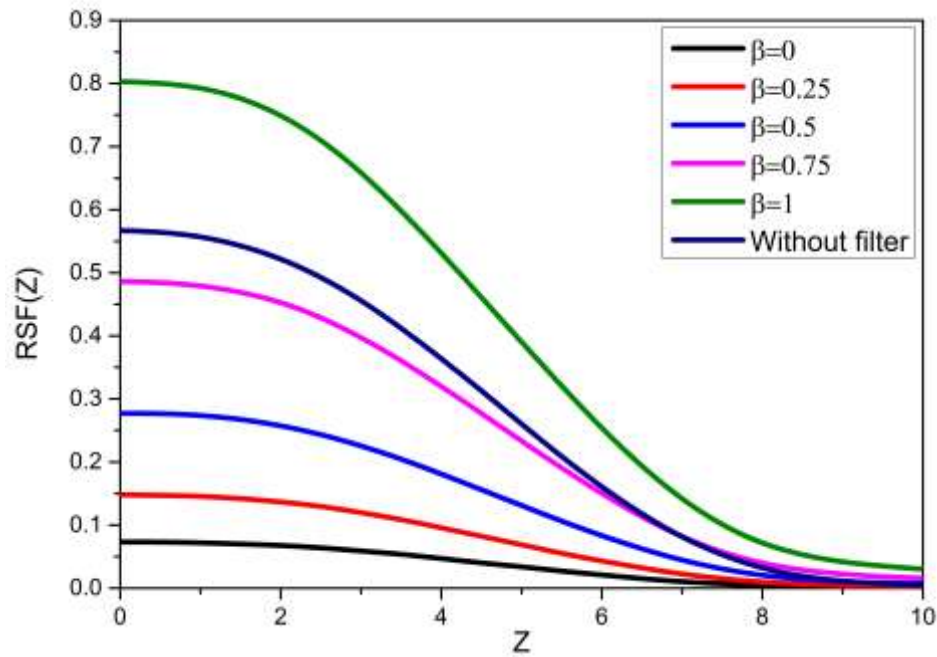
Fig. (4-19): (b) The intensity distribution of the detected thermal image using a system with a filter (at N=2) for unmoving vehicles and at 1.5 Km of distance.

In the case where the vehicle is moving with the linear motion of 80 Km/h and at a distance of 1.5 Km, the intensity of the thermal image becomes very low as shown in figures (4-20): (a, b).

It is clear that the quality of the thermal image becomes very bad to the point where the object cannot be distinguished. Due to the lower values of the intensity distribution of RSF, the detected temperature of the vehicle is very weak and the image results are very blurry. Using the filter helps a lot to improve the image quality as shown in figures (4-20): (a, b). The detected thermal image is still critical for the case of N=1, but at N=2 the intensity distribution is excellent especially when β=1 for the filter.
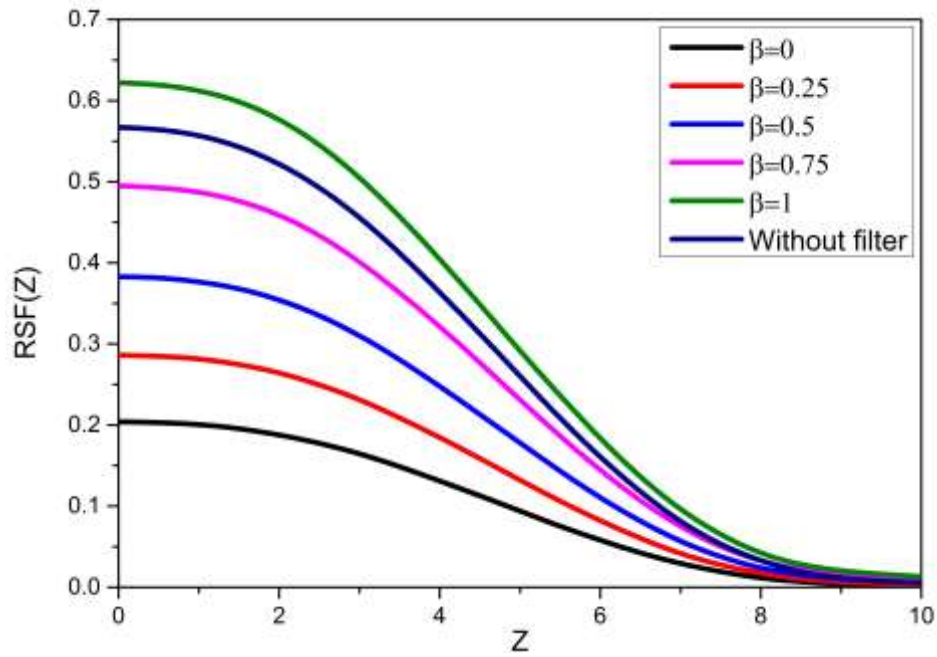
Fig. (4-20): (a) The intensity distribution of the detected thermal image using a system with a filter (at N=1) for moving vehicles with linear motion of (80 Km/h) and 1.5 Km of distance.
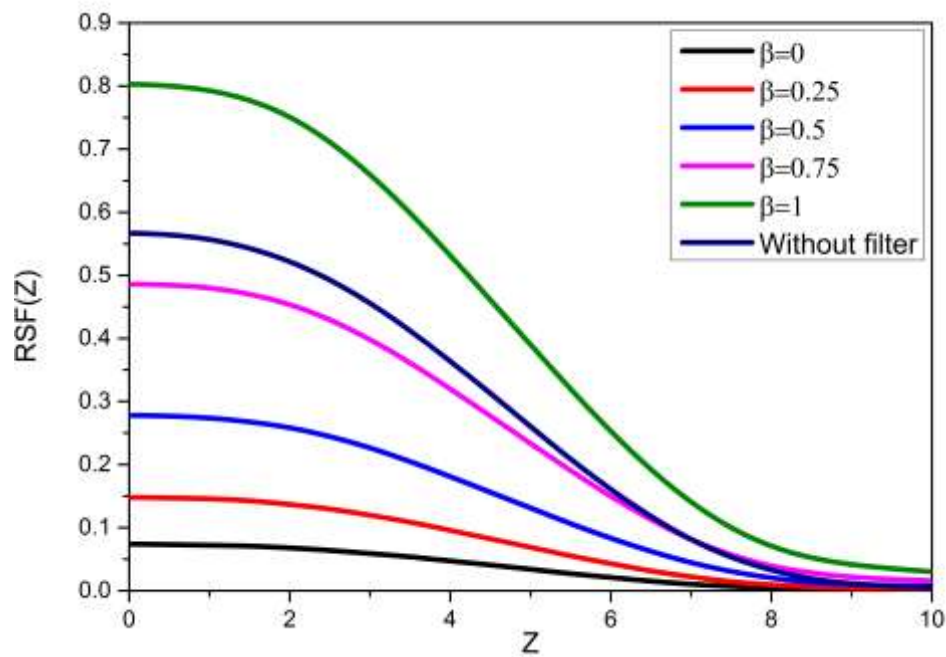

Fig. (4-20): (b) The intensity distribution of the detected thermal image using a system with a filter (at N=2) for moving vehicles with linear motion of (80 Km/h) and 1.5 Km of distance.

Figure (4-21): (a, b) show the intensity distribution of the detected thermal image for an unmoving rectangular object at a distance of 2 Km. This filter is inserted in this case with different values of β and for N=1 and

2, respectively.

The effect of distances is very effect in this case, where the intensity values are very low even when the filter is used. By observing the figures, one can find that the increased in the values of β, the more the detected thermal image begins to tend to be better and clearer, whether it is for a moving or stationary vehicle, especially for N=2. Regardless, this improvement is not beneficial for the detected thermal image, where the intensity doesn't enhance very much and the detected image in such case is not completely improved and unusable. Thus, using the filter at such a distance (more than 2 Km) is useless and doesn't help in improving the image quality. Consequently, distances of more than 2 Km are not
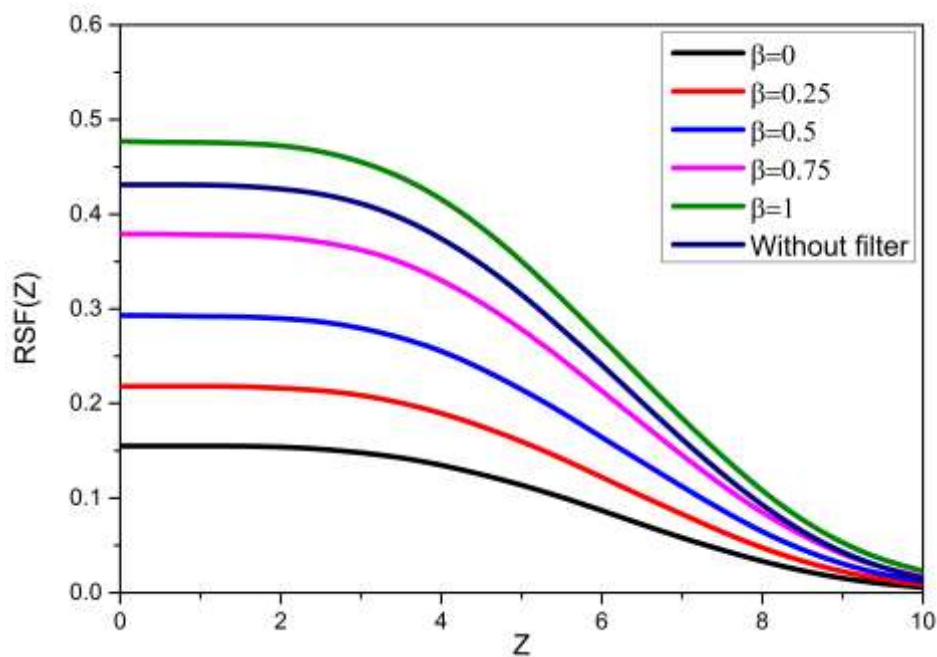
interesting in this study.

Fig. (4-21): (a) The intensity distribution of the detected thermal image using a system with a filter (at N=1) for unmoving vehicles and at 2 Km of distance.
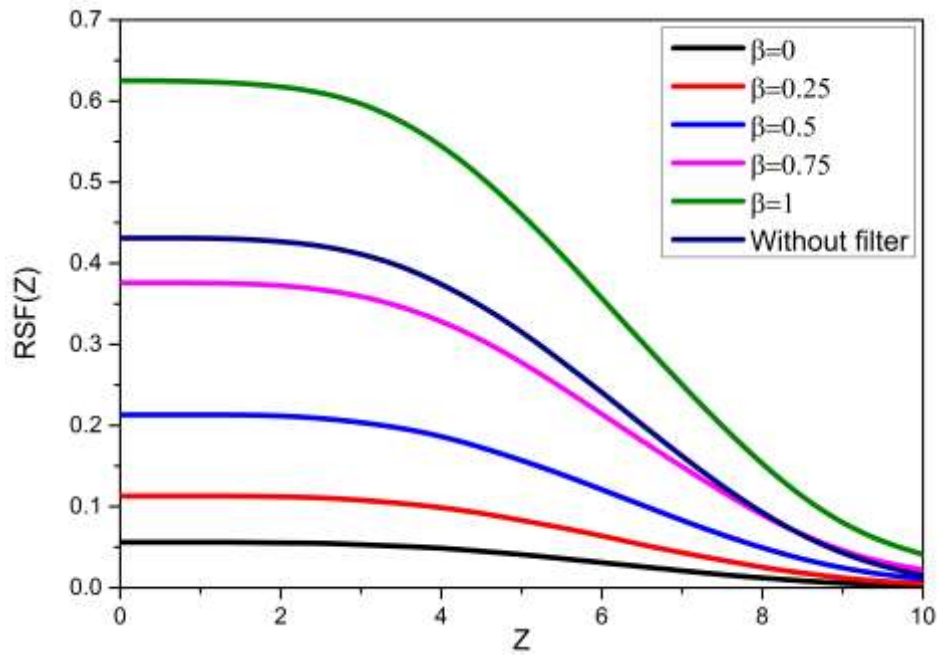
Fig. (4-21): (b) The intensity distribution of the detected thermal image using a system with a filter (at N=2) for unmoving vehicles and at 2 Km of distance.

To distribute the intensity in the image, the heat detected for a vehicle moving at 80Km/h at a distance of 2000m using an optical filter as shown in the following figures (4-22):(a,b).
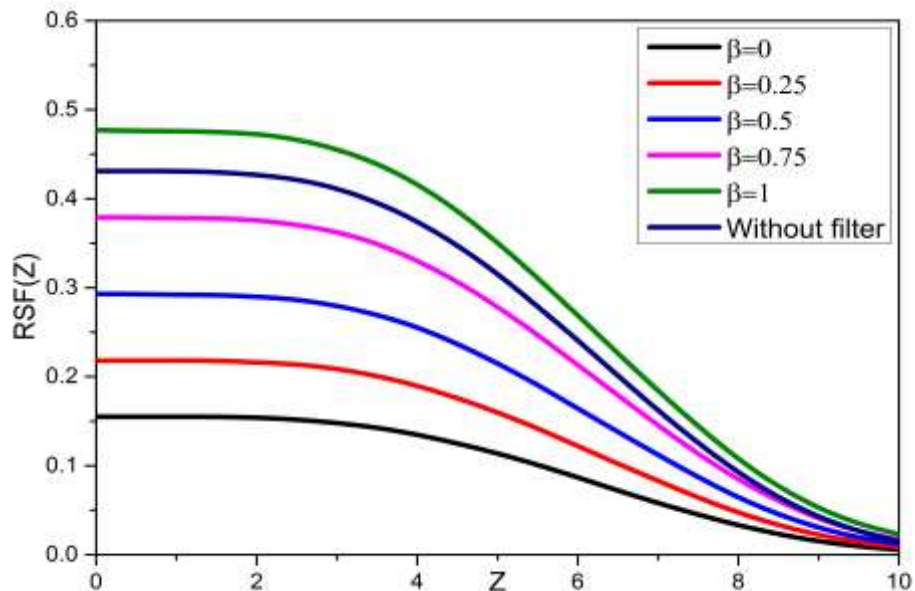

Fig. (4-22): (a) The intensity distribution of the detected thermal image using a system with a filter (at N=1) for moving vehicles with linear motion of (80 Km/h) and at 2 Km of distance.
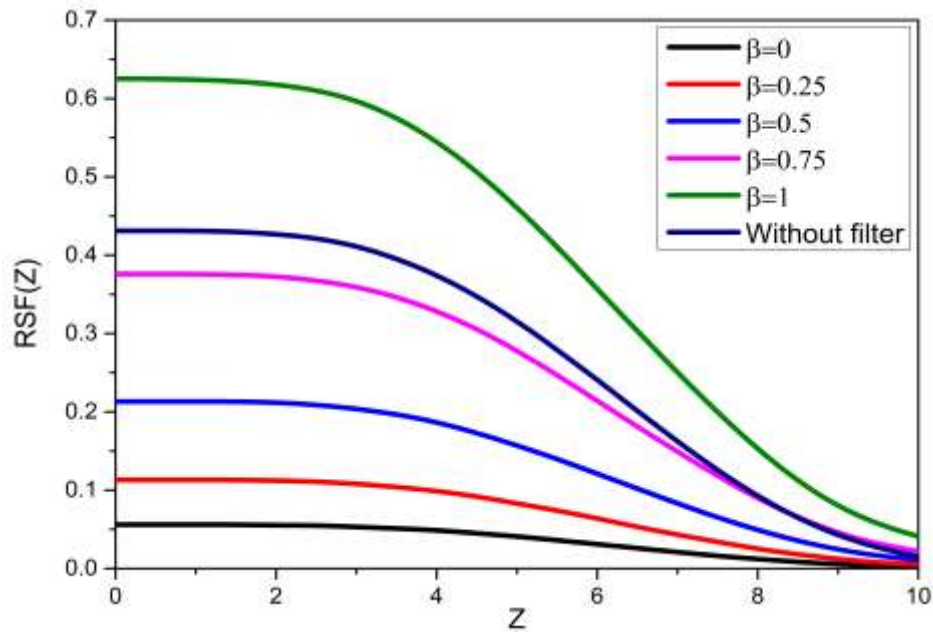
Fig. (4-22): (b) The intensity distribution of the detected thermal image using a system with a filter (at N=2) for moving vehicles with linear motion of (80 Km/h) and at 2 Km of distance.

4-6 Effects of the Bad Weather on the Intensity Distribution of the Detected Thermal Image

One of the important factors, which has a significant effect on the thermal image quality, is the attenuation factor represented by the absorbed/scattered rays from the atmosphere of the environment in which the target is located. This absorption/scattering is because of the presence of microparticles in the atmosphere where the target and the thermal camera are placed. Due to the importance of estimation of the effective recognition distance of the thermal camera in bad weather, in this section, the effect of such factor is investigated for systems operating with (circular, square, and triangular) apertures and for different distances of unmoving targets (vehicles). Distances that are applied, in this study, are (250, 500, 750, 1000, 1500) m.

The bad weather conditions of the target environment negatively affect the distribution intensity values of the thermal image, leading to

form a thermal image of the target which is difficult to identify and distinguish. Increasing the concentration of the dust particles in the atmosphere leads to a decrease in the intensity value of the detected thermal image, and thus, decreases in the distance of detection. Values of the concentration of the particles (PM) were recorded by the meteorological station located in the Ain AL-Tamer area of Kerbala City. These values of PM are (10, 20, 30, 40, 50 $\mu g/m^3$).

From eq. (3-31), the effective visibility range values can be calculated depending on the concentration of the particles PM_{10}. The calculated values of the effective visibility range are (1.1, 0.64, 0.46, 0.37, 0.31) Km corresponding to (10, 20, 30, 40, 50 $\mu g/m^3$) of particle concentrations PM. For different distances between the vehicle and the thermal camera, the calculation of the RSF is performed by using equations (3-33), (3-34), and (3-35) for the three different apertures.

(4-6-1) Effects of the Bad Weather on the RSF for System Operates with Circular Aperture

Figures (4-23): (a, b, c, d, e) show the intensity distributions of the detected thermal image corresponding to the particle concentrations of (10, 20, 30, 40, 50 $\mu g/m^3$), respectively and for different values of distances. The curves denote the RSF of the detected thermal imaging camera operating with a circular aperture.

Figure (4-23): (a(represents the intensity distributions of the detected thermal image when the weather has dust particles with a concentration of 10 $\mu g/m^3$. For different distances of the target under detection, it is found that the maximum intensity value of the RSF is for the case where the distance between the thermal camera and the target

is 250 m. Meanwhile, the increase in the distances between the thermal camera and the target leads to a decrease in the intensity value of the RSF main peak. Arguably that the maximum intensity is less than the same case when the weather doesn't have microparticles with a high concentration. From the figure, it is clear that the limitation of the clarity of the detected thermal image is at the distance of 1 Km. Therefore, the detected thermal images at distances more than 1 Km are useless. This is because of the particle concentrations in the environment, where the target is located, leading to distortion of the resulting thermal image to the point where it is completely blurred. The main reason for this situation is that when infrared radiation spreads through the atmosphere, it will suffer from many phenomena such as absorption and scattering, which leads to a reduction in the received signal before it arrives at the detectors of the thermal imaging device.
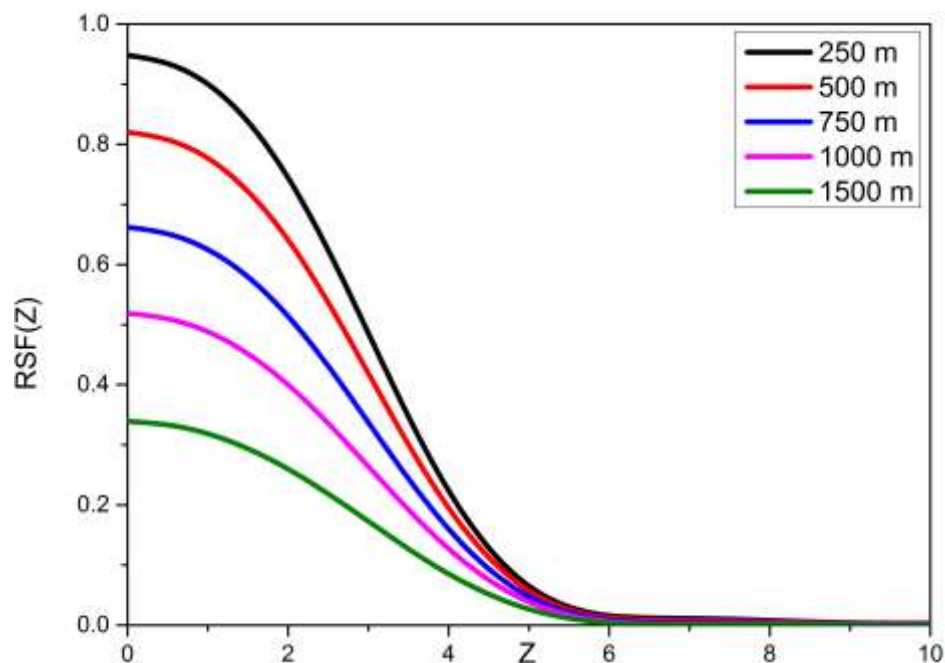

Fig. (4-23): (a) The intensity distribution of the detected thermal image using a system operating with the circular aperture for unmoving vehicles with a concentration of particles PM=10 $\mu g/m^3$ of different distances.

In the same advanced context, the same situation can apply to the
higher concentration of dust particles in the atmosphere. Therefore, the
higher concentrations of particles the higher absorption and scattering of
the spreading thermal rays that come from objects, and thus the more
distorted image compared to an image detected in an environment free
from these particles. All this can be noticed from figures (4-23): (b, c, d, e)
of the unmoving vehicle located at different distances and when the
particle concentrations are (20, 30, 40, and 50 $\mu g/m^3$), respectively.
In these figures, the effect of PM concentration is very clear where
at 50 $\mu g/m^3$ of particle concentration, figure (4-23): (e), the real detection
distance is less than 500 m.

Fig. (4-23): b: The intensity distribution of the detected thermal image using a system
operating with the circular aperture for unmoving vehicles with a concentration of
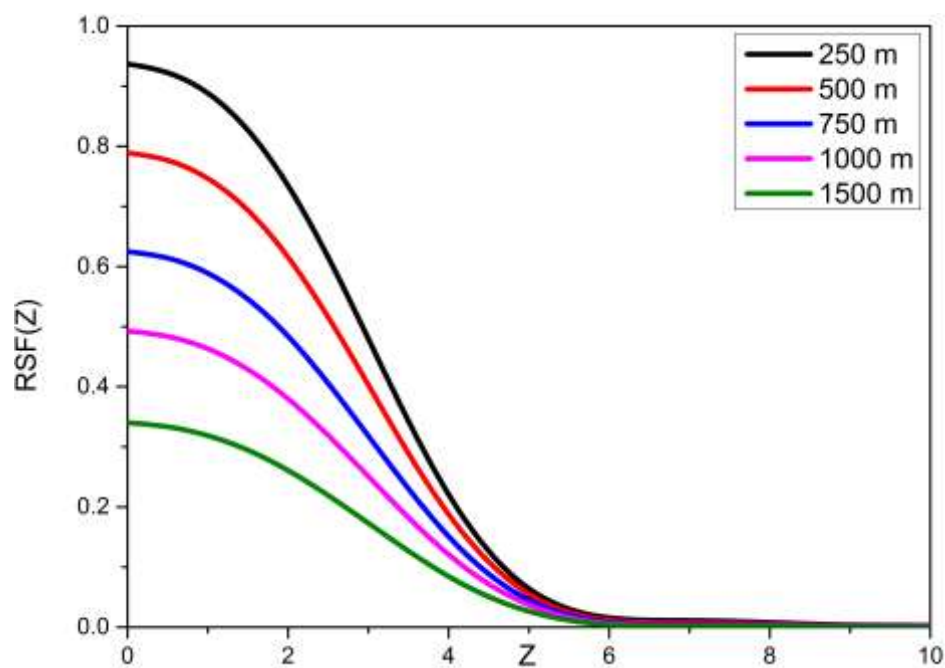particles PM=20 $\mu g/m^3$ of different distances.

Fig. (4-23): c: The intensity distribution of the detected thermal image using a system operating with the circular aperture for unmoving vehicles with a concentration of particles PM=30 $\mu g/m^3$ of different distances.
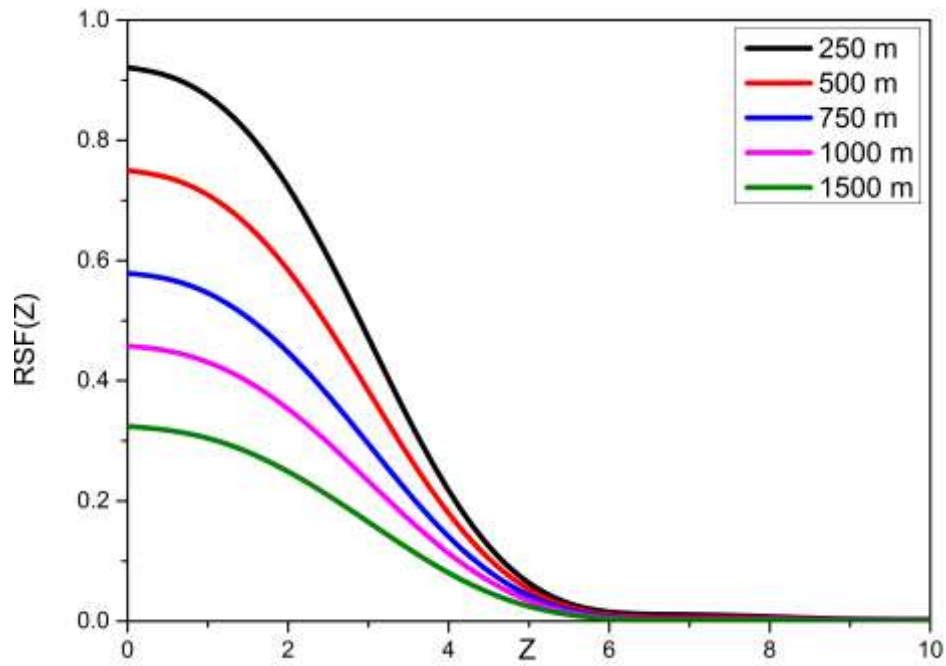

Fig. (4-23): d: The intensity distribution of the detected thermal image using a system operating with the circular aperture for unmoving vehicles with a concentration of particles PM=40 $\mu g/m^3$ of different distances.
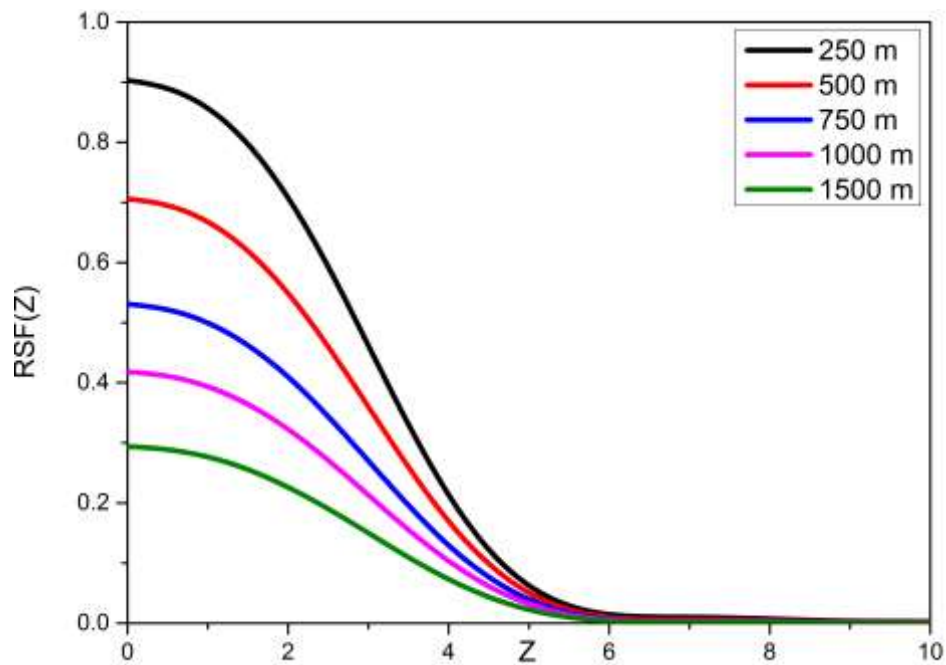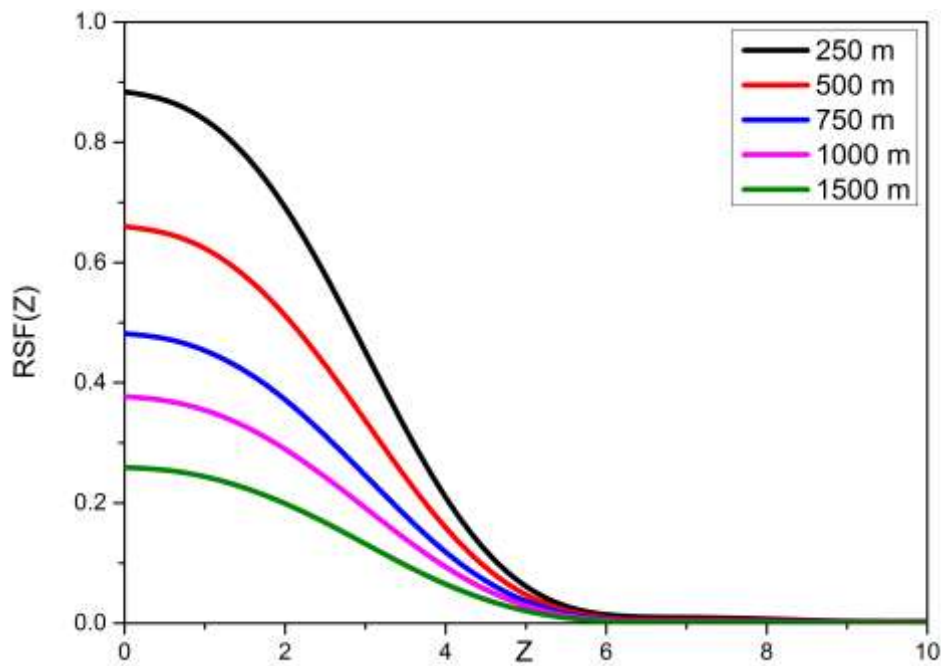
Fig. (4-23): e: The intensity distribution of the detected thermal image using a system operating with the circular aperture for unmoving vehicles with a concentration of particles PM=50 $\mu g/m^3$ of different distances.

(4-6-2) Effects of the Bad Weather on the RSF for System Operates with Square Aperture

Figures (4-24): (a, b, c, d, e) show the intensity distributions of the detected thermal image corresponding to the particle concentrations of (10, 20, 30, 40, 50 $\mu g/m^3$), respectively and for different values of distances. This figure represents the RSF of the detected thermal imaging camera operating with a square aperture.

The same behavior, for the intensity values of the main peak of RSF, is observed in the system operating with the circular aperture. From the figures, which represent the RSF at different concentrations and different distances between the thermal camera and targets, the reduction in the intensity values is apparent when the distance increases. Also, the limitation of the good quality thermal image restricts to the effective

ranges which depend on the particle concentrations contained in the weather. For example, at a concentration of particles of 10 µg/m³, the effective range is 1100 m, which is theoretically calculated using eq. (3-31). From figure (4-24): (a), the limitation of a good quality detected thermal image is captured at less than 1000 m. This is identical to the theoretical calculation of the effective range. In the same cases, figures (4-24): (b, c, d, e) the limitation of the good quality intensity of the detected thermal images are (> 1000, >750, >500, >250), respectively.

Fig. (4-24): a: The intensity distribution of the detected thermal image using a system operating with the square aperture for unmoving vehicles with a concentration of particles PM=10 µg/m³ of different distances.

Fig. (4-24): b: The intensity distribution of the detected thermal image using a system operating with the square aperture for unmoving vehicles with a concentration of particles PM=20 $\mu g/m^3$ of different distances.

Fig. (4-24): c: The intensity distribution of the detected thermal image using a system operating with the square aperture for unmoving vehicles with a concentration of particles PM=30 $\mu g/m^3$ of different distances.
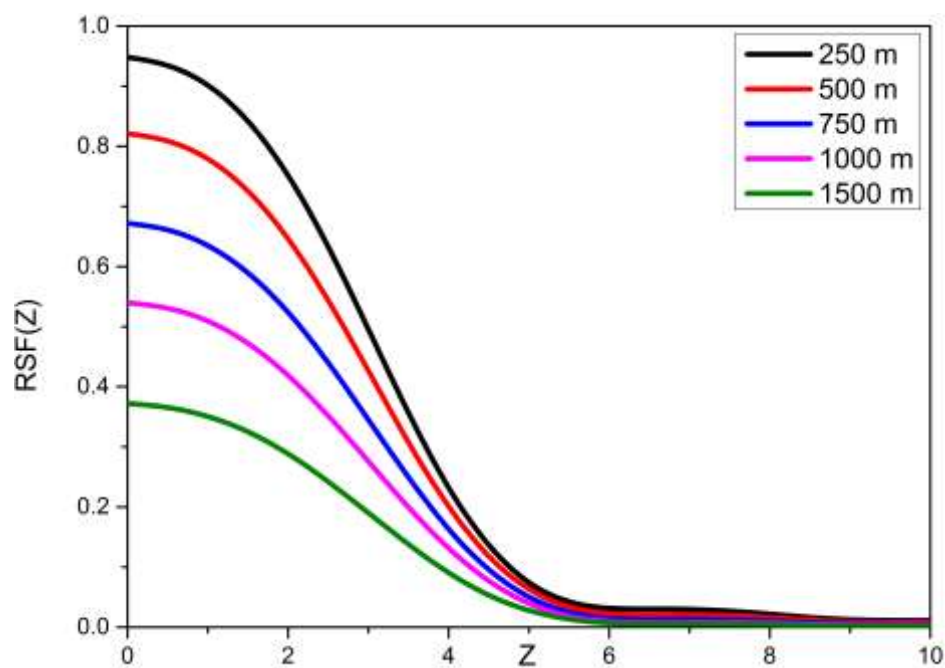
Fig. (4-24): d: The intensity distribution of the detected thermal image using a system operating with the square aperture for unmoving vehicles with a concentration of particles PM=40 $\mu g/m^3$ of different distances.
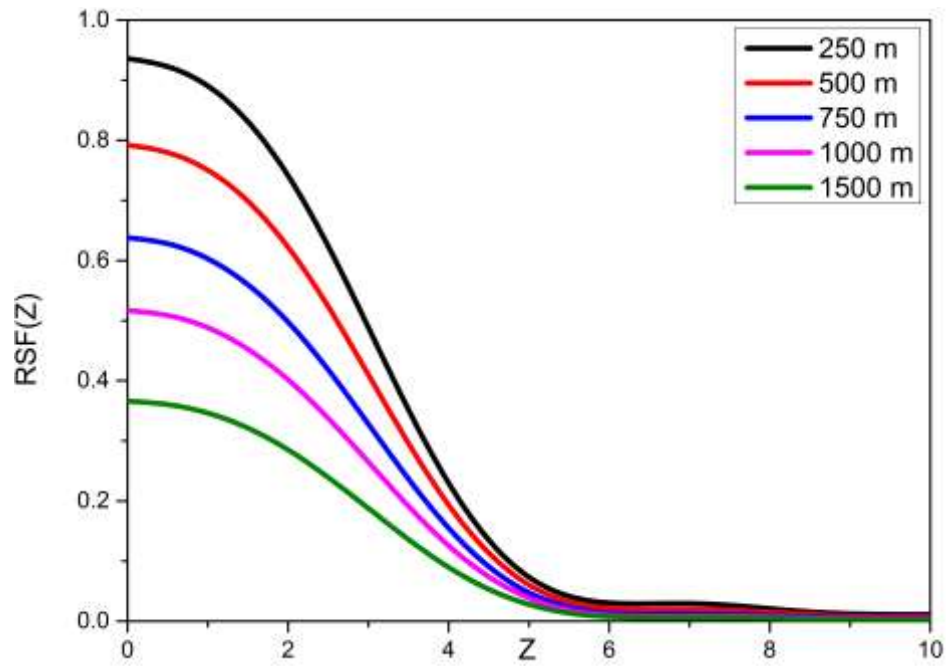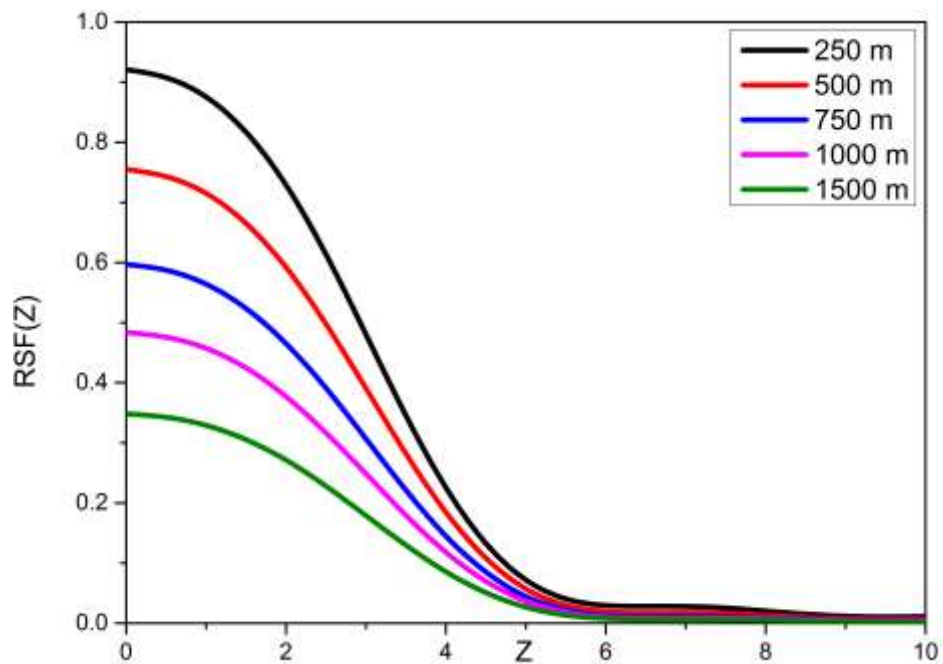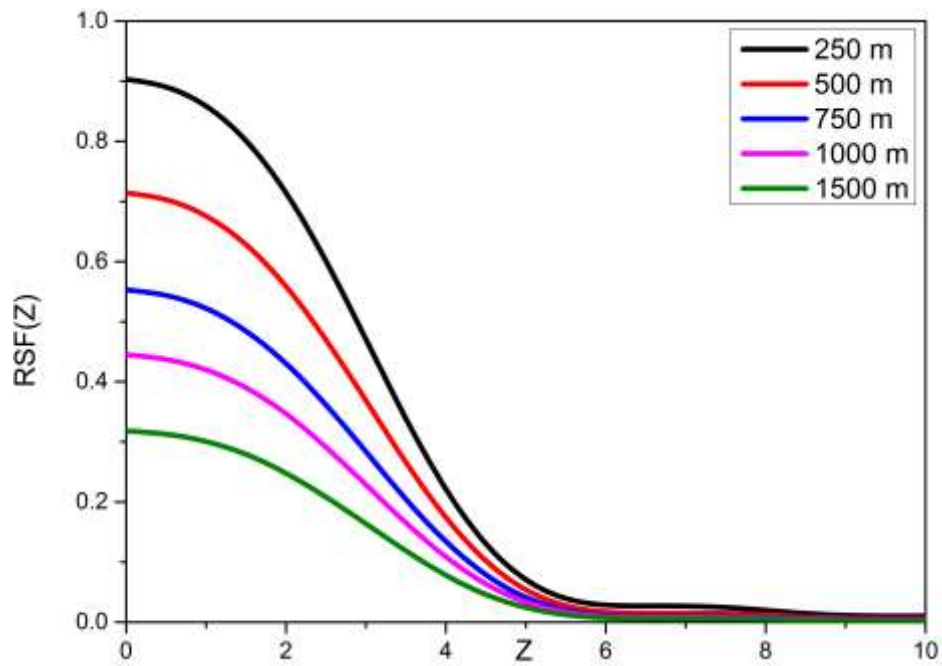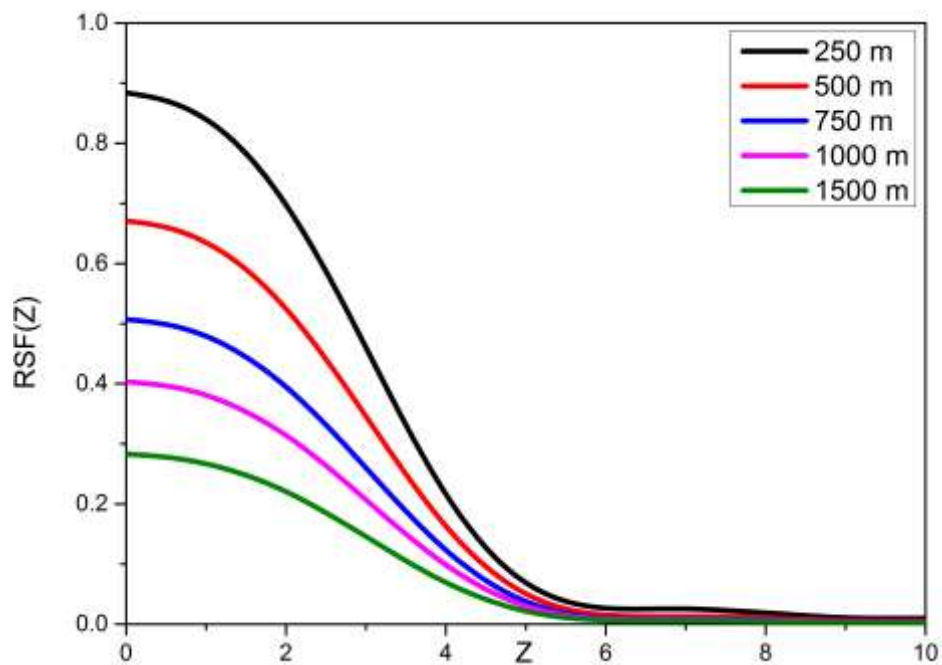

Fig. (4-24): e: The intensity distribution of the detected thermal image using a system operating with the square aperture for unmoving vehicles with a concentration of particles PM=50 $\mu g/m^3$ of different distances.

(4-6-3) Effects of the Bad Weather on the RSF for System Operates with Triangular Aperture

In the triangular aperture, the behavior of the intensity distribution of RSF is similar to the situation in the other two cases (circle, square). The intensity distribution of the detected thermal image is affected by the amount of particles in the weather where the camera and targets are located. This is clear from figures (4-25): (a, b, c, d, e) which show the intensity distributions of the detected thermal image corresponding to the particle concentrations of (10, 20, 30, 40, 50 $\mu g/m^3$), respectively and for different values of distances for imaging camera system operates with a triangular aperture.

Fig. (4-25): a: The intensity distribution of the detected thermal image using a system operating with the triangular aperture for unmoving vehicles with a concentration of particles PM=10 $\mu g/m^3$ of different distances.

Fig. (4-25): b: The intensity distribution of the detected thermal image using a system operating with the triangular aperture for unmoving vehicles with a concentration of particles PM=20 $\mu g/m^3$ of different distances.

Fig. (4-25): c: The intensity distribution of the detected thermal image using a system operating with the triangular aperture for unmoving vehicles with a concentration of particles PM=30 $\mu g/m^3$ of different distances.
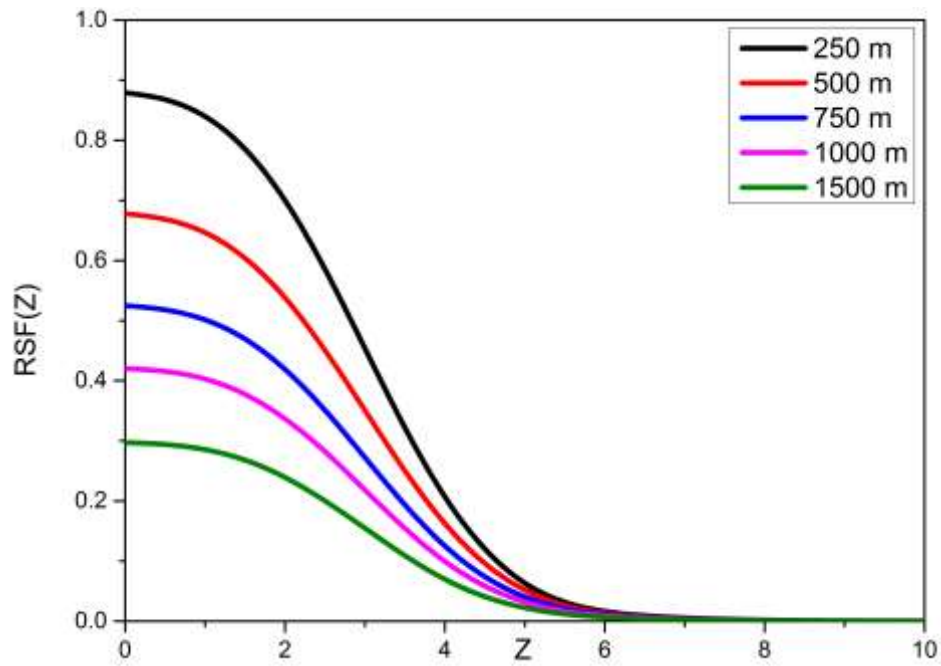
Fig. (4-25): d: The intensity distribution of the detected thermal image using a system operating with the triangular aperture for unmoving vehicles with a concentration of particles PM=40 $\mu g/m^3$ of different distances.
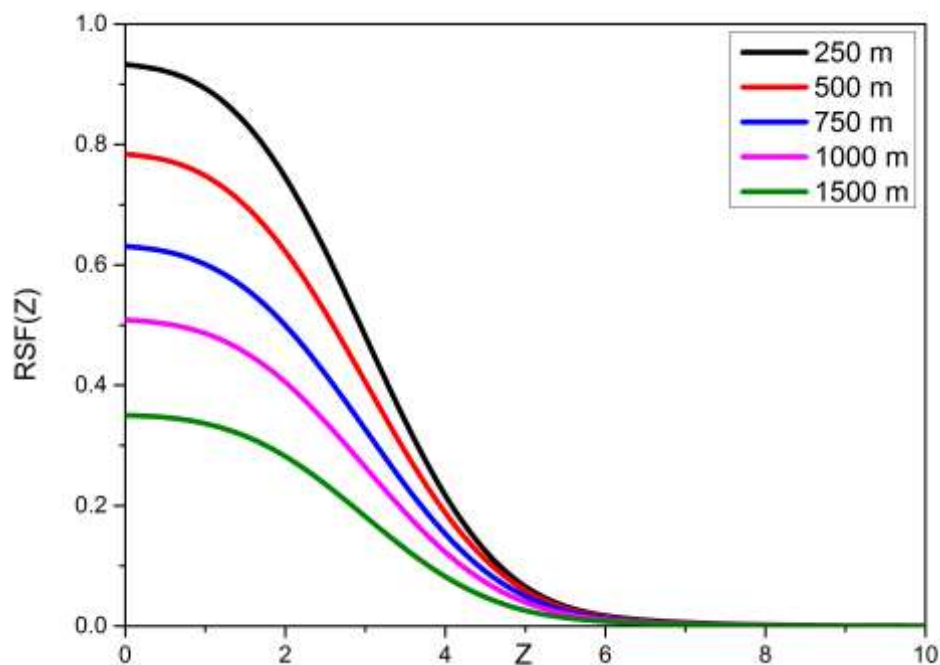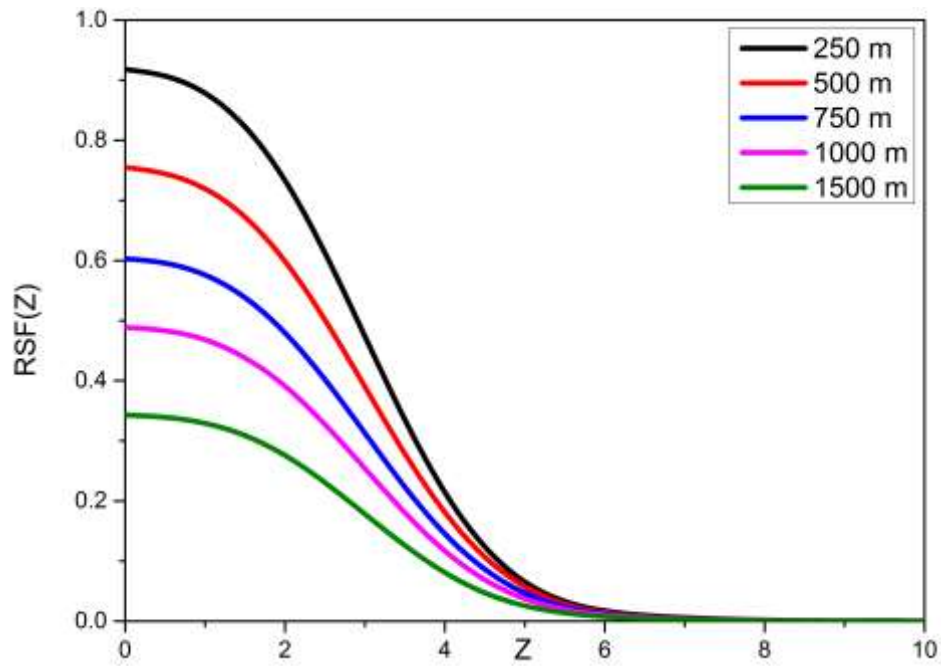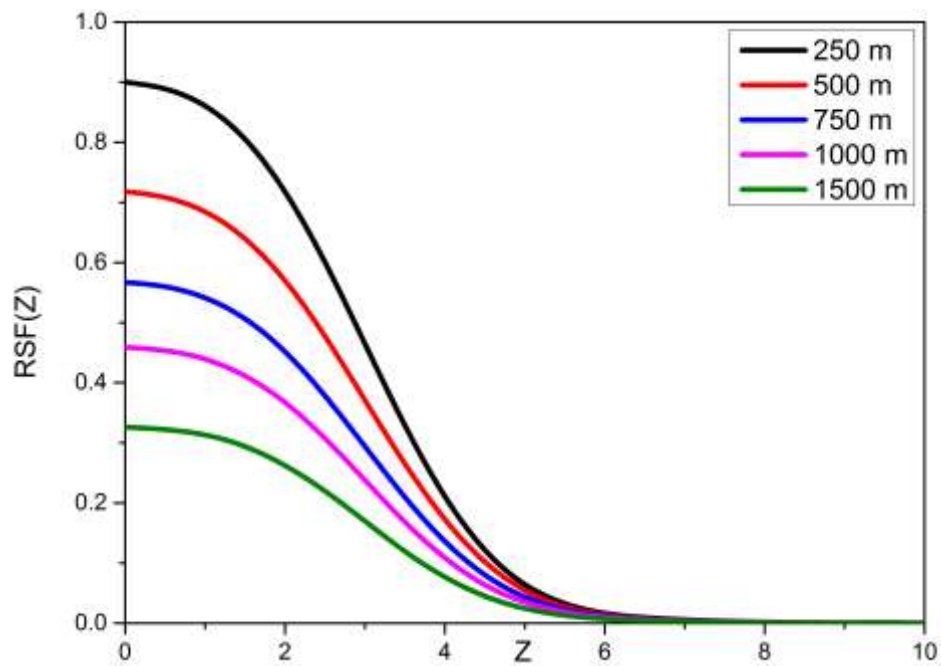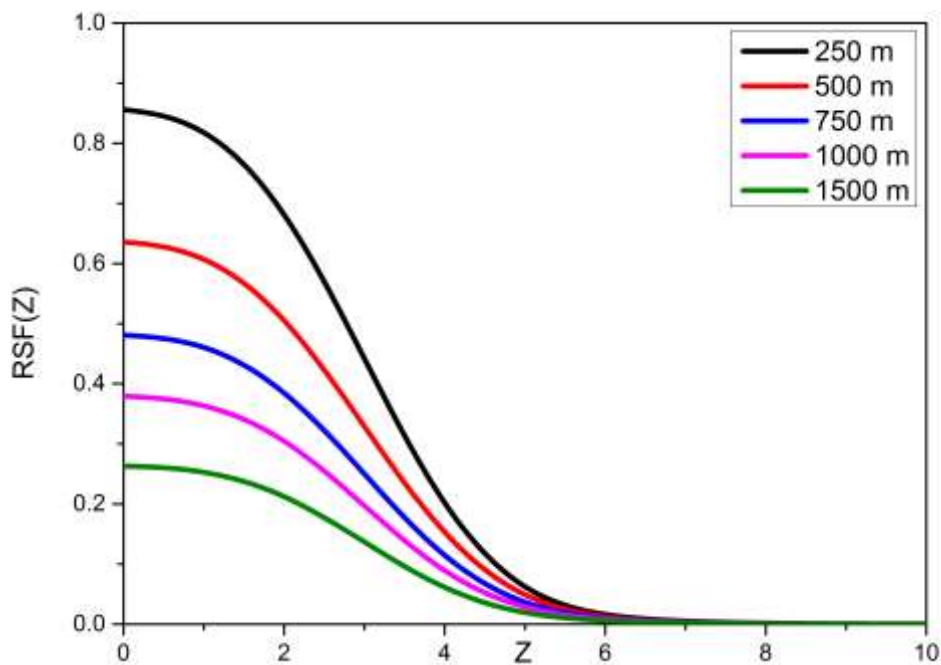

Fig. (4-25): e: The intensity distribution of the detected thermal image using a system operating with the triangular aperture for unmoving vehicles with a concentration of particles PM= 50 $\mu g/m^3$ of different distances.

The greater of distance at which the targets are located, the concentration of dust particles will increase, and thus the absorption/scattering will increase. Figure (4-26) shows the relation between the absorption of the incoming thermal rays and the distance between the thermal imaging device and the target. This figure proves that the absorption is proportional to the distance for any optical system. As a result, the increase in the absorption/scattering of the incoming thermal rays results in intensity degradation in the RSF, leading to produce a detected thermal image with a high distortion compared to the image detected in an environment free of dust particles. This has been clarified in figure (4-27), which shows the relation between the concentration of the dust particles and the absorption of the thermal rays that come to the thermal camera.
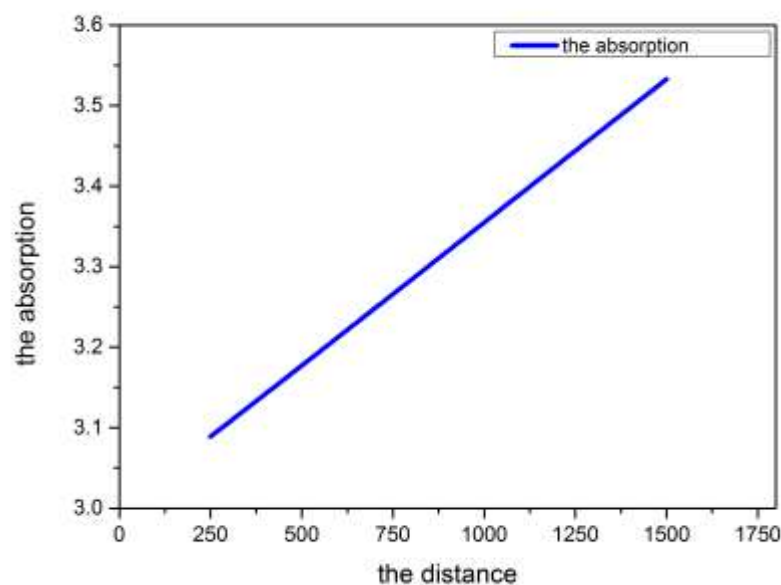
Fig. (4-26) The relation between the absorbance and the distance between the thermal camera and objects to a vehicle in an environment where the concentration of dust particles is 10 μg/m³.
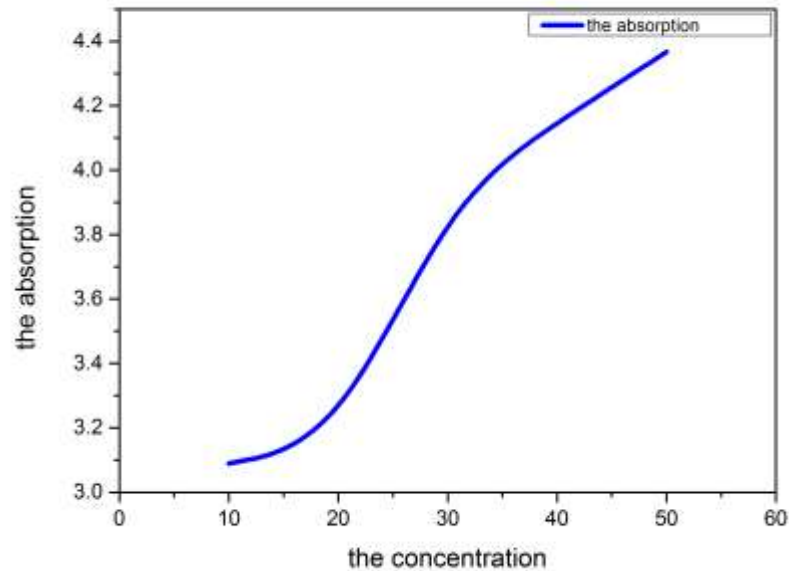
Fig. (4-27) The relation between the absorbance and the concentrations of dust particles.

Eventually, for all cases (in all three apertures) the captured thermal images of a vehicle depend on the distances, nonetheless in all cases the detected thermal image is completely distorted at the distance of 1500 m. Therefore, the intensity distribution at the distance of 1.5 Km will be neglected in the next section.

As well as, for all cases, the value of the intensity at the central peak is always lower than the situation when the weather is free of particles. This means that the effect of such particles exist even if the concentration of the particles is low.

(4-6-4) Comparison Between the Effect of Different Apertures on the Intensity Distribution of the Detected Thermal Image at Bad Weather Conditions

In order to know the preference of any of the used apertures in the optical systems and at bad weather conditions and for specific distances, the highest value of the central peak of the rectangular spread function was selected to know which aperture is the best when used. Figures (4-28), (4-29), (4-30), (4-31), and (4-32) show a comparison between the maximum intensity value of the RSF of the detected thermal image using systems operating with different apertures (circle, square, triangle) at bad weather condition with concentrations of particles of (PM= 10, 20, 30, 40, 50 µg/m^3), respectively. Different distances were selected to investigate which aperture is better in each case. At distances of (250 and 500) m, the performance of circle and square apertures are similar and better than the triangular aperture. This judgment can apply to all cases of particle concentration. Furthermore, at far distances (750 and 1000), the square aperture gives a better intensity value compared to the other apertures (circle, triangle). In the end, to give a final decision in the comparison between the used apertures, the difference in the intensity value is not very significant. Thus, these differences don't affect very much in the thermal image quality. Meanwhile, distance is a very effective factor in all cases of different concentrations of dust particles that contain in the weather.

Fig. (4-28) A comparison between the maximum intensity value of the detected thermal image using systems operating with different apertures at bad weather conditions (PM= 10 μg/m^3) for different distances.

Fig. (4-29) A comparison between the maximum intensity value of the detected thermal image using systems operating with different apertures at bad weather conditions (PM= 20 μg/m^3) for different distances.

Fig. (4-30) A comparison between the maximum intensity value of the detected thermal image using systems operating with different apertures at bad weather conditions (PM= 30 $\mu g/m^3$) for different distances.
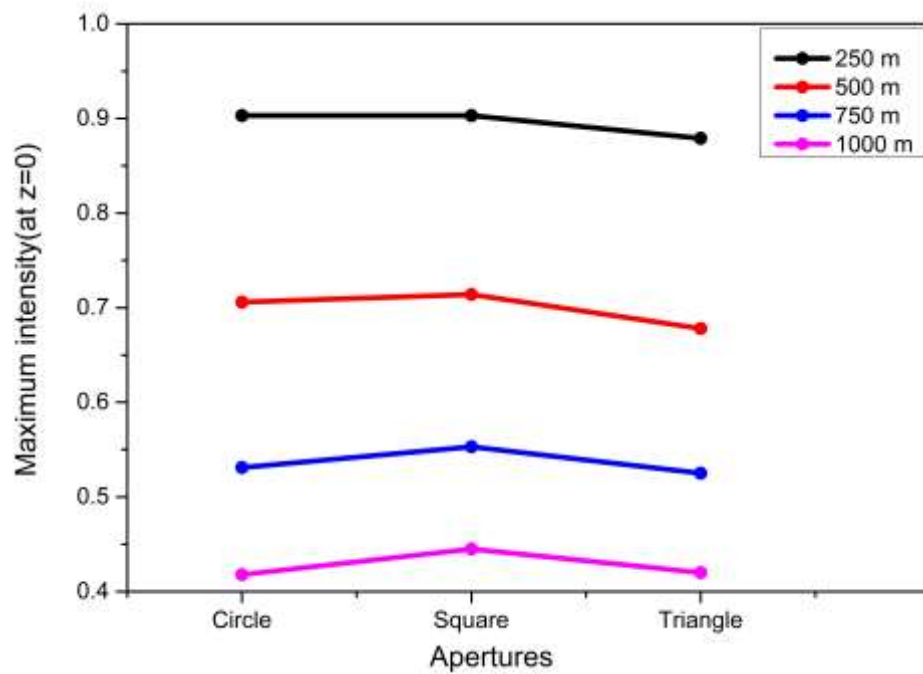
Fig. (4-31) A comparison between the maximum intensity value of the detected thermal image using systems operating with different apertures at bad weather conditions (PM= 40 $\mu g/m^3$) for different distances.
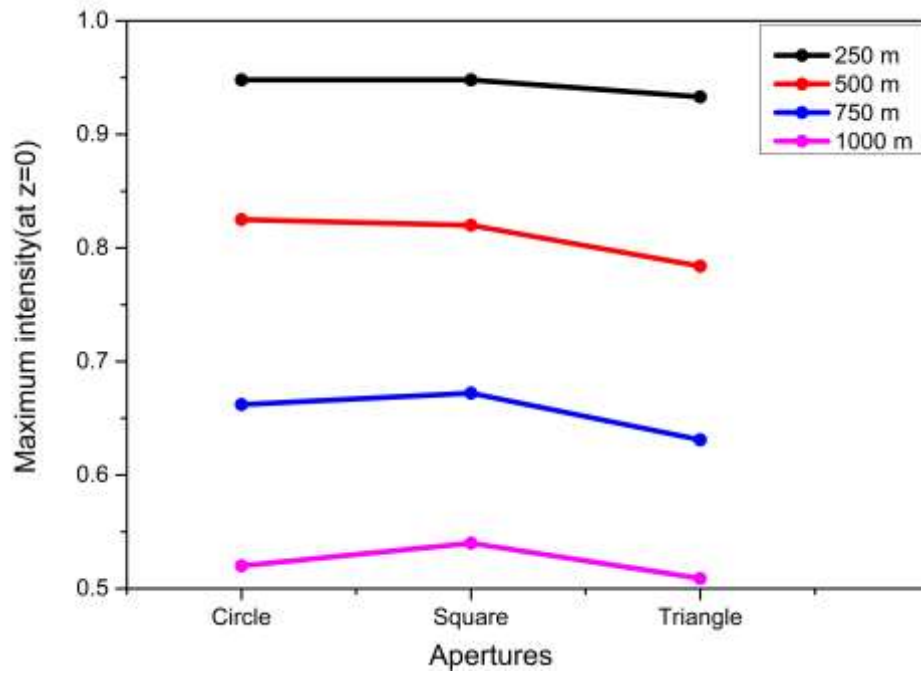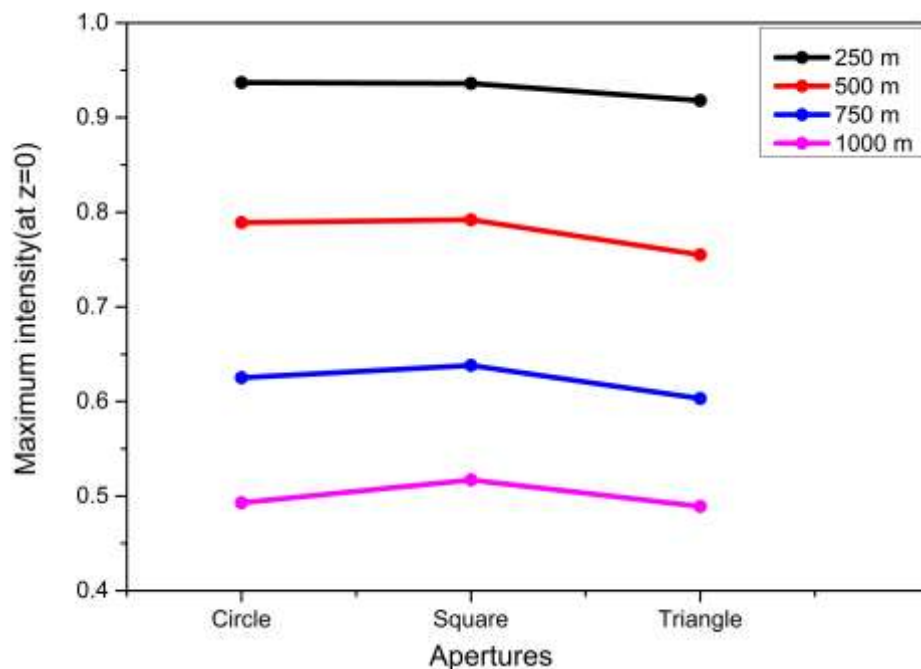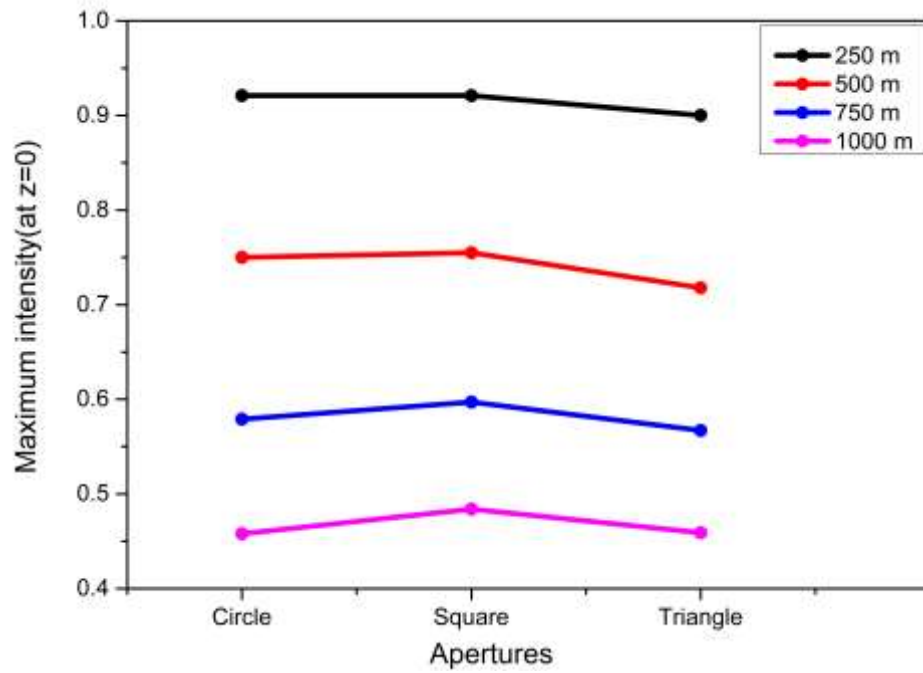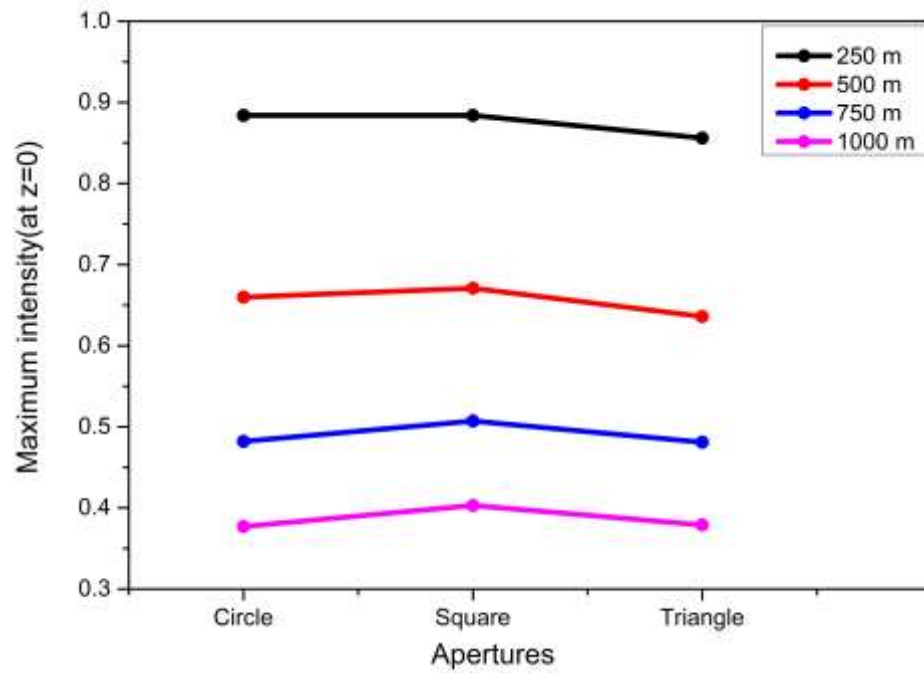
Fig. (4-32) A comparison between the maximum intensity value of the detected thermal image using systems operating with different apertures at bad weather conditions (PM= 50 $\mu g/m^3$) for different distances.

Chapter Five

Conclusions and Future Works

5-1 Conclusions

1. The intensity distribution of the thermal image plays a fundamental and important role in observing and identifying targets, as the rectangular spread function (RSF) is one of the most important used tools in the process of evaluating the efficiency of the thermal camera.

2. It was found that the greater the distance between the thermal camera and objects (250, 500, 750, 1000, 1500, 2000, 3000, 4000) m, the less clear the image becomes.

3. For unmoving targets, a good detection range with a high-resolution thermal image is obtained at ranges of (250-1000) m, above this range, particularly at (1000-2000) m, the thermal image becomes a blur and the target can detect but cannot recognize. a range of more than 2000 m is impossible to detect and recognize the target for this types of thermal camera.

4. The linear motion of objects (velocity) is a very important parameter that affects the intensity distribution of the detected thermal image. For the selected linear motion values, the high speed of the target, the intensity value of RSF reduces and thus, the accuracy of the detected thermal image decreases. The best detection of the thermal image is obtained for the target moving at a speed of 40 Km/h. For higher linear motions the intensity value of RSF decreases.

5. Speed shows a clear effect on the intensity distribution in the image detected for vehicles located at close distances and a small effect on the intensity distribution in the image detected for vehicles located at long distances.

6. the three apertures (circular, square, and triangular) have a good efficiency to detect the thermal image. Additionally, there is no significant difference

in the intensity value of the detected thermal image for the three different

apertures.

7. The triangular optical aperture is considered the best aperture in distances of less than 1.5 Km. Producing a good thermal image because the percentage of efficiency of the thermal imaging depends on many other parameters, which are out of the field of this study.

8. For all cases of distances, that were selected in this work, and for all linear motions that were investigated, using the parabolic filter is very helpful for improving the thermal imaging system by improving the intensity distribution of the detected thermal images.

9. In the parabolic filter, the parameter N=2 is always better than N=1, by increasing the intensity values of RSF. Moreover, increasing the value of the β parameter leads to an increase in the intensity value of the main peak of RSF, which leads to distinguishing and identifying the targets, and increasing the range of detection.

10. The weather conditions, which are represented by dust particles present in the atmosphere of the environment in which the target resides, are affected obviously by the detected thermal images at the region under investigation.

11. The obtained results proved that the greater of the concentration of particles containing in the target environment, the more distortion increases in the image. This is due to an increase in the absorption of thermal radiation emitted from the object by these particles.

5-2 Suggestions for the Future Work

A study of the rectangular spread function for optical systems that suffer .1
from different aberrations and with different orders.

A study of the rectangular spread function for optical systems with the use .2
of other optical filters.

Using other shapes of apertures (Rhombic, Hexagonal) to investigate the .3
intensity distribution in the thermal image.

Investigation of the intensity distribution of another shape of objects .4
(triangular or Elliptical).

Using a multi-synthesis aperture to improve the thermal imaging system. .5

References

S. U. Umar und A. H. Muhammad, *Evaluation And Enhancement of Contract in Digital Images*, J. Univ. Anbar Pure Sci. **7**, (2013). [1]

A. Prakash, *Thermal remote sensing: concepts, issues and applications*, Int. Arch. Photogramm. Remote Sens. **33**, 239 (2000). [2]

R. Vadivambal und D. S. Jayas, *Applications of thermal imaging in agriculture and food industry—a review*, Food bioprocess Technol. **4**, 186 (2011). [3]

E. F. J. Ring, *The discovery of infrared radiation in 1800*, Imaging Sci. J. **48**, 1 (2000). [4]

E. John, *High power mid-wave and long-wave infrared light emitting diodes : device growth and applications .*, Thesis (2009). [5]

D. J. McCafferty, *Applications of thermal imaging in avian science*, Ibis (Lond. 1859). **155**, 4 (2013). [6]

A. Akula, N. Khanna, R. Ghosh, S. Kumar, A. Das, und H. K. Sardana, *Adaptive contour-based statistical background subtraction method for moving target detection in infrared video sequences*, Infrared Phys. Technol. **63**, 103 (2014). [7]

N. P. Avdelidis und A. Moropoulou, *Emissivity considerations in building thermography*, Energy Build. **35**, 663 (2003). [8]

K. J. Havens und E. J. Sharp, *Thermal Imaging Techniques to Survey and Monitor Animals in the Wild: A Methodology* (Academic Press, 2015). [9]

A. Manickavasagan und H. Jayasuriya, *Imaging with electromagnetic spectrum: Applications in food and agriculture*, Imaging with Electromagn. Spectr. Appl. Food Agric. **9783642548**, 1 (2014). [10]

Gondek, *History of infrared detectors A.*, Opto-Electronics Rev. **22**, 77 (2010). [11]

L. SOFRADIR-EC, *or MWIR infrared imaging: Which is best for your application*, SOFRADIR-EC, Infrared Imaging White Pap. Fairfield, New Jersey (2013). [12]

T. Williams, *Thermal imaging cameras: characteristics and performance* (CRC press, 2009). [13]

C. S. Sanoj, N. Vijayaraj, und D. Rajalakshmi, *Vision approach of human detection and tracking using focus tracing analysis*, in *2013 International Conference on Information Communication and Embedded Systems (ICICES)* (IEEE, 2013), S. 64–68. [14]

J. M. Lloyd, *Thermal imaging systems* (Springer Science & Business Media, 2013). [15]

R. Gade und T. B. Moeslund, *Thermal cameras and applications : a survey*, Mach. Vis. Appl. 245 (2014). [16]

J. Zeng, L. Lin, und F. Deng, *Infrared thermal imaging as a nonradiation method for detecting thermal expression characteristics in normal female breasts in China*, Infrared Phys. Technol. **104**, 103125 (2020). [17]

J. A. Tsanakas und P. N. Botsaris, *An infrared thermographic approach as a hot-spot detection tool for photovoltaic modules using image histogram and line profile analysis*, Int. J. Cond. Monit. **2**, 22 (2012). [18]

N. O. Nwazor und S. I. Orakwue, *A review of night vision technology*, Aust. J. Sci. Technol. **4**, 265 (2020). [19]

D. L. In, *An Advanced Radiometric Calibration Approach For Uncooled Thermal Cameras*, Photogramm. Rec. 1 (2017). [20]

T. Zhao, H. Niu, A. Anderson, J. Viers, T. Zhao, H. Niu, A. Anderson, Y. Chen, und J. Viers, *A Detailed Study on Accuracy of Uncooled Thermal Cameras by Exploring the Data Collection Workflo*, Proc. SPIE **10664**, (2018). [21]

C. O'Neill und R. Lucier, *Understanding cooled vs uncooled optical gas imaging*, Air Qual. Meas. Methods Technol. (2019). [22]

References

M. J. Haque, *Night Vision Technology : An Overview*, Int. J. Comput. Appl. **167**, 37 (2017). [23]

K. J. Gaston und A. Sánchez De Miguel, *Environmental Impacts of Artificial Light at Night*, Annu. Rev. Environ. Resour. **47**, 373 (2022). [24]

M. Rai, T. Maity, und R. K. Yadav, *Thermal imaging system and its real time applications: a survey*, J. Eng. Technol. **6**, 290 (2017). [25]

J. Merchant, *Infrared temperature measurement theory and application*, Mikron Instruments Co. Oakland, NJ, USA (2008). [26]

P. Venegas, J. Guerediaga, L. Vega, und J. Molleda, *Infrared Thermography for Temperature Measurement and Non-Destructive Testing*, Sensors 2014, 12305 (2014). [27]

B. B. Lahiri, S. Bagavathiappan, T. Jayakumar, und J. Philip, *Infrared Physics & Technology Medical applications of infrared thermography : A review*, Infrared Phys. Technol. **55**, 221 (2012). [28]

N. Ludwig, D. Formenti, M. Gargano, und G. Alberti, *Skin temperature evaluation by infrared thermography: Comparison of image analysis methods*, Infrared Phys. Technol. **62**, 1 (2014). [29]

A. Akula, R. Ghosh, und H. K. Sardana, *Thermal Imaging And Its Application In Defence Systems*, Acad. Sci. Innov. Res. (AcSIR), Cent. Sci. Instruments Organ. Chandigarh -160030, India **335**, 333 (2011). [30]

Y. Montembeault, P. Lagueux, V. Farley, A. Villemaire, und K. C. Gross, *Hyper-Cam: Hyperspectral IR imaging applications in defence innovative research*, in *2010 2nd Workshop on Hyperspectral Image and Signal Processing: Evolution in Remote Sensing* (IEEE, 2010), S. 1–4. [31]

F. K. Amon, N. P. Bryner, A. J. Lock, und A. P. Hamins, *Performance Metrics for Fire Fighting Thermal Imaging Cameras: Small-and Full-Scale Experiments (NIST TN 1499)*, Tech. Note (NIST TN), Natl. Inst. Stand. Technol. (2008). [32]

A. Szajewska, *Development of the thermal imaging camera (TIC) technology*, Procedia Eng. **172**, 1067 (2017). [33]

R. Vadivambal und D. S. Jayas, *Applications of Thermal Imaging in Agriculture and Food Industry-A Review*, Food Bioprocess Technol. **4**, 186 (2011). [34]

A. Manickavasagan und N. D. G. White, *Applications of Thermal Imaging in Agriculture – A Review*, Can. Soc. Eng. Agric. Biol. Syst. 1 (2005). [35]

C. Burke, M. Rashman, S. Wich, A. Symons, C. Theron, und S. Longmore, *Optimizing observing strategies for monitoring animals using drone-mounted thermal infrared cameras*, Int. J. Remote Sens. **40**, 439 (2019). [36]

R. Gade und T. B. Moeslund, *Thermal cameras and applications: a survey*, Mach. Vis. Appl. **25**, 245 (2014). [37]

R. Usamentiaga, P. Venegas, J. Guerediaga, L. Vega, J. Molleda, und F. G. Bulnes, *Infrared thermography for temperature measurement and non-destructive testing*, Sensors **14**, 12305 (2014). [38]

A. C. Goldberg, S. W. Kennerly, J. W. Little, T. A. Shafer, C. L. Mears, H. F. Schaake, M. Winn, M. Taylor, und P. N. Uppal, *Comparison of HgCdTe and quantum-well infrared photodetector dual-band focal plane arrays*, Opt. Eng. **42**, 30 (2003). [39]

T. W. Tuer, *Thermal imaging systems relative performance: 3-5 micrometers vs 8-12 micrometers*, Sci. Appl. Inc., Ann Arbor, MI. (1977). [40]

R. Usamentiaga, P. Venegas, J. Guerediaga, L. Vega, J. Molleda, und F. G. Bulnes, *Infrared thermography for temperature measurement and non-destructive testing*, Sensors **14**, 12305 (2014). [41]

W. K. Wong, Z. Y. Chew, C. K. Loo, und W. S. Lim, *An Effective Trespasser Detection System Using Thermal Camera An Effective Trespasser Detection System* [42]

References

Using Thermal Camera, in *Second International Conference on Computer Research and Development An* (2010), S. 2–7.

K. V. Kumar, B. Sambaiah, D. K. Sagar, und R. Sayanna, *Point spread functions of defocused optical systems with hanning amplitude filters*, Int. J. Innov. Res. Sci. Eng. Technol **2**, 4293 (2013). [43]

U. Gupta und M. Vadhavaniya, *Analysis of Target Tracking Algorithm in Thermal Imagery*, Int. J. Comput. Appl. **71**, 34 (2013). [44]

R. Ishimwe, K. Abutaleb, und F. Ahmed, *Applications of thermal imaging in agriculture—A review*, Adv. Remote Sens. **3**, 128 (2014). [45]

M. Venkanna und D. K. Sagar, *Amplitude filters in shaping the point spread function of optical imaging systems*, in *International Conference on Optics and Photonics 2015*, Bd. 9654 (SPIE, 2015), S. 60–64. [46]

M. Štumper und J. Kraus, *Thermal imaging in aviation*, MAD-Magazine Aviat. Dev. **3**, 13 (2015). [47]

T. Fu, J. Stipancic, L. Miranda-Moreno, S. Zangenehpour, und N. Saunier, *Traffic Data Collection Using Thermal Camera Under Varying Lighting and Temperature Conditions in Multimodal Environments*, in *TAC 2016: Efficient Transportation-Managing the Demand-2016 Conference and Exhibition of the Transportation Association of Canada* (2016). [48]

M. Bardou, P. Seng, L. Meddeb, J. Gaudart, E. Honnorat, und A. Stein, *Modern approach to infectious disease management using infrared thermal camera scanning for fever in healthcare settings*, J. Infect. **74**, 95 (2017). [49]

S. J. Mambou, P. Maresova, O. Krejcar, A. Selamat, und K. Kuca, *Breast cancer detection using infrared thermal imaging and a deep learning model*, Sensors **18**, 2799 (2018). [50]

B. T. Miethig, Convolutional neural network detection and classification system using an infrared camera and image detection uncertainty estimation, PhD Thesis,The University of McMaster, 2019. [51]

S. E. H. Kiashari, A. Nahvi, H. Bakhoda, A. Homayounfard, und M. Tashakori, *Evaluation of driver drowsiness using respiration analysis by thermal imaging on a driving simulator*, Multimed. Tools Appl. **79**, 17793 (2020). [52]

M. Mazur-Milecka, N. Głowacka, M. Kaczmarek, A. Bujnowski, M. Kaszyński, und J. Rumiński, *Smart city and fire detection using thermal imaging*, in *2021 14th International Conference on Human System Interaction (HSI)* (IEEE, 2021), S. 1–7. [53]

A. A. Kharnoob und A. F. Hassan, *Effect of hexagonal synthetic aperture on the optical system with focal error*, in *Journal of Physics: Conference Series*, Bd. 1999 (IOP Publishing, 2021), S. 12047. [54]

A. A. Kharnoob und A. F. Hassan, *The effect of focal error on the point spread function for hexagonal aperture*, AIP Conf. Proc. **020021**, (2022). [55]

A. F. A. Raheem, A. A. Raheem, und F. K. Fuliful, *Investigation of IR atmospheric transmission under different concentrations of particulate matter PM10*, in *AIP Conference Proceedings*, Bd. 2547 (AIP Publishing LLC, 2022), S. 30008. [56]

A. F. A. Raheem, A. A. Raheem, und F. K. Fuliful, *Investigation of thermal imaging under bad weather conditions*, in *AIP Conference Proceedings*, Bd. 2386 (AIP Publishing LLC, 2022), S. 70004. [57]

A. F. A. Raheem, A. A. Raheem, und F. K. Fuliful, *Detection and analyzing the quality of thermal imager for moving object at different ranges*, in *AIP Conference Proceedings*, Bd. 2414 (AIP Publishing LLC, 2023), S. 30016. [58]

B. Jähne, *Applications and tools*, Digit. Image Process. 3 (2005). [59]

V. A. Kotkar und S. S. Gharde, *Review of various image contrast enhancement* [60]

techniques, Int. J. Innov. Res. Sci. Eng. Technol. **2**, (2013).

M. Born und E. Wolf, *Principles of optics: electromagnetic theory of propagation, interference and diffraction of light* (Elsevier, 2013). [61]

S. A. Ahmed, Calculation of MTF for Optical Disk Modulator by Using Fractal Function, MSc Thesis, University of Technology, 2008. [62]

Y. Lin, T. Feng, S. Lan, J. Liu, und Y. Xu, *On-chip diffraction-free beam guiding beyond the light cone*, Phys. Rev. Appl. **13**, 64032 (2020). [63]

L. Learning, *Limits of Resolution: The Rayleigh Criterion*, Fundam. Heat, Light Sound (2021). [64]

J. C. Wyant, *1.0 measurement of paraxial properties of optical systems*, Course Notes, Univ. Arizona, Tuscon, AZ (2015). [65]

K. H. K. Al-lamy, Desing Study of Various Synthetic Aperture Configuration, MSc Thesis, University of Technology, 2008. [66]

T. Yue, J. Suo, J. Wang, X. Cao, und Q. Dai, *Blind optical aberration correction by exploring geometric and visual priors*, in *Proceedings of the IEEE Conference on Computer Vision and Pattern Recognition* (2015), S. 1684–1692. [67]

J. Sasián, *Introduction to aberrations in optical imaging systems* (Cambridge University Press, 2013). [68]

V. N. Mahajan, *Aberration theory made simple*, Bd. 6 (SPIE Press, 1991). [69]

W. T. Welford, *Aberrations of optical systems* (CRC Press, 1986). [70]

W. Fadl, *Design Optical Modulator by Using Fractal Function Geometry*. [71]

A.A.Raheem, *Study the Image of Line Object for Optical System Using Synthetic Circular Aperture*, J. kerbala Univ. **7**, (2009). [72]

P. Debevec, *Rendering synthetic objects into real scenes: Bridging traditional and image-based graphics with global illumination and high dynamic range photography*, in *Acm siggraph 2008 classes* (2008), S. 1–10. [73]

A. A. Gowen, B. K. Tiwari, P. J. Cullen, K. McDonnell, und C. P. O'Donnell, *Applications of thermal imaging in food quality and safety assessment*, Trends food Sci. Technol. **21**, 190 (2010). [74]

J. H. Lee, J.-S. Choi, E. S. Jeon, Y. G. Kim, T. Thanh Le, K. Y. Shin, H. C. Lee, und K. R. Park, *Robust pedestrian detection by combining visible and thermal infrared cameras*, Sensors **15**, 10580 (2015). [75]

T. H. A. Al-bedary, Energy distribution of apodized laser beam in annular system, MSc Thesis, University of Technology, 2007. [76]

Range Calculation of Night Vision Devices, MSc Thesis,University of Z. A.Hasan, .Babylon, 2000 [77]

K. V. Kumar, B. Sambaiah, D. K. Sagar, und R. Sayanna, *Point Spread Functions of Defocused Optical Systems with Hanning Amplitude Filters*, **2**, 4293 (2013). [78]

W. H. Tarkhan, *The Effect of Astigmatism Aberration on Point Spread Function for Optical System Using Different Apertures*, AL-Qadisiyah J. Pure Sci. **23**, 100 (2018). [79]

Q. K. Ahmed, *New Method for Calculating Cumulative Line Energy Using Pupil Function Technique A new relation has been derived to calculate the cumulative line energy*, **2**, 7 (2006). [80]

A. B. H. Al-Jizany, *A. B. H. Al-Jizany, Studying Of Image Intensity Distribution Of Elliptical Object (Elliptical Spread Function)*, Ibn AL-Haitham J. Pure Appl. Sci. **22**, (2017). [81]

M. Bath, P. Sund, und L. G. Mansson, *Method for determining the two-dimensional presampling modulation transfer function in digital radiography*, Med. Imaging 2001 Phys. Med. Imaging **4320**, 268 (2001). [82]

B. Wang und K. J. Ciuffreda, *Depth-of-focus of the human eye: theory and clinical* [83]

References

implications, Surv. Ophthalmol. **51**, 75 (2006).

S. Banerji, M. Meem, A. Majumder, B. Sensale-Rodriguez, und R. Menon, *Extreme-depth-of-focus imaging with a flat lens*, Optica **7**, 214 (2020). [84]

S. Bae und F. Durand, *Defocus magnification*, in *Computer graphics forum*, Bd. 26 (Wiley Online Library, 2007), S. 571–579. [85]

V. V Mayer und E. I. Varaksina, *Study of Babinet's principle and Rayleigh criterion through elementary theory and simple experiments*, Eur. J. Phys. **42**, 65302 (2021). [86]

J. Demmerle, E. Wegel, L. Schermelleh, und I. M. Dobbie, *Assessing resolution in super-resolution imaging*, Methods **88**, 3 (2015). [87]

G. Cox, *Optical imaging techniques in cell biology* (CRC Press, 2006). [88]

D. E. Wolf und D. E. Wolf, *The Optics of Microscope Image Formation*, **81**, 11 (2007). [89]

A. H. Al-hamadan, G. S. Karam, und A. S. Al-saedi, *Evaluation The image Quality And The optimum Aberrations Balance For an optical System With Different Apertures*, ARPN J. Eng. Appl. Sci. **12**, 6671 (2017). [90]

T. L. S. a Candle, S. Chaos, und I. DirectX, *The Colour Image Processing Hand*, IEEE Spectr. 76T3 (1998). [91]

A. Mahmood, S. A. Khan, S. Hussain, und E. M. Almaghayreh, *An adaptive image contrast enhancement technique for low-contrast images*, IEEE Access **7**, 161584 (2019). [92]

C. D. Claxton und R. C. Staunton, *Measurement of the point-spread function of a noisy imaging system*, JOSA A **25**, 159 (2008). [93]

P. Jia, X. Wu, Z. Li, B. Li, W. Wang, Q. Liu, A. Popowicz, und D. Cai, *Point spread function estimation for wide field small aperture telescopes with deep neural networks and calibration data*, Mon. Not. R. Astron. Soc. **505**, 4717 (2021). [94]

J. Herbel, T. Kacprzak, A. Amara, A. Refregier, und A. Lucchi, *Fast point spread function modeling with deep learning*, J. Cosmol. Astropart. Phys. **2018**, 54 (2018). [95]

M. J. Riedl, *Optical design fundamentals for infrared systems*, Bd. 48 (SPIE press, 2001). [96]

T. P. Johnson und J. Sasian, *Image distortion, pupil coma, and relative illumination*, Appl. Opt. **59**, G19 (2020). [97]

R. B. Schulz und W. Semmler, *Fundamentals of optical imaging*, Mol. Imaging I 3 (2008). [98]

A.A.Raheem und Q. H. Obaid, *Study the Effect of elliptical Aperture on Intensity Distribution of Bar Object Image*, J. kerbala Univ. **8**, (2010). [99]

J. E. Harvey, J. B. Breckinridge, R. G. Irvin, und R. N. Pfisterer, *Novel designs for minimizing diffraction effects of large segmented mirror telescopes*, in *Current Developments in Lens Design and Optical Engineering XIX*, Bd. 10745 (SPIE, 2018), S. 121–134. [100]

A.A.Raheem, F. K. Fuliful, und S.H.Hadi, *Study the Image of Line Object for Optical System Contain to Gaussian Filter Using Different Apertures*, J. Babylon Univ. **19**, 167 (2011). [101]

K. Singh, R. Rattan, und N. K. Jain, *Diffraction images of truncated sine and square wave periodic objects in the presence of linear image motion*, Appl. Opt. **12**, 1846 (1973). [102]

A. H. Al-hamadani und G. S. Karam, *Apodization Defocused Optical Imaging System with Different Apertures using Hanning Amplitude Filter*, Adv. Phys. Theor. Appl. **68**, 5 (2017). [103]

P. Shailaja, N. Kumar, R. Andra, und K. Sagar, *Tailoring the point spread function of an aberrated optical imaging system with Hanning aperture*, **0**, 349 (2017). [104]

M. Venkanna und D. K. Sagar, *Amplitude filters in shaping the point spread function of optical imaging systems*, Proc. SPIE 9654, Int. Conf. Opt. Photonics 2015, 96540A (15 June 2015) (2022). [105]

A. H. Al-hamdani und G. Karam, *Apodization Defocused Optical Imaging System with Different Apertures using Hanning Amplitude Filter*, Adv. Phys. Theor. Appl. 4 (2017). [106]

N. Qasim und A. H. Al-hamadani, *Image Resolution Enhancement for Parabolic Apodized Optical System*, Int. J. Mech. Eng. Image **7**, 1970 (2022). [107]

G. S. Karam, A. H. Al-Hamadani, N. Qasim, N. S. Karam, A. A. Raheem, und Q. Khaled, *Effect of Parabolic Filter on the Resolution of Point Spread Function for Apodized Optical Environment System*, J. Green Eng. **11**, 2238 (2021). [108]

M. Keshavulu Goud, R. Komala, A. Naresh Kumar Reddy, und S. Goud, *Point spread function of asymmetrically apodized optical systems with complex pupil filters: the one-dimensional case with slit aperture*, Acta Phys. Pol. A **122**, 90 (2012). [109]

J. S. Lee und A. E. Willner, *Analysis of Gaussian optical receivers*, J. Light. Technol. **31**, 2687 (2013). [110]

D. Perić, B. Livada, M. Perić, und S. Vujić, *Thermal imager range: Predictions, expectations, and reality*, Sensors **19**, 3313 (2019). [111]

J. A. Khalati, *Experimental Study of the Influence of Dust Particle on Link Range of Free Space Laser Communication System*, J. Coll. basic Educ. **24**, (2018). [112]

M. I. Malik, K. A. Assaf, und A. A. Muhsin, *Optimal Analysis of Laser Beam Propagation Through Dust Storm*, Int. J. Inf. Res. Rev. **3**, 2946 (2016). [113]

D. Perić, B. Livada, M. Perić, und S. Vujić, *Thermal imager range: Predictions, expectations, and reality*, Sensors (Switzerland) **19**, (2019). [114]

الخلاصة

التصوير الحراري هو شكل فعال من أشكال تكنولوجيا الرؤية الليلية، مع القدرة على العمل في غياب تام لأي ضوء.

ان مبدأ عمل التصوير الحراري هو التقاط جزء الأشعة تحت الحمراء من الطيف الكهرومغناطيسي المنبعث من الأجسام لأن هذه الأجسام تصدر موجات كهرومغناطيسية عندما تكون درجة حرارتها أعلى من الصفر المطلق.

تستخدم كاميرات التصوير الحراري على نطاق واسع في التطبيقات العسكرية لقدرتها على توفير الرؤية الليلية والمراقبة وتحديد الأهداف. تعتمد تطبيقات التصوير الحراري على أطوال موجية محددة من الأشعة تحت الحمراء (3-5) ميكرومتر و (8-14) ميكرومتر.

تعتمد جودة النظام البصري على عدد من العوامل التي تؤثر بدورها على شدة الصورة ، مثل العوامل الهندسية لتصميم النظام البصري التي ينتج عنها الانعراج والانحراف ، والعوامل المتعلقة بطبيعة الهدف وخصائصه, محيط (نوع الهدف ، سرعته و البعد الذي يقع عنده الهدف).

في هذا العمل ، تم التعامل مع نظام بصري مثالي. أي أنها تدرس تأثير العوامل المتعلقة بحالة الهدف ومحيطه ، وتحليل التدهور في الشدة ، مما يعطي صورة ضبابية من اجل الوصول إلى قيمة اعلى شدة لتمييز الهدف وليس لاكتشافه فقط.

في هذا البحث سيتم تطبيق شرط التصوير الحراري على دالة الانتشار المستطيل (RSF) لمعرفة توزيع شدة الصورة الحرارية المكتشفة التي تم رصدها في مكان مخصص في محافظة كربلاء.

تم تطبيق أشكال مختلفة من فتحة الكاميرا (دائرة، مربعة، مثلثة) و فلتر بصري لتحسين كفاءة الكاميرا الحرارية.

يتم استخدام برنامج Mathcad لدراسة وتطوير أداء أجهزة التصوير الحراري باستخدام وظيفة RSF كوصف للأهداف، حيث يعتبر النموذج تقنية واعدة للتطبيقات العسكرية التي تحاول تحسين الكاميرا الحرارية في بيئة محافظة كربلاء محافظة.

كلية العلوم

قسم الفيزياء

تحسين كفاءة التصوير الحراري باستخدام أشكال مختلفة لفتحات العدسة

رسالة مقدمة الى مجلس كلية العلوم - جامعة كربلاء

وهي جزء من متطلبات نيل درجة الماجستير في علوم الفيزياء

من قبل

فاطمة رحيم خلف

بإشراف

أ.م. د. أزهر عبد الزهرة رحيم

1445 هـ   م**2023**